Optical Signal Processing of Phase-Modulated Signals for Communication

DAI, Yongheng

A Thesis Submitted in Partial Fulfillment
of the Requirements for the Degree of
Doctor of Philosophy
in
Electronic Engineering

The Chinese University of Hong Kong
September 2011

ABSTRACT OF THESIS ENTITLED:

Optical Signal Processing of Phase-Modulated Signals for Communication

Submitted by Dai, Yongheng

for the degree of Doctor of Philosophy in Electronic Engineering at the Chinese University of Hong Kong in September 2011

Optical signal processing is a key technique to overcome the speed limitation of electronic devices and to bypass the energy-hungry optic-to-electric/electric-to-optic conversion in fiber optic communication networks. Compared with present amplitude-modulated signals, phase-modulated signals such as binary phase shift keying (BPSK) and quadrature phase shift keying (QPSK) are promising for use in high capacity optical networks owing to their excellent transmission performance. This thesis investigates new techniques and optical circuits for optical signal processing of signals in these advanced modulation formats.

In the past few decades of fiber-optic communication, on-off keying (OOK) format is almost the only one used in commercial communication systems. In newly deployed systems, however, advanced modulation formats, especially phase-modulated formats, are favored to combat the transmission performance degradation at high bit rates. Subsequently, it would be common that different modulation formats are adopted in different parts of the whole network. Therefore, format conversion is crucial to enhance the stability and efficiency of communication networks. OOK to

BPSK conversion based on cross phase modulation is demonstrated in the thesis, where pump-modulated four-wave mixing (FWM) is used for phase doubling and thus avoid the use of high optical power that will otherwise degrade the signal quality through stimulated Brillouin scattering (SBS) effect. The FWM also serves as a wavelength conversion stage and helps to achieve wavelength-preserved format conversion. Format conversion within phase-modulated signals is also demonstrated.

Wavelength conversion plays an important role in wavelength routing and network management in wavelength division multiplexing systems. For phase-modulated signals, phase preserving effects like FWM must be used for the wavelength conversion purpose. However, polarization dependence of FWM is a major obstacle for its practical implementation. In this thesis, polarization insensitive FWM is achieved in a birefringent photonic crystal fiber (PCF). The new technique enables polarization-insensitive wavelength conversion of differential phase shift keying (DPSK) signal with a single pump in a linear structure. With an additional pump, a larger conversion bandwidth can be realized. The large bandwidth has also been utilized to achieve polarization-insensitive wavelength multicasting of DPSK signal.

Demodulation is a critical process to convert phase modulation to intensity modulation before the phase-encoded information can be detected by a photoreceiver. To enhance the flexibility in network management, demodulators capable of working at variable bit rates are desirable for applications like dynamic bandwidth allocation.

In the thesis, a delay asymmetric nonlinear loop mirror (DANLM) is first demonstrated to achieve bit-rate variable demodulation using a tunable optical delay introduced by wavelength conversion together with dispersion. The polarization dependence of the DANLM is suppressed using two orthogonal pumps in the setup. To obtain a larger range of operating bit-rates, dual-pump FWM is also used to increase the wavelength conversion bandwidth. To address the bulkiness of the DANLM, we further improve the setup by using a fiber Bragg grating together with a nonlinear PCF in a linear structure to achieve bit-rate tunable demodulation.

Clock recovery module provides a synchronous signal for digital optical communication and is a fundamental element for optical signal processing. Clock recovery of intensity-constant nonreturn-to-zero (NRZ)-DPSK signal is difficult to be achieved since no clock tones or only weak clock tones exist in the signal. Most of the reported NRZ-DPSK clock recovery schemes work at fixed bit rate or a very limited range of bit rates. We first demonstrate a wideband clock recovery circuit for NRZ-DPSK signal by combining the preprocessing with a conventional fiber-based delay interferometer (DI) and bit-rate transparent clock extraction using SBS. Subsequently, by replacing the conventional DI with the DANLM, clock recovery circuit for NRZ-DPSK signal over an extended range of bit-rates is achieved. These techniques promise to provide enhanced flexibility in future optical network management.

Wireless communication can utilize the wide bandwidth of optical system to generate

or to process microwave signals. As a novel technology to provide high bit-rate wireless service, ultra-wideband (UWB) communication has attracted growing interest. We demonstrate the use of delayed interference of a $\pi/2$ phase-shift keying signal in a fiber-based DI to generate UWB monocycle pulses at low cost and power consumption. Pulse position modulation of the monocycle pulses has also been achieved.

摘要

光信號處理是一項很重要的技術。它能夠處理電子設備無法處理的高速通訊信號，並且避免在光纖通訊網絡中光電/電光信號轉換所帶來的高能耗。和目前使用的強度調製信號相比，由於相位調製信號出色的傳輸特性，它們更適合於高速大容量的光網路，比如二相相移鍵控或者四相相移鍵控。本文將探討可用於處理這類高級調製格式的新技術和子系統。

在光纖通訊過去的數十年，二進位啟閉鍵控幾乎是唯一被商用通信系統採用的格式。但是近年來，新鋪設的系統更鍾愛高級調製格式，尤其是相位調製格式，以之對抗高速傳送下的性能惡化。因此，在網路的不同區域採用不同調製格式的情況會變得普遍，從而格式轉換將有助於網路的穩定性和效率。本文展示了二進位啟閉鍵控到二相相移鍵控的轉換。該轉換基於交叉相位調製，而我們增加了一級泵浦調製的四波混頻來避免受激布裏淵散射的危害。此外，它也提供波長轉換的功能，以實現波長不變的格式轉換變。我們也展示相位調製信號之間的格式轉換。

波長轉換是在波分複用系統中實現波長路由和網路管理的重要技術。對於相位調製信號，必須是像四波混頻這樣相位敏感的效應才能用於實現波長轉換。然而，在實際應用中，四波混頻的偏振依賴性是一個難題。本文在一條帶有雙折射的光子晶體光纖實現了偏振不敏感的四波混頻。這個新技術只需要一個泵浦就可以線上型結構中實現差分二相相移鍵控偏振不敏感的波長轉換。當我們再

多加一個泵浦的時候，寬頻的波長轉化就可以實現。這個寬頻特性也可以被運用到相位調製信號的偏振不敏感的波長多播應用中。

解調制是相位調製信號必需的一種處理。它把載入在相位上的資訊轉換到強度上，以方便光電接收器的探測。碼率可變的解調器可被運用到像動態帶寬分配這樣的應用中，來增強網路管理的靈活性。本文採用時延不對稱的非線性環路鏡實現了這個功能。利用雙正交泵浦的四波混頻，該環路鏡的偏振依賴被克服。而為了覆蓋更寬的碼率範圍，雙平行泵浦的四波混頻被用來增加了波長轉換的帶寬，即增加了光學時延。此外，利用光纖布拉格光柵，線型結構的碼率可變解調器解決了該類解調器體積較大的問題。

時鐘恢復模組為數位光通訊提供了同步准直信號，是光信號處理中的重要元素。由於不歸零差分二相相移鍵控號幾乎沒有時鐘信息，要恢復它們的時鐘就比較困難。過去的這類時鐘恢復工作，主要工作在一個固定的碼率，或者是小範圍變動的碼率。利用光纖延遲干涉儀的預處理和受激布裹淵散射的全碼率時鐘提取，我們首先展示了一個寬頻的相位調製信號時鐘恢復模組。然後再採用了時延不對稱的非線性環路鏡來代替延遲干涉儀，碼率可調的時鐘恢復模組也被實現。這類技術有利於提高光網路管理的靈活性。

無線通訊可以利用寬頻的光學系統去產生和處理微波信號。作為一項提供高速無線服務的新技術，擴譜通訊引起了越來越多的興趣。我們利用對 π /2 相移鍵控信號的延遲干涉處理，來生成了單週期脈衝信號。這個方案只需極低的成本

和能耗。

ACKNOWLEDGEMENT

I would like to present my supervisor, Prof. Chester Shu, with my huge gratitude for his invaluable guidance, support and help during my study. His insight of academic research and comprehensive knowledge of optical communications have enlightened me to surmount obstacles. He has shared all my frustration and mistakes through the whole journey, although I really wish I could have more success to share with him. With his care, patience and tolerance, the four-year study is memorable and enjoyable. I owe all my success, if any, to him.

In addition, I would like to thank Prof. Hon Ki Tsang and Prof. Kam Tai Chan, who have provided me a laboratory with advanced equipment.

I would like to thank Ms. Lai Ching Ho for her instructions of lab safety, suggestions of equipment use, and arrangement of facilities. I am deeply grateful to Dr. Mei Po Fok, Mr. Lap Kit Cheng, and Mr. Kin Pang Lei for instructing me in the operation of equipment. I would like to take this opportunity to thank everyone in the photonic group Dr. Kejian Chen, Dr. Caiming Sun, Dr. Chao Li, Dr. Hao He, Dr. Tao Yang, Dr. Xia Chen, Dr. Lin Xu, Mr. Zhongxiang Zhang, Ms. Mengyu Chen, Mr. Chi Yan Wong, Mr. Jiangbing Du, Mr. Liang Wang, Mr. Ming Gai Lo, Ms. Jingjing Liu, Mr. Zili Ma, Ms. Xuelei Fu, Mr. Yimin Chen, Mr. Zhenzhou Cheng, Mr. Ke Xu, Ms. Ka Yan Fung, who have created a harmonious and invigorating atmosphere during my

study.

I would like to thank my family and my friends for their unconditional support. Special thanks are given to my sister, Ms. Yongli Dai, who loves me as a mother, a teacher and a friend all the time. I am grateful to my girlfriend, Ms. Qi Wang, whose love is a most amazing gift I can have. Thanks are also given to my roommate, Mr. Tan Jin.

TABLE OF CONTENT

ABSTRACT i

ACKNOWLEDGEMENT iv

TABLE OF CONTENT vi

1 INTRODUCTION 1

1.1 Overview of Optical Signal Processing 3

1.2 Optical Signal Processing of Phase-Modulated Signals 6

1.3 Outline of The Thesis 8

References 11

2 FORMAT CONVERSION OF PHASE- MODULATED SIGNALS 15

2.1 Introduction to Advanced Modulation Formats 17

2.2 Precoding and Decoding of BPSK and QPSK Formats 21

2.3 NRZ-OOK to RZ-BPSK Conversion 30

2.4 RZ-BPSK to RZ-QPSK Conversion 38

References 44

3 WAVELENGTH CONVERSION OF DPSK SIGNALS 46

3.1 Polarization-Insensitive FWM 49

3.1.1 Polarization-Insensitive FWM in Conventional HNLF 51

3.1.2 Polarization-Insensitive FWM in a Birefringent PCF 54

3.2 Widely Tunable Wavelength Conversion of RZ-DPSK Signal 59

3.3 Polarization-Insensitive Multicasting of RZ-DPSK Signal 68

References 78

4 BIT-RATE VARIABLE DEMODULATION OF DPSK SIGNALS 82

4.1 Introduction to Delay-Asymmetric Nonlinear Loop Mirror 84

4.1.1 Demodulation of DPSK Based on DI 84

4.1.2 Working Principle of DANLM 87

4.2 Polarization-Insensitive Operation of DANLM 90

4.3 Wideband Operation of DANLM 95

4.4 Bit-Rate Variable Demodulator in Linear Structure 101

References 111

5 BIT-RATE VARIABLE CLOCK RECOVERY OF NRZ-DPSK SIGNALS 115

5.1 Bit-Rate Transparent Clock Recovery Using SBS Loop 117

5.2 Wideband Clock Recovery of NRZ-DPSK Signal Using Fiber-Based DI.. 120

5.3 Bit-Rate Tunable Clock Recovery of NRZ-DPSK Signal Using DANLM. 131

References 141

6 DELAYED INTERFERENCE OF PSK SIGNAL TO GENERATE UWB SIGNALS 145

6.1 Introduction to Photonic Generation of UWB Signal 147

6.2 Monocycle Pulse Generation Using Fiber-Based DI 154

Reference 162

7 THESIS SUMMARY AND FUTURE WORK 165

7.1 Summary 165

7.2 Future Work 168

References 170

APPENDICES i

Appendix A. List of Publication i

Appendix B. List of Figures iv

Appendix C. Abbreviations xiv

Optical Signal Processing of Phase-Modulated Signals for Communications

1 INTRODUCTION

Telecommunication service has been as important as water and electricity supply for the human being and the modern society. Among the various communication forms, fiber-optic communication is the backbone to transmit the vast volume of information. Starting from point-to-point links, today's fiber-optic communication is based on complicated optical fiber networks with numerous nodes. The transmission speed of commercial communication systems has also increased from hundreds of Mbit/s to today's 40 Gbit/s.

Unlike water and electricity supply networks, where the traffic is homogeneous and changeless for all users, optical fiber networks carry specified and time-varying optical signal for exclusive users. (Since digital communication dominates in the fiber-optic communication, optical signal in this thesis refers to digital optical signal hereinafter.) Processing of optical signal is therefore vital to correct operation of optical fiber networks, guaranteeing the right information to be sent to the right user. Currently, the processing of optical signal is dominated by commercial electronic processors, where the optical signal has to been converted to electrical signal and back again to optical signal after electronic signal processing. This method leads to at

least two problems. One is the high power consumption related to optic-to-electric/electric-to-optic conversion; the other is limited processing speed of electronic processors. The two problems will become more and more severe as the information traffic increases.

To reduce the power consumption, optical signal processing, which directly process the optical signal and avoid conversion between electrical signal and optical signal, is blooming. The processing can be implemented in an optoelectronic manner or an all-optical manner, using optic-electric effects or nonlinear optical effects. The latter requires the control signal used to process the optical signal be also in the optical domain. The processing speed of the all-optical method is also far beyond the limitation of electrical devices. On the other hand, the optoelectronic manner benefits from simple implementation of multichannel optical signal processing.

1.1 Overview of Optical Signal Processing

The purposes of optical signal processing can be roughly divided into three main categories: routing and switching, regeneration, and performance monitoring.

Routing and switching is necessary for successful signal transmission from its source to destination through an optical fiber network with many possible paths. When a data packet reaches one network node, this function will notify the node of the next node that the data packet should be sent to and start the hop to that node. To achieve the complex function, many processing techniques have been developed, including optical logic operation, packet envelop detection, optical label erasing and rewriting, tunable optical delay, wavelength conversion, wavelength exchange, wavelength multicasting, reconfigurable add-drop multiplexing and de-multiplexing, data format conversion, and pulse format conversion [1-6]. These techniques will help to find the right path, prepare the right data packet, and sent the packet to the right node.

Regeneration is a function that can be implemented in a network node, or in the middle of a transmission link. It aims to recover the quality of a degraded signal and hence to increase the transmission distance. Traditionally, regeneration includes re-amplification, re-shaping, and re-timing. As PSK and quadrature amplitude modulation (QAM) have shown their excellent quality for future high-capacity transmission [7], phase regeneration should be added to the regeneration category [8]. To amplify the optical signal, different optical amplifiers like semiconductor optical

amplifier (SOA), erbium-doped fiber amplifier (EDFA), Raman amplifier, and optical parametric amplifier (OPA) are developed [9,10]. Amplitude and phase regenerators based on nonlinear effects of self-phase modulation (SPM), cross-phase modulation (XPM), four-wave mixing (FWM), and other parametric processes are also explored [11-13]. For retiming, optical clock signals can be recovered using optical phase-locking loop, SOA-ring laser, Fabry-Perot filter, self-pulsating laser diode, and stimulated Brillouin scattering (SBS) loop [14-17].

Optical performance monitoring [18] is critical for intelligent management of optical networks, especially dynamic networks where the transmission link is reconfigurable. By monitoring the signal qualities like optical signal-to-noise ratio (OSNR), residual chromatic dispersion (CD), polarization mode dispersion (PMD), and optical nonlinear impairments, one can measure the quality of service, detect faults, and recover the normal operation of optical networks.

In fact, optical signal processing is already beyond the scope of the optical signal itself. Microwave photonics, which utilizes the wide bandwidth of photonic devices to process electronic signals optically, is one of the examples. It includes many topics like photonic generation of microwave signals, photonic true-time delay beam forming, microwave photonic filters, microwave photonic analog-to-digital conversion, and wireless communication based on radio-over-fiber technology. Owing to the recent maturity of high-speed optoelectronic devices [19], this

technology is becoming promising.

1.2 Optical Signal Processing of Phase-Modulated Signals

The world's first commercial communication link based on optical fiber was setup in Chicago in 1977, working at 44.736 Mbit/s. Over the past thirty-five years, amplitude-modulated signals, mainly on-off keying (OOK), dominate in the fiber-optic communication systems, in both 2.5-Gbit/s systems and 10-Gbit/s systems. To handle the increasing transmission traffic, new 40-Gbit/s communication systems are going to beat the older ones in the market. However, high-speed transmission systems have lower tolerance to PMD and CD and also require higher OSNR. The nonlinear effects in 40-Gbit/s systems are also more injurious to transmission performance than in 10-Gbit/s ones. To successfully deliver high-speed communication systems, many advanced techniques are necessary, including forward error correction, distributed amplification, CD-management, PMD-management, advanced coding and modulation, etc. Among them, advanced modulation is the most critical one. In advanced modulation techniques, in addition to the modulation of amplitude, phase and polarization of light may also be modulated to enhance the transmission performance or to carry more data, like optical dual-binary (ODB), QAM, and polarization-switched quadrature phase-shift keying (PS-QPSK). Advanced modulation formats can also be purely phase-modulated signals, like binary phase-shift keying (BPSK) and quadrature phase-shift keying (QPSK).

Optical signal processing techniques for phase-modulated signals are more

challenging compared with that of amplitude-modulated signals. Unlike the latter, direct approaches to process the phase of an optical wave are limited to phase-sensitive processes like FWM or cascaded sum-frequency generation (SFG)/ difference-frequency generation (DFG) in special nonlinear medium. Other phase-insensitive nonlinear effects, including SPM, XPM, and cross gain modulation (XGM), can be utilized to achieve some limited functions, such as to process the amplitude of phase-modulated signals [20-21] without causing any disturbance to the phase information. Besides, in subtly designed system architecture, phase-insensitive processes can also be applied to phase-modulated signals [22] but offering relatively low cost efficiency. In brief, the development of optical signal processing techniques on phase-modulated signals can be separated into two patterns: brand-new techniques that have never been used for amplitude-modulated signals [13] and techniques borrowed from those of amplitude-modulated signals [20-22].

1.3 Outline of The Thesis

The thesis research focuses on the development of optical signal processing techniques for phase-modulated signals, including format conversion, wavelength conversion, demodulation, and clock recovery. The research work is also extended to optical processing of electronic signals. In chapter 1, an overview of optical signal processing is given. The processing techniques of phase-modulated signals can either inherit from those of amplitude-modulated signals or can be based on completely new functions.

Various modulation formats are coexisting in current networks, and conversion between these formats is desirable in constructing a flexible network. Chapter 2 first gives a brief introduction to phase-modulated formats. Emphasis is put on binary and quadrature PSK formats, including their precoding and decoding methods. Nonreturn-to-zero (NRZ)-OOK to return-to-zero (RZ)-BPSK conversion is then demonstrated, where pump-modulated FWM is utilized to enhance the conversion performance and to provide additional functions. Some technical details on BPSK to QPSK conversion are also provided in this chapter.

Wavelength conversion is a mature technology for amplitude-modulated signals, while it is not the same case for phase-modulated signals. One critical problem is the random polarization of optical signal transmitted in the optical fiber networks. For OOK signal, the problem can be easily overcome by using SPM for wavelength

conversion, which cannot be applied to phase-modulated signals due to its phase insensitivity. Chapter 3 addresses the polarization sensitivity of FWM-based wavelength conversion techniques for differential phase shift keying (DPSK) signal. Using birefringence in a highly nonlinear photonic crystal fiber (PCF), wide bandwidth and polarization-insensitive wavelength conversion can be achieved simultaneously. This technique is subsequently extended to wavelength multicasting of RZ-DPSK signal, where multiple-pump FWM is used.

Chapter 4 reports our work on bit-rate tunable demodulation of DPSK signals. Demodulation is a process to convert phase-encoded data to amplitude-encoded one for detection, and is also a useful method to generate ODB and alternate mark inversion (AMI) signals. In this chapter, bit-rate tunable demodulation of DPSK signal is demonstrated using either a loop structure or a linear structure, based on wavelength conversion together with dispersion to provide a tunable optical delay. Polarization-insensitive operation in the loop mirror is achieved using FWM with dual-orthogonal pumps. To broaden the range of bit rates covered by the loop mirror, FWM with dual-parallel pumps has been used to enlarge the wavelength conversion bandwidth. At last, bit-rate tunable demodulation is demonstrated in a linear structure using cascaded FWM, which is favored by its compactness.

Clock recovery techniques are well-established for amplitude-modulated signals, where the varying amplitude provides strong clock information. For purely

phase-modulated signals, the constant intensity envelop contains no information about the clock. Thus, preprocessing is required to extract the clock information in the initial stage. Most of the reported demonstrations can only work at a fixed bit rate or over a small range of variation. Efforts described in chapter 5 explore the techniques to build a clock recovery unit working over a large range of bit rates. A wideband clock recovery circuit is demonstrated for intensity-constant NRZ-DPSK signal, using a fiber-based delay interferometer (DI) and a loop mirror based on SBS effect. Replacing the DI with a delay-asymmetric nonlinear loop mirror (DANLM), an improved clock recovery circuit working over an extended range of bit rates is achieved.

Processing of phase-modulated signals can bring applications in additional areas. In Chapter 6, we demonstrate the use of delayed interference of a phase-modulated signal to generate ultra-wideband (UWB) signal for wireless communication. This approach benefits from its simple structure, low cost, and low power consumption. Finally, a summary of the thesis is given in chapter 7. Suggested schemes for improvement on the demonstrated techniques of optical signal processing are also described.

References

[1] X. Chen, Y. Yu, and X. Zhang, "All-optical logic minterms for three-input demodulated differential phase-shift keying signals at 40 Gbit/s," IEEE Photon. Technol. Lett., vol. 23, no. 2, pp. 118-120, Jan. 2011.

[2] F. Fresi, C. Porzi, M. Guina, L. Orsila, L. Poti, and A. Bogoni, "Wavelength transparency of all-optical packet envelop detection circuit for RZ-format optical packet switching applications," IEEE Photon. Technol. Lett., vol. 21, no. 20, pp. 1565-1567, Oct. 2009.

[3] N. Calabretta, H.-D. Jung, E. Tangdiongga, H. Dorren, "All-optical packet switching and label rewriting for data packets beyond 160 Gbit/s," IEEE Photon. J., vol. 2, no. 2, pp. 113-129, Apr. 2010.

[4] N. Alic, J. R. Windmiller, J. B. Coles, and S. Radic, "Two-pump parametric optical delays," IEEE Sel. Topics Quantum Electron., vol. 14, no. 3, pp. 681-690, May/Jun. 2008.

[5] L. K. Oxenløwe, R. Slavik, M. Galili, H. C. H. Mulvad, A. T. Clausen, Y. Park, J. Azana, and P. Jeppesen, "640 Gbit/s timing jitter-tolerant data processing using a long-period fiber-grating-based flat-top pulse shaper," IEEE Sel. Topics Quantum Electron., vol. 14, no. 3, pp. 566-572, May/Jun. 2008.

[6] R. Elschner, C.-A. Bunge, B. Huttl, A. G. i Coca, C. Schmidt-Langhorst, R. Ludwig, C. Schubert, and K. Petermann, "Impact of pump-phase modulation on FWM-based wavelength conversion of D(Q)PSK signals," IEEE Sel. Topics Quantum Electron., vol. 14, no. 3, pp. 666-673, May/Jun. 2008.

[7] P. J. Winzer and R.-J. Essiambre, "Advanced modulation formats for high-capacity optical transport networks," J. Lightw. Technol., vol. 24, no. 12, pp. 4711-4728, Dec. 2006.

[8] A. Bogris and D. Syvridis, "RZ-DPSK signal regeneration based on dual-pump phase-sensitive amplification in fibers," IEEE Photon. Technol. Lett., vol. 18, no. 20, pp. 2144-2146, Oct. 2006.

[9] E. Bettini, A. Galtaorssa, L. Palmieri, M. Santagiustina, L. Schenato, and L. Ursini, "Polarized backward Raman amplification in unidirectionally spun fibers," IEEE Photon. Technol. Lett., vol. 20, no. 1, Jan. 2008.

[10] Y. Liang, J. Li, P. C. Chui, and K. K. Y. Wong, "High-sensitivity optical preamplifier for WDM systems using an optical parametric amplifier," IEEE Photon. Technol. Lett., vol. 21, no. 20, pp. 1562-1564, Oct. 2009.

[11] P. V. Mamyshev, "All-optical data regeneration based on self-phase modulation effect," in Proc. of ECOC 1998, Madrid, Spain, pp. 475-476.

[12] A. Striegler and B. Schmauss, "All-optical DPSK signal regeneration based on cross-phase modulation," IEEE Photon. Technol. Lett., vol. 16, no. 4, pp. 1083-1085, Apr. 2004.

[13] R. Slavik et al., "All-optical phase and amplitude regenerator for next-generation telecommunications systems," Nature Photon., vol. 4, pp. 690-695, 2010.

[14] Y. Yu, X. Zhang, and D. Huang, "All-optical clock recovery from NRZ-DPSK signal," IEEE Photon. Technol. Lett., vol. 18, no. 22, pp. 2356-2358, Nov. 2006.

[15] G. Contestabile, M. Presi, N. Calabretta, and E. Ciaramella, "All-optical clock

recovery for NRZ-DPSK signals," IEEE Photon. Technol. Lett., vol. 18, no. 23, pp. 2544-2546, Dec. 2006

[16]X. Tang, J. C. Cartledge, A. Shen, F. V. Dijk, and G.-H. Duan, "All-optical clock recovery for 40-Gbit/s MZM-generated NRZ-DPSK signals using a self-pulsating DBR laser," IEEE Photon. Technol. Lett., vol. 20, no. 17, pp. 1443-1445, Sep. 2008.

[17]D. L. Butler, J. S. Wey, M. W. Chbat, G. L. Burdge, and J. Goldhar, "Optical clock recovery from a data stream of an arbitrary bit rate by use of stimulated Brillouin Scattering," Opt. Lett., vol. 20, no. 6, pp. 560-562, Mar. 1995.

[18]D. C. Kilper, R. Bach, D. J. Blumenthal, D. Einstein, T. Landolsi, L. Ostar, M. Preiss, and A. E. Willner, "Optical performance monitoring," J. Lightw. Technol., vol. 22, no. 1, pp. 294-304, Jan. 2004.

[19]L. Yang and G. B. Giannakis, "Ultra-wideband communications: an idea whose time has come," IEEE Signal Process. Mag., vol. 21, no. 6, pp. 26-54, Nov. 2004.

[20]A. Striegler and B. Schmauss, "All-optical DPSK signal regeneration based on cross-phase modulation," IEEE Photon. Technol. Lett., vol. 16, no. 4, pp. 1083-1085, Apr. 2004.

[21]K. Cvecek, K. Sponsel, G. Onishchukov, B. Schmauss, and G. Leuchs, "2R-regeneration of an RZ-DPSK signal using a nonlinear amplifying loop mirror," IEEE Photon. Technol. Lett., vol. 19, no. 3, pp. 146-148, Feb. 2007.

[22]M. Shin, P. S. Devgan, V. S. Grigoryan, and P. Kumar, "SNR improvement of

DPSK signals in a semiconductor optical regenerative amplifier," IEEE Photon. Technol. Lett., vol. 18, no. 1, pp. 49-51, Jan. 2006.

2 FORMAT CONVERSION OF PHASE-MODULATED SIGNALS

Phase-modulated signals have many advantages over amplitude-modulated signals, but the former cannot completely replace the latter owing to their low cost and easy implementation. The transition from amplitude-modulated signals to phase-modulated signals in commercial communication systems has begun for quite a while. For example, Huawei [1] started to deliver the 40-Gbit/s systems in 2008. The systems can provide three versions for different application scenarios with different modulation formats: ODB, differential-phase return-to-zero OOK and differential QPSK (DQPSK). Systems optimized for the operation of different data formats will coexist in the fiber-optic communication networks. To enhance the efficiency and reliability of the networks, as well as smooth transition of modulation formats, all-optical data format conversion is a desirable function expected to be mounted in the gateways between different communication networks. Furthermore, format conversion between different types of phase-modulated signals is also interesting as the transmission of multi-level modulated signals like QPSK is cost effective for aggregated ultra-high speed data stream. However, in distributing data signals to sub-networks, it can be more cost effective to decompose the QPSK to BPSK signals, which are less complicated to handle. The format conversion can be used in a gateway that provides a cross-connect between two networks at different levels.

Format conversion includes both pulse formation conversion and modulation formation conversion. The former is not as significant as the latter and is also relatively easy to demonstrate. In this chapter, we focus on modulation formation conversion between amplitude-modulated signals and phase-modulated signals, although sometimes pulse format conversion also occurs. Section 2.1 gives a brief introduction to advanced modulation formats. Details on the precoding and decoding of binary PSK and quadrature PSK formats are discussed in the following section. In section 2.3, pump-modulated FWM is used after a XPM stage to achieve NRZ-OOK to RZ-BPSK conversion. Lastly, some technical details on RZ-BPSK to RZ-QPSK format conversion is given in section 2.4.

2.1 Introduction to Advanced Modulation Formats

An optical wave has four physical parameters that can be modulated to represent information, including amplitude, phase, polarization, and frequency. Frequency modulation of lightwave is much less spectrally efficient and hard to realize at high speed compared with the other modulation formats, so it is scarcely adopted in fiber-optic communication systems. It can be also taken as a special kind of phase modulation. The other three parameters can be all used for high-capacity optical networks, although the pure polarization-modulated format, polarization-shift keying (PolSK), is not so popular.

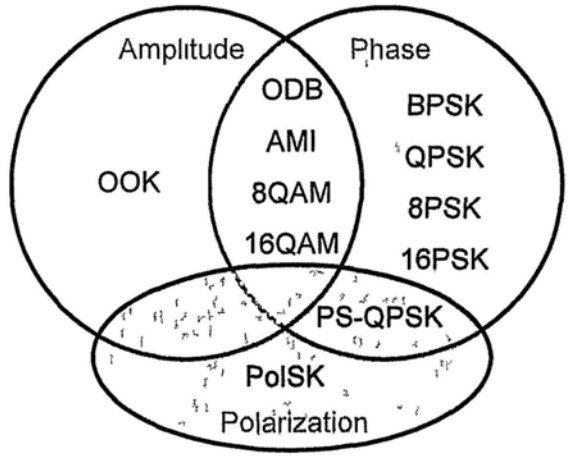

Fig. 2.1. Modulation formats in optical fiber communication systems. OOK: on-off keying; ODB: optical dual-binary; AMI: alternate mark inversion; 8QAM: 8 quadrature amplitude modulation; 16QAM: 16 quadrature amplitude modulation; BPSK: binary phase-shift keying; QPSK: quadrature phase-shift keying; 8PSK: 8 phase-shift keying; 16PSK: 16 phase-shift keying; PS-QPSK: polarization-switched QPSK; PolSK: polarization-shift keying.

Fig. 2.1 shows most of the modulation formats that have attracted intensive interest. Some of them are well-known and maturely implemented in commercial communication systems and the others are still under testing in laboratories. OOK is the basic format with pure amplitude modulation and is most widely used in present 10-Gbit/s communication systems. ODB and AMI belong to the category of advanced amplitude-modulated formats with mixed phase modulation. The phase modulation depth is π. In ODB format, the π-phase change occurs only in 1-bits if there are an odd number of 0-bits between two successive 1-bits. In AMI format, the π-phase change always occurs in every 1-bit, which is actually same as the differential-phase return-to-zero OOK format proposed by Huawei [1]. Fig. 2.2 shows a data sequence "11010011000101" represented in the two formats. The additional phase modulation is not able to carry data but can enhance the transmission performance, especially in increasing the tolerance to nonlinear impairments [2].

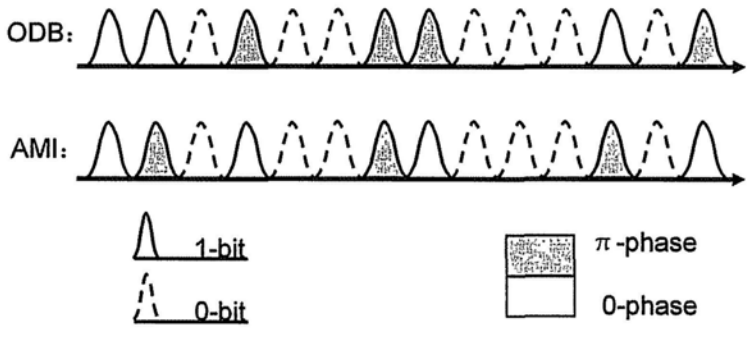

Fig. 2.2. A data sequence "11010011000101" modulated in ODB and AMI formats.

PSK format is an advanced modulation format with constant intensity and uses

different phase to represent information. As photodiodes only respond to optical intensity, data encoded in a PSK format cannot be simply detected. Coherent detection has been developed to fully retrieve the information of an optical field. It is necessary for multilevel formats like 8PSK and 16PSK or even higher. However, the complication is also irksome. For BPSK or QPSK, they can be implemented in a differential way, i.e. differential BPSK (DBPSK; hereinafter, DPSK refers to DBPSK) and DQPSK, after a precoding process in the transmitter. Data modulated in a DBSPK or DQPSK format can be demodulated by a DI and then directly detected by a photodiode. Actually, BPSK and QPSK signal can also be detected after demodulation in a DI if a decoder is to be mounted in the receiver. Details will be discussed in next section.

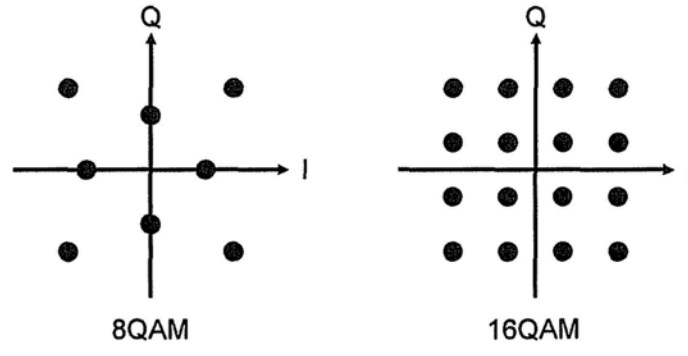

Fig. 2.3. Constellation diagrams of 8QAM and 16QAM.

QAM is another kind of advanced modulation format with mixed amplitude and phase modulation. In contrast to ODB and AMI, both amplitude and phase modulations carry information and hence the spectral efficiency is enhanced. Fig. 2.3 shows the constellation diagrams of 8QAM and 16QAM. Each dot in the 8QAM

diagram represents three bits of data, so an 8QAM signal carries triple amount of information as compared to an OOK signal at the same baud rate. Accordingly, a 16QAM signal carries four times of information compared to that of OOK. However, the sophisticated variation of amplitude and phase makes coherent detection the only way to retrieve the data encoded in these formats.

PS-QPSK is a fairly new advanced modulation format proposed in 2009 and found to own the best power efficiency among all the modulation formats [3] in a coherent communication system. The power efficiency can be understood as the required OSNR to reach a given bit-error ratio: the lower the OSNR, the higher the power efficiency. This feature is extremely desirable in high-speed optical communication, where the obtained OSNR is usually relatively low. PS-QPSK signal is actually the combination of a PolSK signal and a QPSK signal, which carries three bits of data in a single baud. The PolSK signal and QPSK signal are independent, so a PS-QPSK signal can be realized by modulating the polarization of a QPSK signal.

2.2 Precoding and Decoding of BPSK and QPSK Formats

As coherent detection is beyond the scope of the thesis, only directly-detected formats will be investigated. Among the advanced modulation formats, ODB, AMI, BPSK, and QPSK can be detected without a complicated coherent system. ODB and AMI can be treated simply as OOK format, while BPSK and QPSK require precoding or decoding to obtain the data after demodulation in a DI. The requirement is due to the use of DI. Fig. 2.4 shows transmission systems using DPSK/DQPSK or BPSK/QPSK modulation formats. It includes four important elements: modulation, demodulation, precoding, and decoding.

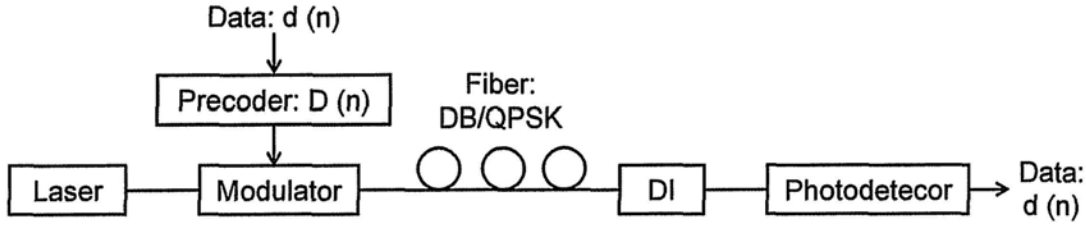

(a) DB/QPSK transmission system

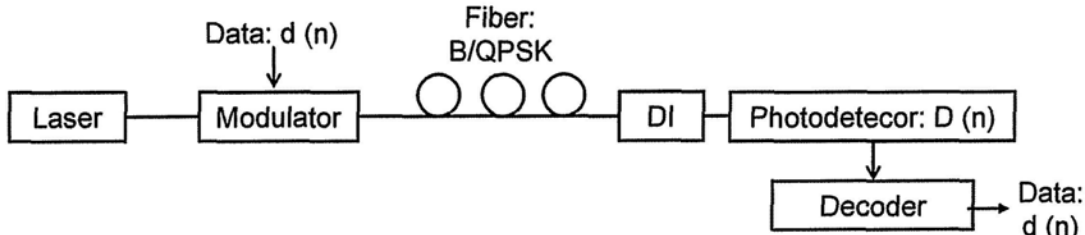

(b) B/QPSK transmission system

Fig. 2.4. Transmission systems using (a) DB/QPSK formats and (b) B/QPSK formats. DI: delay interferometer. d (n): the original data; D (n): transformed data with certain logic relation to the original data.

The difference of PSK and differential PSK signal is just the difference between precoding and decoding. They have the same transmission performance in optical fibers. This feature makes the all-optical format conversion between amplitude-modulated signal and phase-modulated signal meaningful as all-optical conversion to differential PSK signals is not achievable yet due to the lack of optical precoder and decoder.

For the binary PSK, the modulation is relatively easy and the signal can be generated by either a phase modulator (PM) or a Mach-Zehnder modulator (MZM). Demodulation can be accomplished using a fiber-based DI, as shown in Fig. 2.5. The DI can be easily manufactured by splicing two 3-dB couplers together, with different lengths of the two branches to introduce a relative delay. For the demodulation purpose, the delay should be equal to one baud period of a binary PSK signal. Another parameter of DI is the relative phase shift between the two branches. It should be set to proper values for the right demodulation of different PSK signals.

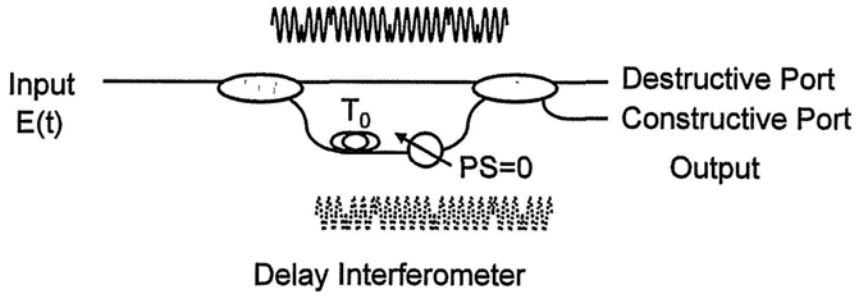

Fig. 2.5. Demodulation of binary PSK signal in a fiber-based DI. PS: phase shift.

Demodulation is based on interference between the signal itself and its delayed copy. In a DI, the input PSK signal is equally split by the first coupler into two copies and the two copies propagate through their respective branches, experiencing different delay and phase shift. The two copies are combined by the second coupler, where the interference occurs. The process can be analytically expressed as

$$\begin{cases} E_{\text{portl}} = \frac{1}{\sqrt{2}} \cdot \frac{1}{\sqrt{2}} \cdot E(t) + \frac{i}{\sqrt{2}} \cdot \frac{i}{\sqrt{2}} \cdot E(t-T_0) \cdot e^{j\varphi_{ps}} \\ \quad = \frac{1}{2}(E(t) - E(t-T_0) \cdot e^{j\varphi_{ps}}) \\ E_{port2} = \frac{i}{\sqrt{2}} \cdot \frac{1}{\sqrt{2}} \cdot E(t) + \frac{1}{\sqrt{2}} \cdot \frac{i}{\sqrt{2}} \cdot E(t-T_0) \cdot e^{j\varphi_{ps}} \\ \quad = \frac{i}{2}(E(t) + E(t-T_0) \cdot e^{j\varphi_{ps}}) \end{cases} \tag{2-1}$$

where $E(t)$ is the field of input PSK signal, E_{portl} and E_{port2} are the fields of output demodulated signals, and φ_{ps} is the value of phase shift.

For binary PSK, the value can be 0 or π. If the $\varphi_{ps} = 0$,

$$\begin{cases} E_{\text{portl}} = E_{\text{destructive}} = \frac{1}{2}(E(t) - E(t-T_0)) \\ E_{port2} = E_{constructive} = \frac{i}{2}(E(t) + E(t-T_0)) \end{cases} \tag{2-2}$$

The intensities are proportional to

$$\begin{cases} |E_{\text{destructive}}|^2 = \frac{1}{2}|E(t)|^2(1 - \cos(\varphi(t) - \varphi(t-T_0))) \\ |E_{constructive}|^2 = \frac{1}{2}|E(t)|^2(1 + \cos(\varphi(t) - \varphi(t-T_0))) \end{cases} \tag{2-3}$$

The signals at the destructive and constructive ports are complementary to each other. If a balanced detector is used to add the two signals together, the demodulated signal

is

$$\left|E_{balanced}\right|^2 = \left|E(t)\right|^2 \cos(\varphi(t) - \varphi(t - T_0)) \quad (2\text{-}4)$$

This indicates if there is no phase change between two successive bits, the demodulated signal is a 1-bit; if there is a π-phase change, the demodulated signal is a 0-bit. However, in the modulation of a binary PSK signal, 1-bit generates a π-phase shift of the CW light and 0-bit generates no phase shift. Phase shift of CW light is different from phase change between two successive bits, but with a fixed logic relation. To retrieve the original data from the demodulated signal, precoding or decoding is required to solve the logic relation.

In precoding, if original data d (n) to be carried is 1-bit, no phase change should be added to the signal according to the demodulation rules and hence the same phase shift should be introduced to the CW light in two successive bits. Otherwise, a π-phase change should be added to the signal for 0-bit. Table 2.1 shows the operation of precoding, where "~" means "not". The precoded data D (n) is the one used to modulate a CW light to generate a DPSK signal. The precoding process can be summarized to D (n) = d (n) ·D (n-1) + ~ d (n) ·~D (n-1).

Table 2.1: Precoding of DPSK signal

Original Data d(n)	Phase Change	Precoded Data D(n)	Demodulated Data
1	0	D(n) = D(n-1)	1
0	π	D(n) = ~ D(n-1)	0

In decoding, the original data d (n) is directly used to modulate a CW light to

generate a BPSK signal. If the demodulated data is 1-bit, the current bit is the same to its previous one. Otherwise, it changes from its previous one, as shown in Table 2.2. The operation can be summarized to $d(n) = D(n) \cdot d(n-1) + \sim D(n) \cdot \sim d(n-1)$, where D (n) is the demodulated data. It shows that decoder has the same logic operation to precoder, except with different input/output definition. This feature also validates in the case of quadrature PSK signals to be discussed later on. The reference bit d (0) is physically to be 1 for the constructive port and balanced port, and to be 0 for the destructive port.

Table 2.2: Decoding of BPSK signal

Demodulated Data D(n)	Decoded Data d(n)
1	d(n) = d(n-1)
0	d(n) = ~ d(n-1)

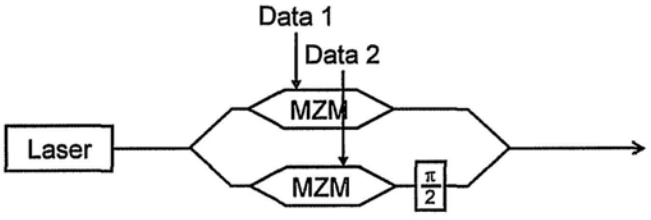

(a) Parallel QPSK modulator

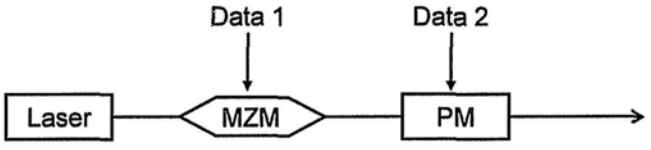

(b) Serial QPSK modulator

Fig. 2.6. Quadrature PSK modulators: (a) parallel scheme; (b) serial scheme. MZM: Mach-Zehnder modulator; PM: phase modulator.

Quadrature PSK signals can be generated by modulators in either a serial structure or

a parallel structure, as shown in Fig. 2.6. Each scheme introduces a distinctive relation between the original data and demodulated data of the signal, and hence different precoding or decoding algorithm.

Demodulation of quadrature PSK signals is also implemented in a DI. Similar to that of binary PSK, the delay should be one bit period, while the phase shift needs to be carefully set to facilitate the detection. The demodulation can also be described by equation (2-1). With balanced detection used,

$$\left|E_{balanced}\right|^2 = \left|E(t)\right|^2 \cos(\varphi(t) - \varphi(t - T_0) + \varphi_{ps}) \qquad (2\text{-}5)$$

When the phase shift is set to $\pm \pi/4$, the phase variation of quadrature PSK with four values of 0, $\pm \pi/2$, and π, will just lead to two different outputs after demodulation, as indicated in Table 2.3. Combining the results of two DI with different phase shift of $\pm \pi/4$, data carried in quadrature PSK format can be retrieved. Here, we define output after DI with phase shift of $\pi/4$, $-\pi/4$ to be I and Q channel, respectively.

Table 2.3: Demodulation of quadrature PSK signal

Phase Change	Demodulated Data: I (Phase shift= π /4)	Demodulated Data: Q (Phase shift= - π /4)
0	1	1
π /2	0	1
π	0	0
3 π /2	1	0

As mentioned, precoding and decoding in quadrature PSK format also depend on the type of modulators used, parallel or serial. In the parallel modulator shown in Fig 2.6 (a), each MZM provides a π-phase modulation, and one of them experiences an

additional half-π phase shift before being combined together coherently. The output is

$$E_{out} = \frac{E_0 e^{j\omega t}}{\sqrt{2}}(e^{j\cdot Data_1\cdot\pi} + e^{j\cdot Data_2\cdot\pi+\frac{\pi}{2}}) \tag{2-6}$$

The logic relation between original data (d_1 (n), d_2 (n)) and precoded data (D_1 (n), D_2 (n)) in DQPSK format is indicated in Table 2.4. With a phasor defined by (D_1, D_2) in the complex plane, the relation can be explained by rotation of the phasor. Taking the original data "00" as an example, the phase change should be π in order to get "00" after demodulation according to Table 2.3. A π-phase change means a phasor (D_1 (n-1), D_2 (n-1)) should be rotated by 180° and thus (~D_1 (n-1), ~D_2 (n-1)) is obtained for (D_1 (n), D_2 (n)).

Table 2.4: Precoding of DQPSK modulation in parallel scheme

Original Data $d_1(n)$ | $d_2(n)$	Phase Change	Precoded Data $D_1(n)$ | $D_2(n)$
00	π	~D_1(n-1) | ~D_2(n-1)
01	π /2	~D_2(n-1) | D_1(n-1)
10	3 π /2	D_2(n-1) | ~D_1(n-1)
11	0	D_1(n-1) | D_2(n-1)

Summarizing Table 2.4,

$$\begin{cases} D_1(n) = d_1(n)\cdot d_2(n)\cdot D_1(n-1) + d_1(n)\cdot\sim d_2(n)\cdot D_2(n-1) + \\ \qquad \sim d_1(n)\cdot d_2(n)\cdot\sim D_2(n-1) + \sim d_1(n)\cdot\sim d_2(n)\cdot\sim D_1(n-1) \\ D_2(n) = d_1(n)\cdot d_2(n)\cdot D_2(n-1) + d_1(n)\cdot\sim d_2(n)\cdot\sim D_1(n-1) + \\ \qquad \sim d_1(n)\cdot d_2(n)\cdot D_1(n-1) + \sim d_1(n)\cdot\sim d_2(n)\cdot\sim D_2(n-1) \end{cases} \tag{2-7}$$

In the serial modulator shown in Fig. 2.6 (b), the MZM (D_1) provides a π-phase modulation while the PM (D_2) provides a half-π modulation. The logic relation

between original data and precoded data in the serial scheme is shown in Table 2.5. The phase modulation on a CW light in a serial modulator can be easily calculated by $\pi \cdot D_1 + \pi/2 \cdot D_2$, so the logic relation can be obtained using an algebraic expression: Phase change = $\pi \cdot (D_1(n) - D_1(n-1)) + \pi/2 \cdot (D_2(n) - D_2(n-1))$. Taking the original data "01" as an example, the phase change should be $\pi/2$ in order to obtain "01" after demodulation according to Table 2.3. However, $D_2(n) - D_2(n-1)$ cannot be equal to 0 to generate a half-π phase shift. If $D_2(n) - D_2(n-1) = 1$, $D_1(n) = D_1(n-1)$; if $D_2(n) - D_2(n-1) = -1$, $D_1(n) - D_1(n-1) = \pm 1$. Thus, $D_2(n)$ is always different from $D_2(n-1)$ and hence equal to $\sim D_2(n-1)$, while $D_1(n) = D_1(n-1) \cdot \sim D_2(n-1) + \sim D_1(n-1) \cdot D_2(n-1) = XOR(D_1(n-1), D_2(n-1))$. Similar summarization can be made as that in equation (2-7).

Table 2.5: Precoding of DQPSK modulation in serial scheme

Original Data $d_1(n) \mid d_2(n)$	Phase Change	Precoded Data $D_1(n) \mid D_2(n)$
00	π	$\sim D_1(n-1) \mid D_2(n-1)$
01	$\pi/2$	$xor(D_1(n-1), D_2(n-1)) \mid \sim D_2(n-1))$
10	$3\pi/2$	$\sim xor(D_1(n-1), D_2(n-1)) \mid \sim D_2(n-1)$
11	0	$D_1(n-1) \mid D_2(n-1)$

For QPSK signal, decoding is required to retrieve the data after demodulation by a DI. The logic operation is actually the same as that of the precoder as mentioned before. In Table 2.6, the relation between the demodulated data and the decoded data of a QPSK signal generated by a parallel modulator is shown. The demodulated data discloses the rotation of phasor ($d_1(n)$, $d_2(n)$) according to Table 2.3, and the

rotation subsequently discloses the relation between two successive bits of the original data.

Table 2.6: Decoding of QPSK modulation in parallel scheme

Demodulated Data $D_1(n) \mid D_2(n)$	Phase Change	Decoded Data $d_1(n) \mid d_2(n)$
00	π	$\sim d_1(n-1) \mid \sim d_2(n-1)$
01	$\pi/2$	$\sim d_2(n-1) \mid d_1(n-1)$
10	$3\pi/2$	$d_2(n-1) \mid \sim d_1(n-1)$
11	0	$d_1(n-1) \mid d_2(n-1)$

Summarizing Table 2.6,

$$\begin{cases} d_1(n) = D_1(n)\cdot D_2(n)\cdot d_1(n-1) + D_1(n)\cdot \sim D_2(n)\cdot d_2(n-1) + \\ \qquad \sim D_1(n)\cdot D_2(n)\cdot \sim d_2(n-1) + \sim D_1(n)\cdot \sim D_2(n)\cdot \sim d_1(n-1) \\ d_2(n) = D_1(n)\cdot D_2(n)\cdot d_2(n-1) + D_1(n)\cdot \sim D_2(n)\cdot \sim d_1(n-1) + \\ \qquad \sim D_1(n)\cdot D_2(n)\cdot d_1(n-1) + \sim D_1(n)\cdot \sim D_2(n)\cdot \sim d_2(n-1) \end{cases} \quad (2\text{-}8)$$

Again, the reference bits $d_1(0)$, $d_2(0)$ are physically to be 1 for the constructive port and balanced port, and to be 0 for the destructive port.

For the case of QPSK generated in a serial modulator, the decoding method is shown in Table 2.7.

Table 2.7: Decoding of QPSK modulation in serial scheme

Demodulated Data $D_1(n) \mid D_2(n)$	Phase Change	Decoded Data $d_1(n) \mid d_2(n)$
00	π	$\sim d_1(n-1) \mid d_2(n-1)$
01	$\pi/2$	$\text{xor}(d_1(n-1), d_2(n-1)) \mid \sim d_2(n-1))$
10	$3\pi/2$	$\sim\text{xor}(d_1(n-1), d_2(n-1)) \mid \sim d_2(n-1)$
11	0	$d_1(n-1) \mid d_2(n-1)$

2.3 NRZ-OOK to RZ-BPSK Conversion

A basic format conversion between amplitude-modulated signals and phase-modulated signals is the conversion from OOK signal to BPSK signal. The conversion utilizes the XPM effects in SOA [4] or highly nonlinear fiber (HNLF) [5, 6], where the OOK signal is the pump in XPM. Although favored for its compactness and high modulation efficiency, the SOA-approach has two problems. The first one is the significant XGM, which transfers amplitude modulation to the generated BSPK signal. The other is the slow recovery time of SOA, which leads to the pattern effect. Approaches based on XPM in optical fiber are desirable for the ultrafast response and small disturbance to the constant intensity of BPSK signal. However, the phase modulation efficiency in fiber is not very high and is governed by the following equation [5]

$$\varphi = 2\gamma P L_{eff} \tag{2-9}$$

where φ is phase shift of the XPM probe, γ is nonlinear coefficient, P is optical power of XPM pump, and L_{eff} is the effective length of nonlinear fiber. Using the typical value of nonlinear coefficient, γ=11.5 $\text{km}^{-1}\text{W}^{-1}$, the required pump power is ~ 21.5 dBm to introduce a π-phase shift in a highly nonlinear fiber with an effective length of 1 km. Unfortunately, SBS threshold of a NRZ-OOK signal in such a fiber is ~ 19 dBm, according to the equation in [7]

$$g_B P_{th} L_{eff} / A_{eff} \approx 21 \tag{2-10}$$

where g_B (estimated to be 3×10^{-12} m/W for 100-ps pulse.) is the peak value of Brillouin gain, P_{th} is SBS threshold power, and A_{eff} (~11.5 μm^2) is the effective area

of the fiber. The SBS can dramatically degrade the OOK signal and hence the phase modulation of the probe. It is easy to see that the increase of the fiber length is not a good manner to solve this problem since it will also decrease the SBS threshold. Fibers with higher nonlinear coefficient are a better solution except that this kind of fibers is rarely accessible yet.

To avoid the SBS-induced degradation in HNLF, the generated BPSK signal usually has a phase shift less than π, which reduces the power efficiency of BPSK format. To increase the phase modulation depth, pump-modulated FWM is an effective method [8, 9]. The method has been utilized to restore a DPSK signal or to reduce the driving voltage of a PM. In the OOK to BPSK format conversion, the XPM pump just needs to introduce a $\pi/2$-phase shift of the probe if a pump-modulated FWM process follows the XPM to double the phase modulation depth as shown in Fig. 2.7, which would reduce the pump power to ~ 18.5 dBm and is lower than the SBS threshold.

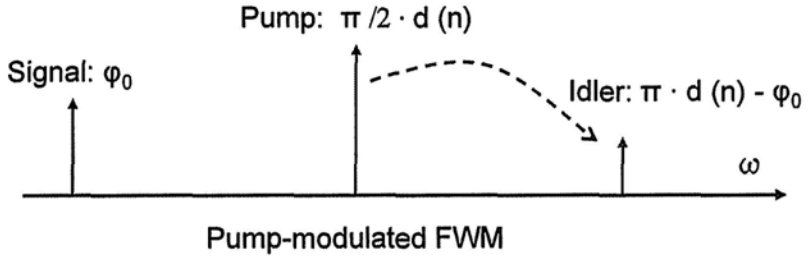

Fig. 2.7. Pump-modulated FWM to double the phase modulation depth.

Fig. 2.8 shows the experimental setup to convert NRZ-OOK to RZ-BPSK signal using the XPM-plus-FWM approach. The choice of NRZ pulse format of OOK and

RZ pulse format of BPSK leads to less frequency chirp of the generated BPSK signal [10]. The NRZ-OOK signal is generated from a CW light which is modulated by a 10-Gbit/s pseudo-random bit sequence (PRBS) in a MZM. Combined with a XPM probe, a 10-GHz pulse train, the optical signals are amplified to a total power of ~ 20 dBm by an EDFA and fed into a 1-km HNLF, which has an effective area of 11.4 μm^2 and a nonlinear coefficient of 11.7 $km^{-1}W^{-1}$. In the HNLF, 1-bits of the NRZ-OOK signal add a $\pi/2$-phase shift to the pulsed probe through XPM while 0-bits introduce nothing. The generated $\pi/2$-BPSK signal is filtered out by an optical bandpass filter and combined with another CW light to perform the pump-modulated FWM in a highly nonlinear PCF. After optical filtering, a π-BPSK signal is generated, which owns high receiver sensitivity.

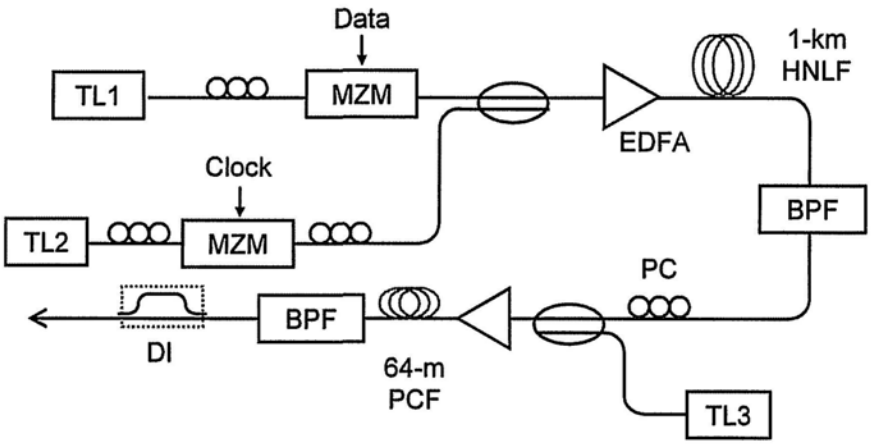

Fig. 2.8. Experimental setup of NRZ-OOK to RZ-BPSK conversion using XPM plus FWM. TL: tunable laser; BPF: optical bandpass filter; PCF: photonic crystal fiber; DI: delay interferometer.

The influence of SBS in the format conversion process is shown in Fig. 2.9. When

the optical power of NRZ-OOK signal is below the SBS threshold, the demodulated BPSK signal at the constructive port of DI has little noise although the eye opening is small. When the OOK signal power increases, the eye opening is also enlarged, but becomes noisier due to SBS.

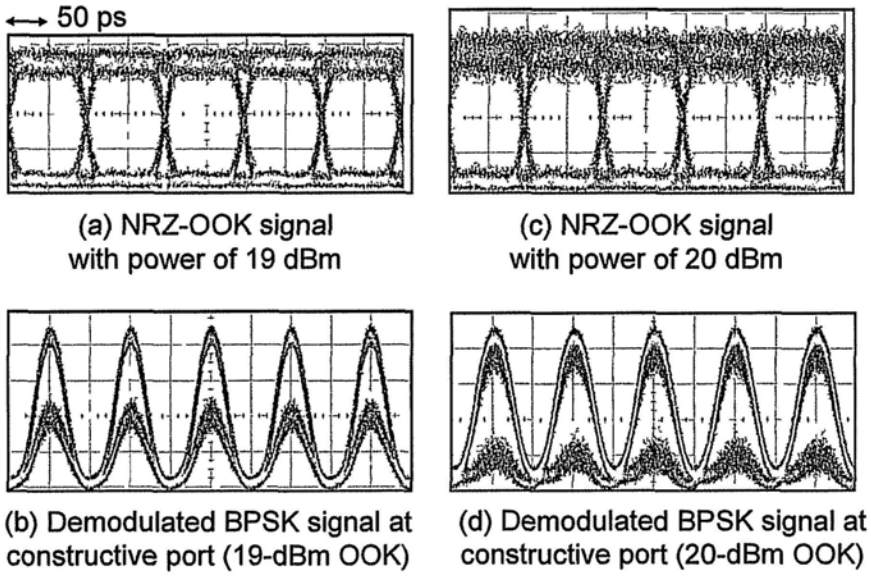

Fig. 2.9. Influence of SBS on OOK to BPSK conversion. (a, b) NRZ-OOK signal with power under SBS threshold and the corresponding generated BPSK signal; (c, d) NRZ-OOK signal with power above SBS threshold and the corresponding generated BPSK signal.

Another problem in this approach is FWM. As shown in Fig. 2.10, when the XPM pump and probe are close in wavelength, FWM between them is strong and leads to a slight variation of intensity, which is similar to XGM in SOA. The effect can be avoided by increasing the wavelength spacing between the light waves, as shown in the inset of Fig. 2.10. In our experiment, we set the wavelengths of OOK signal and

the pulsed probe in the XPM stage to 1550.9 and 1557.3 nm, respectively, and set the power of OOK signal to ~ 18.5 dBm to generate a π/2-BPSK signal. After phase doubling by pump-modulated FWM in the PCF, π-BPSK signal is finally generated, as shown in Fig. 2.11. The total optical power for pump-modulated FWM in the 64-m PCF is 23 dBm.

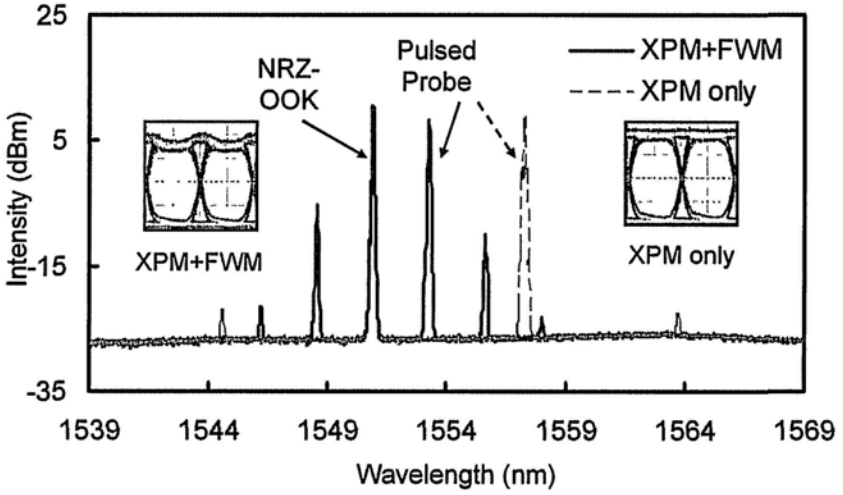

Fig. 2.10. Optical spectra in format conversion when FWM between the XPM-pump and XPM-probe varies. Inset: eye diagrams of NRZ-OOK signal when FWM is present and absent.

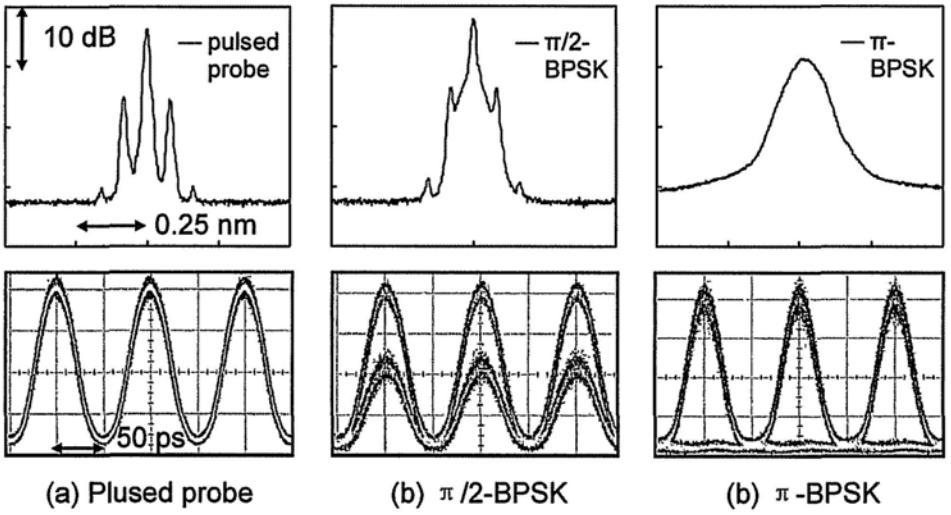

Fig. 2.11. Format conversion from NRZ-OOK to BPSK signal.

Apart from converting π/2-BPSK to π-BPSK signal, the FWM stage also performs as a wavelength conversion stage. Specifically, it can convert the wavelength of π-BPSK signal back to that of the original NRZ-OOK signal, realizing a wavelength-preserved format conversion. As shown in Fig. 2.12, by setting the wavelength of the CW light in the pump-modulated FWM to 1563.7 nm, the wavelength of the generated π-BPSK signal is at 1550.9 nm, which is exactly the wavelength of the original NRZ-OOK signal.

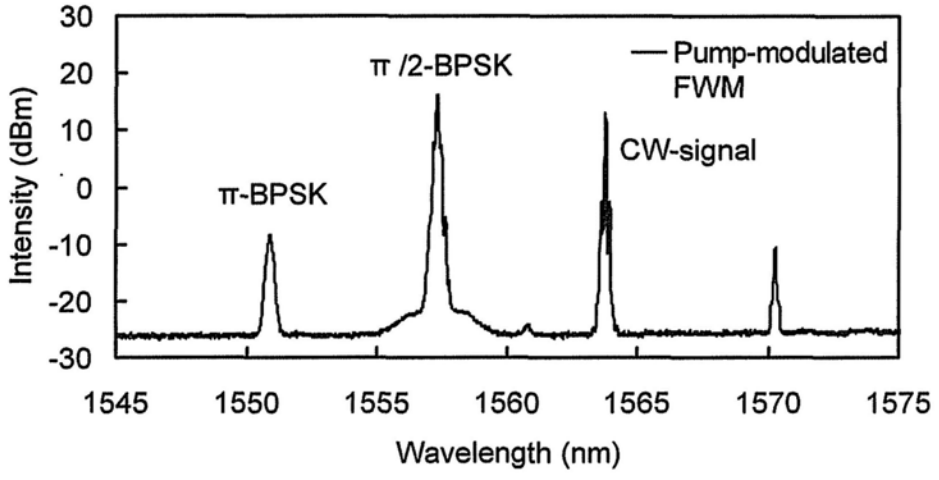

Fig. 2.12. Optical spectrum of pump-modulated FWM to convert π/2-BPSK to π-BPSK signal at the same wavelength of the original OOK signal. CW-signal is set at 1563.7 nm.

Bit error ratios (BER) of different signals are measured. At the error-free level (BER = 10^{-9}), the power penalty of π/2-BPSK signal is found to be 5.4 dB compared with the input NRZ-OOK signal. After phase-doubling by pump-modulated FWM, the power penalty of π-BPSK signal at the same wavelength of the input NRZ-OOK

signal decreases to -1.4 dB. The power gain results from the NRZ-to-RZ pulse format conversion. The BERs of π-BPSK signals at other wavelengths are also measured. In our experiment, the CW-signal for pump-modulated FWM in the PCF is at the long wavelength side of the π/2-BPSK signal and the FWM bandwidth of the PCF is ~ 14 nm. Therefore, π-BPSK signal at a longer wavelength is supposed to have a better performance than that at a shorter wavelength, while the difference is quite small within the FWM bandwidth. Our result shows ~ 0.05 dB difference by comparing the π-BPSK signals at wavelengths of 1550.9 and 1553.9 nm. Beyond the FWM bandwidth, the difference increases to ~ 0.5 dB by comparing two signals at the wavelengths of 1550.0 and 1548.9 nm.

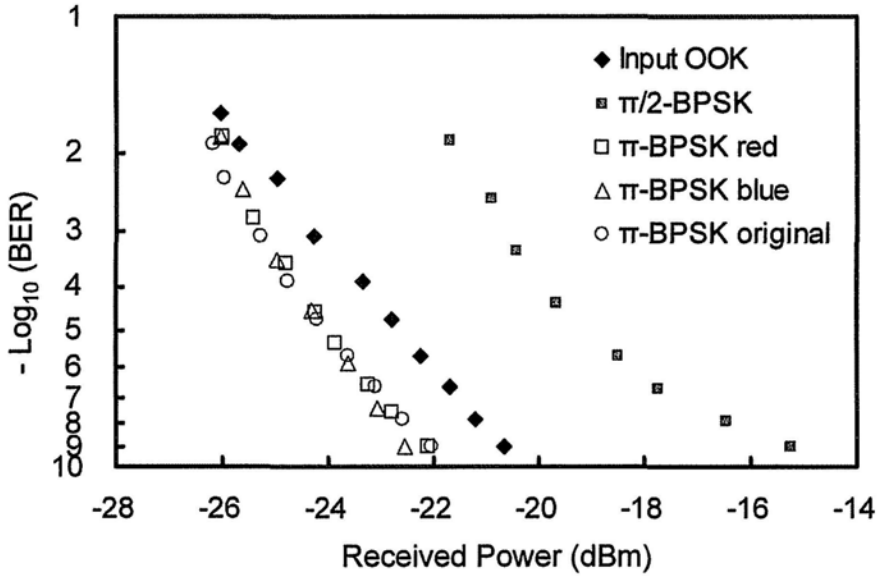

Fig. 2.13. BER measurement of the generated BPSK signals. Π-BPSK red: π-BPSK signal at the wavelength of 1553.9 nm; π-BPSK blue: π-BPSK signal at the wavelength of 1548.9 nm; π-BPSK original: π-BPSK at the wavelength of 1550.9 nm.

To summarize, in the OOK to BPSK format conversion, we use pump-modulated FWM to double the phase of RZ-BPSK signal generated by XPM from a NRZ-OOK signal. The phase doubling process reduces the optical power of OOK signal required to generate the BPSK signal and hence avoids signal degradation caused by SBS. The pump-modulated FWM also works as a wavelength conversion stage, which, in particular, can achieve wavelength-preserved NRZ-OOK to RZ-BPSK format conversion.

2.4 RZ-BPSK to RZ-QPSK Conversion

Similar to the generation of π/2-BPSK signal, but replacing the pulsed probe by a RZ-BSPK signal, the RZ-BPSK signal can be converted to a RZ-QPSK signal after combining with a NRZ-OOK signal. The method has been reported in [11]. In this section, the experiment is repeated to provide some technical details.

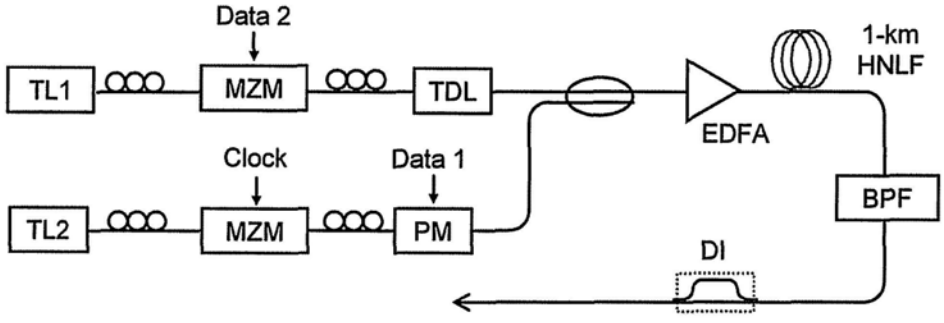

Fig. 2.14. Experimental setup to combine 10-Gbit/s RZ-BPSK and 10-Gbit/s NRZ-OOK to 10-Gbaud/s RZ-QPSK. TL: tunable laser; TDL: tunable optical delay line; BPF: bandpass filter.

Fig. 2.14 shows the experimental setup. A RZ-BPSK signal is generated by modulating a pulse train in a PM and a NRZ-OOK signal is generated by modulating a CW light in a MZM. Both the BPSK and OOK signasl carry a 10-Gbit/s PRBS. A tunable optical delay line is added in the OOK branch to align the two signals in time domain. The two signals are combined together, amplified to a total power of ~ 20 dBm, and launched into a 1-km HNLF with a nonlinear coefficient of 11.7 $km^{-1}W^{-1}$. In the HNLF, the NRZ-OOK signal just needs to add a π/2 phase shift to the RZ-BPSK signal to generate a RZ-QPSK signal, so its optical power is under the

SBS threshold. The generated RZ-QPSK signal is filtered out using an optical bandpass filter and demodulated in a fiber-based DI.

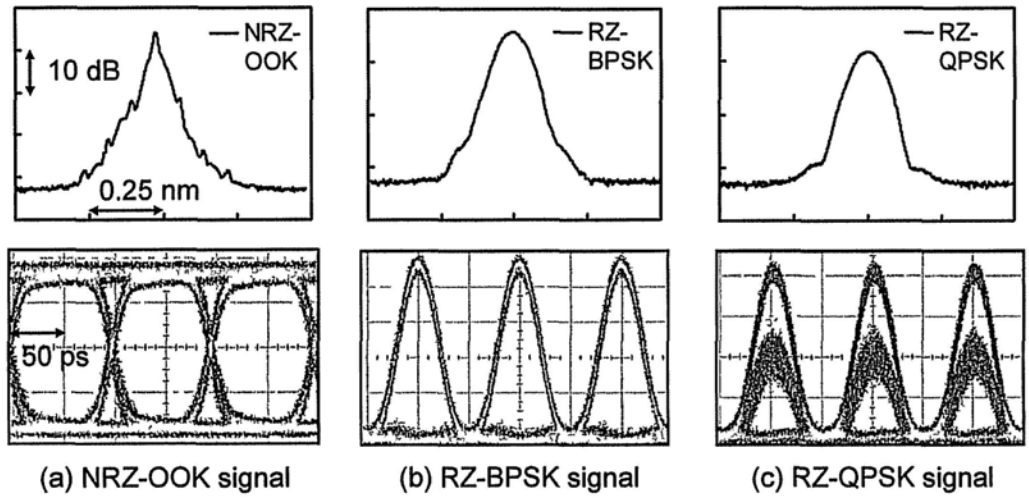

Fig. 2.15. Conversion of 10-Gbit/s NRZ-OOK signal and 10-Gbit/s RZ-BPSK signal to 10-Gbaud/s RZ-QPSK signal. (b, c) demodulated RZ-BPSK signal and RZ-QPSK signal with phase shift in DI set at 0.

The combination of NRZ-OOK signal and RZ-DPSK signal to RZ-QPSK signal is shown in Fig. 2.15. The original RZ-BPSK signal has a modulation depth of π, and the NRZ-OOK signal introduces another $\pi/2$ modulation depth through XPM in the HNLF. The QPSK signal is demodulated by a DI with phase shift of 0, so the demodulated signal has three levels. When the phase is adjusted to $\pm \pi/4$, the demodulated signal will have just two levels. Actually, there are four different outputs when the phase shift is set to $\pi/4$, $3\pi/4$, $5\pi/4$, and $7\pi/4$, as shown in Fig. 2.16. The definition of I/Q channel is the same as that shown in Table 2.3. Here, we adjust the wavelength of the RZ-QPSK signal slightly to introduce different phase shifts in

a fixed DI. In agreement with the theory, the level of 0-bits cannot reach zero intensity. This problem will not exist if a balanced detection is used, which can cancel out the non-zero level. One may note that it is hard to distinguish the four demodulated signals just by their eye diagrams since they are similar to each other. However, their spectral features show a sharp contrast to disclose their identities.

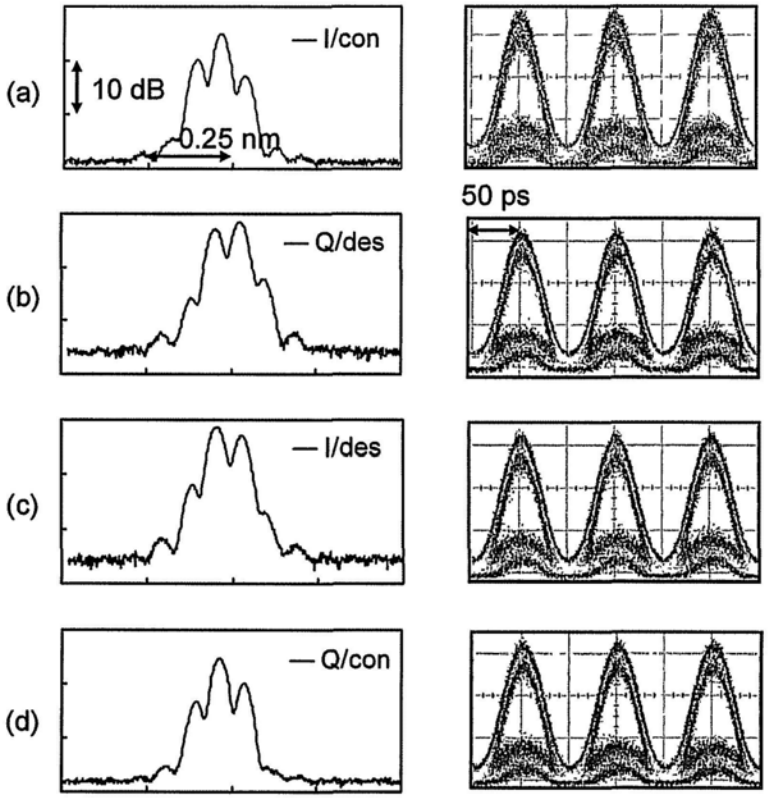

Fig. 2.16. Demodulated signals when the phase shift of DI is set to (a) π/4: constructive port of I channel; (b) 3π/4: destructive port of Q channel; (c) 5π/4: destructive of I channel; (d) 7π/4: constructive port of Q channel.

To measure the BER of the generated RZ-QPSK signal, it is not necessary to use a precoder or decoder, which is required only to recover the data. One can just

compare the detected data with the data supposed to be after demodulation in a DI, which can be calculated using software, according to the logic relation shown in Table 2.8. RZ-BPSK and NRZ-OOK signal carry d_1 (n) and d_2 (n), respectively.

Table 2.8 Demodulation of QPSK signal generated in a serial scheme

Original Data $d_1(n)$ | $d_2(n)$	Phase Change	Demodulated Data I (n) | Q (n)
00	0	11
01	$\pi/2$	01
10	π	00
11	$3\pi/2$	10

The generation of RZ-QPSK signal in the experiment is similar to that in a serial QPSK modulator. To calculate the demodulated data supposed to be, d_1 (n) and d_2 (n) should be synchronized, i.e. a bit from d_1 (n) is combined with a bit from d_2 (n). Therefore, the relative delay between the two data streams has to be measured. As shown in Fig. 2.17, the NRZ-OOK signal advances 14.9 ns compared with RZ-BPSK signal, which corresponds to 149 bits in a 10-Gbaud/s signal. With this information, demodulated data without error can be calculated using Table 2.8. By comparing the result with experimentally detected data, the BER can be obtained.

The measured BERs are plotted in Fig. 2.18. The BERs of I/Q channel are obtained by averaging the BERs measured from destructive and constructive ports at the same optical power. Error-free RZ-QPSK signal can be obtained, but error floor is also found. The power penalty is more than 6 dB compared to the input signals. This

degradation may be caused by the format conversion process as well as the single-ended detection manner. It is believed that the degradation can be mitigated if balanced detection is used.

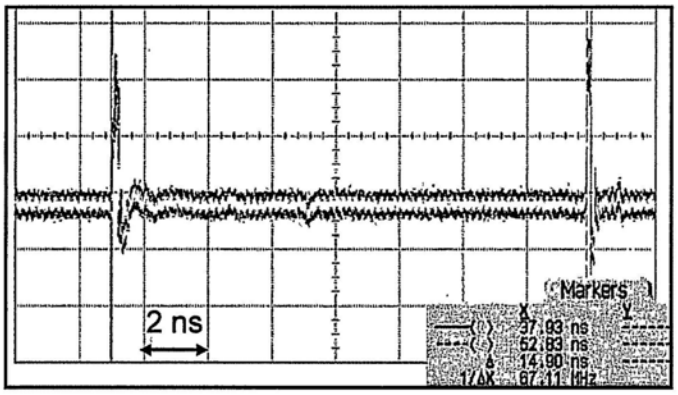

Fig. 2.17. Measurement of relative delay between the NRZ-OOK signal and RZ-BPSK signal.

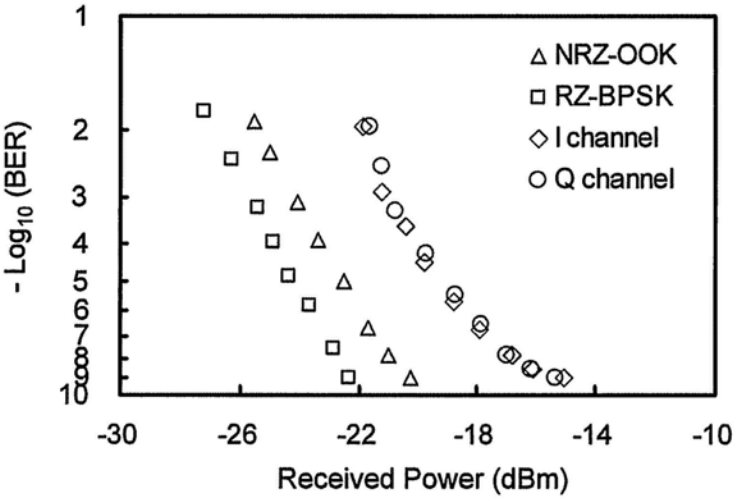

Fig. 2.18. BER measurement of input NRZ-OOK signal, input RZ-BPSK signal, and generated RZ-QPSK signal.

In conclusion, this section shows some technical details in the detection and BER

measurement of QPSK signals using fiber-based DI and single-ended photodetector. The demodulated signals are first indentified to I/Q channels by their optical spectra, and then the logic relation between the transmitted and received data is disclosed. To measure the BER, the relative delay between the two input data streams are measured to calculate the data supposed to be detected by the photodetector.

References

[1] W. X. Wang, "40G, cornerstone to broaden future," Huawei Technol., issue 34, pp. 23-24, Sep. 2008 (in Chinese). http://www.huawei.com/cn/about-huawei/publications/communicate/index-115329-hw_083054.htm

[2] P. J. Winzer and R.-J. Essiambre, "Advanced modulation formats for high-capacity optical transport networks," J. Lightw. Technol., vol. 24, no 12, pp. 4711-4728, Dec. 2006.

[3] M. Karlsson and E. Agrell, "Which is the most power-efficient modulation format in optical links?" Opt. Express, vol. 17, no. 13, pp. 10814-10819, Jun. 2009.

[4] W. Astar and G. M. Carter, "10 Gbit/s RZ-OOK to BPSK format conversion by cross-phase modulation in single semiconductor optical amplifier," Electron. Lett., vol. 42, no. 25, pp. 1472-1474, Dec. 2006.

[5] S. Lee, K. Chow, C. Shu, and C. Lin, "All optical ASK to DPSK format conversion using cross-phase modulation in a nonlinear photonic crystal fiber," in Proc. of CLEO/PR 2005, Tokyo, Japan, Paper CFJ2-5.

[6] C. Schmidt-Langhorst, R. Ludwig, M. Galili, B. Huettl, F. Futami, S. Watanabe, and C. Schubert, "160 Gbit/s all-optical OOK to DPSK in-line format conversion," in Proc. of ECOC 2006, Cannes, France, Paper Th4.3.5.

[7] G. P. Agrawal, Nonlinear Fiber Optics, 3nd ed. (New York: Academic, 2005).

[8] M. P. Fok and C. Shu, "DPSK signal restoration using four-wave mixing in a dispersion-flattened highly nonlinear photonic crystal fiber," in Proc. of OECC 2007, Yokohama, Japan, Paper 13B3-2.

[9] Y. Gao, Y. Xie, and S. He, "Reducing the driving voltage of a phase modulator with cascaded four-wave-mixing processes," J. Opt. Soc. Am. B, vol. 27, no. 11, pp. 2360-2364, Nov. 2010.

[10] S. Kitagawa, S. M. Nissanka, and A. Maruta, "All-optical modulation format conversion from NRZ-OOK to RZ-M-ary PSK based on fiber nonlinearity," in

Proc. of OFC/NFOEC 2008, San Diego, Paper OTuD6.

[11]M. Galili, B. Huettl, C. Schmidt-Langhorst, R. Ludwig, F. Futami, S. Watanabe, and C. Schubert, "All-optical combination of DPSK and OOK to 160 Gbit/s DQPSK data signals," in Proc. of OFC/NFOEC 2007, Anaheim, CA, Paper OThI5.

3 WAVELENGTH CONVERSION OF DPSK SIGNALS

Wavelength conversion is a sub-function implemented in optical cross connects (OXC) to achieve optical switching. It can prevent wavelength blocking and enhance flexibility of wavelength division multiplexing (WDM) system. As shown in Fig. 3.1 (a), OXC is a device used to switch high-speed optical signals in a fiber optic WDM network, such as an optical mesh network. It can have more than three ports.

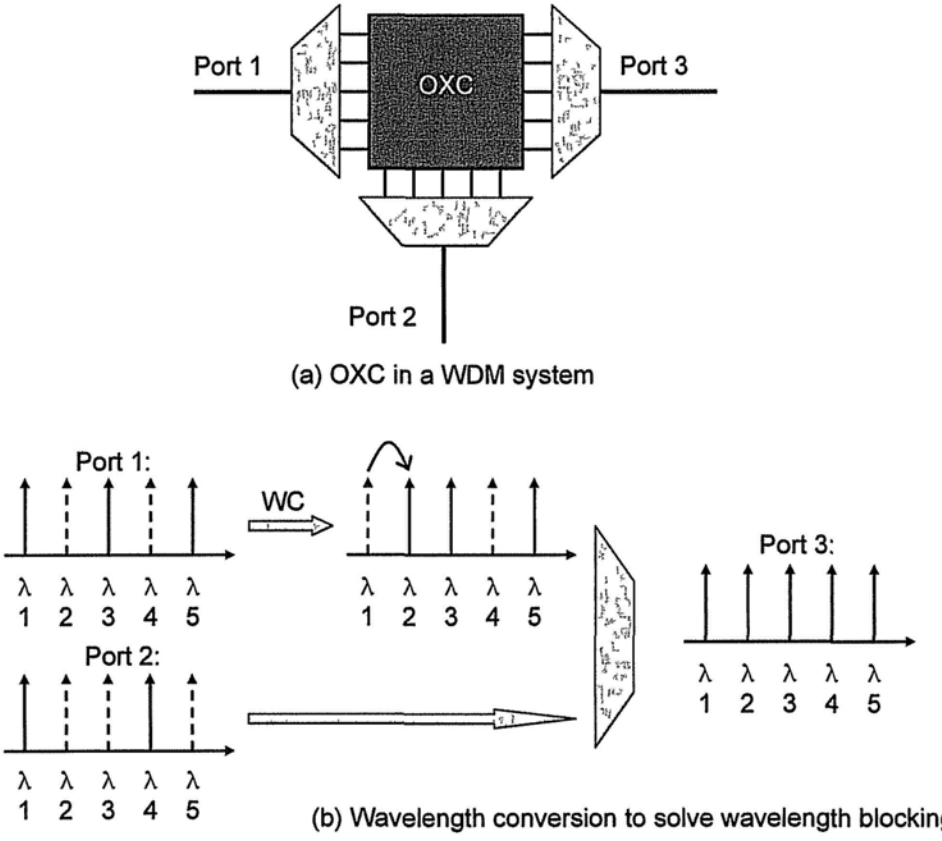

Fig. 3.1. (a) Structure of OXC in a WDM system and (b) solution of wavelength blocking by wavelength conversion (Dash line: vacant channel; solid line: occupied channel). OXC: optical cross connect; WC: wavelength conversion.

Wavelength blocking may occur for wavelength routing in an OXC. For example, as illustrated in Fig. 3.1 (b), channels 1, 3, 5 from port 1 and channels 1, 4 from port 2 are supposed to be switched to port 3 for further transmission. However, the two channels 1 will occupy the same wavelength at port 3, resulting in crosstalk between the information carried by them. At the same time, channel 2 of port 3 is vacant, so the information carried by channel 1 from port 1 can be moved to channel 2 of port 3 by wavelength conversion, avoiding wavelength contention with the other channel 1 from port 2.

All-optical wavelength conversion of amplitude-modulated signals can be achieved using many kinds of nonlinear effects, like SPM, XPM, XGM, or FWM. For phase-modulated signals, wavelength conversion can be implemented in two types of methods. The first one is to convert phase-modulated signals to amplitude-modulated signals, perform the wavelength conversion and convert back to phase-modulated signals [1, 2]. This type of methods can use mature wavelength conversion techniques for amplitude-modulated signals, including SPM to achieve polarization-insensitive wavelength conversion, and provide additional functions like regeneration [2]. However, the conversion between phase and amplitude is usually complicated, costly, bit-rate and format dependent. Moreover, the converted signal will lose the differential coding property [3], although the data can be retrieved using an additional decoder at the receiver side. The other method is to use phase-sensitive parametric processes like FWM and cascaded SFG/DFG to directly convert the phase

information to another wavelength. This kind of methods can achieve wavelength conversion in a single stage, be transparent to bit rates, as well as preserve the differential coding property. However, parametric processes are sensitive to polarization states of the mixing waves, which limit their implementation for polarization-random optical signals in practical networks.

This chapter addresses the problem of polarization-dependence of FWM in wavelength conversion of phase-modulated signals. In section 3.1, four different approaches to achieve polarization-insensitive FWM are introduced. The approach based on a birefringent fiber is used to implement widely tunable wavelength conversion of DPSK signal as described in section 3.2. In the last section, this approach is expanded to achieve polarization-insensitive wavelength multicasting of DPSK signal.

3.1 Polarization-Insensitive FWM

FWM is a phase-sensitive parametric process which evolves several light waves. The basic forms of FWM include partially degenerate FWM which involves three waves or a nondegenerate form which involves four waves, as shown in Fig. 3.2.

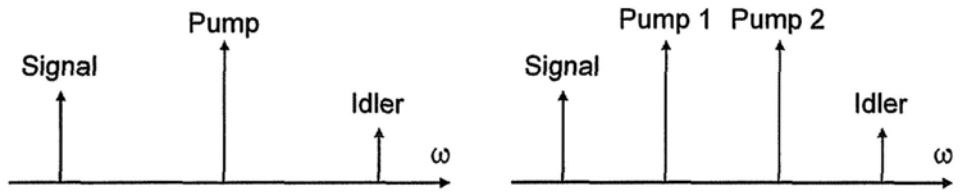

(a) Partially degenerate FWM (b) Nondegenerate FWM

Fig. 3.2. (a) Partially degenerate and (b) nondegenerate FWM.

The phase relation between the waves is

$$E_{idler} = \gamma |E_s| |E_p|^2 e^{j(2\omega_p - \omega_s) + (2\varphi_p - \varphi_s)} \tag{3-1}$$

$$E_{idler} = \gamma |E_s| |E_{p1}| |E_{p2}| \cdot e^{j(\omega_{p1} + \omega_{p2} - \omega_s) + (\varphi_{p1} + \varphi_{p2} - \varphi_s)} \tag{3-2}$$

where γ is nonlinear coefficient; ω and φ are the frequency and phase of each wave, respectively; equation (3-1) is for the partial degenerate FWM and (3-2) for the nondegenerate one. When applied to phase-modulated signals, the pump phase should be constant and hence the phase of the idler is an image of that of the input signal, i.e. the phase information of signal is converted to a new wavelength.

As mentioned, FWM is a polarization-sensitive process. When the polarization of input signal is orthogonal to that of the pump, the idler cannot be effectively generated. Unfortunately, after long-distance transmission in fiber-optic network, the

polarization of signal is impossible to be predicted. Therefore, advanced FWM scheme that is insensitive to the signal polarization is desired. Polarization-insensitive FWM has been realized using dual-pump arrangements [4, 5], polarization diversity loop [6], or twisted fiber [7]. The dual-pump approach is easy to implement, but requires one additional pump. The polarization diversity loop has the problem of stability, and the twisted fiber requires much effort to fabricate.

3.1.1 Polarization-Insensitive FWM in Conventional HNLF

Polarization-insensitive FWM can be achieved in a conventional HNLF using dual-orthogonal pumps [4], dual-parallel pumps [5], or single pump in polarization-diversity loop [6]. As shown in Fig. 3.3, the dual-pump approaches are implemented in a linear structure (Fig. 3.3 (c)), while the single-pump one is in a loop structure (Fig. 3.3 (e)).

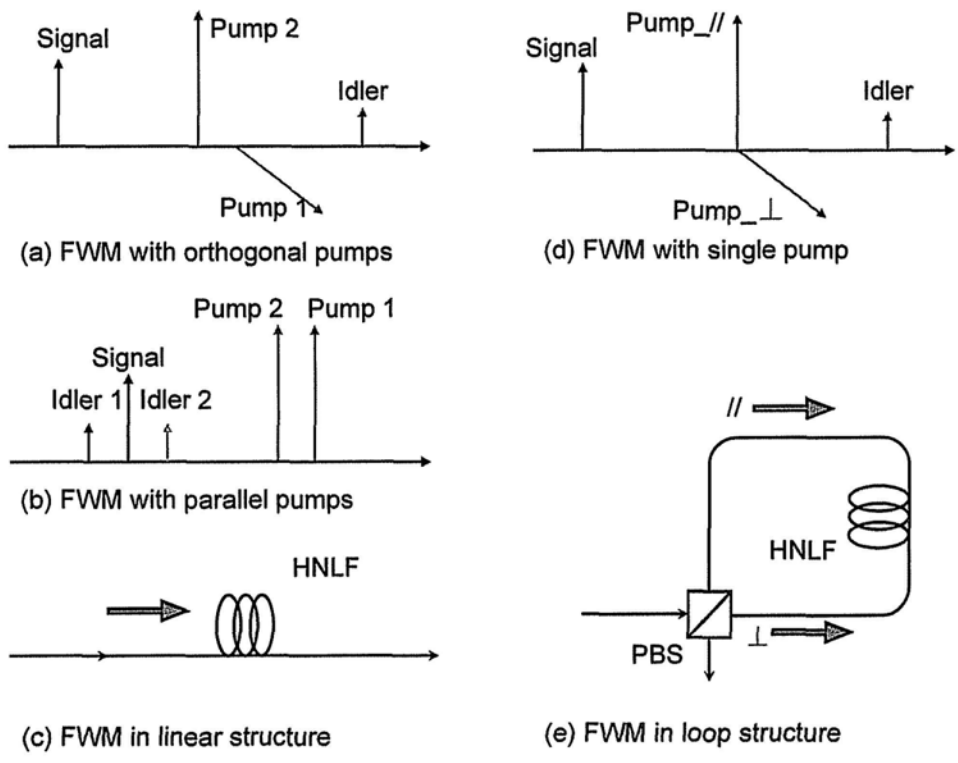

Fig. 3.3. Polarization-insensitive FWM in conventional HNLF. PBS: polarization beam splitter.

In FWM with dual-orthogonal pumps shown in Fig. 3.3 (a), the wavelengths of the

two pumps are close to each other. Assuming the input signal has a polarization direction with a relative angle of θ to the direction of pump 1, the generated idler is

$$\begin{aligned} E_{idler} &= \gamma E_1(E_s^* E_2) + \gamma E_2(E_s^* E_1) \\ &= \left(\gamma |E_s||E_1||E_2| \sin\theta \cdot \hat{p}_2 + \gamma |E_s||E_1||E_2| \cos\theta \cdot \hat{p}_1\right) e^{jt(\omega_1+\omega_2-\omega_s)} \end{aligned} \quad (3\text{-}3)$$

where γ, ω_1, ω_2, ω_s are the conversion efficiency, frequency of pump 1, pump 2, and signal, respectively. As the two orthogonal pumps are quite close to each other in frequency, the difference of efficiency is neglected here. Thus, the power of the idler is insensitive to θ since

$$\begin{aligned} |E_{idler}|^2 &= E_{idler} \cdot E_{idler}^* \\ &= (\gamma |E_s||E_1||E_2|)^2 (\sin^2\theta + \cos^2\theta) \\ &= (\gamma |E_s||E_1||E_2|)^2 \end{aligned} \quad (3\text{-}4)$$

In FWM with dual-parallel pumps shown in Fig. 3.3 (b), the frequency detuning between the two pumps should be much smaller than that between pumps and signal. This arrangement makes the parametric beating between pumps and signal insignificant compared with the beating between the two pumps. The FWM will generate two idlers that are insensitive to polarization of the input signal. Taking idler 1 as example,

$$\begin{aligned} E_{idler1} &= \gamma(\Delta\omega_{p1-p2}) E_s (E_2 E_1^*) + \gamma(\Delta\omega_{p1-s}) E_s E_2 (E_1 E_s^*) \\ &\quad + \gamma(\Delta\omega_{p2-s}) E_s E_1 (E_2 E_s^*) \\ &\approx \gamma(\Delta\omega_{p1-p2}) (E_2 E_1^*) E_s \\ \gamma(\Delta\omega_{p1-s}) &<< \gamma(\Delta\omega_{p1-p2}), \gamma(\Delta\omega_{p2-s}) << \gamma(\Delta\omega_{p1-p2}) \end{aligned} \quad (3\text{-}5)$$

where $\Delta\omega$ is the frequency detuning between two beating lightwaves in a parametric process. The power of idler is

$$\begin{aligned}|E_{idler1}|^2 &= E_{idler1}\cdot E_{idler1}^* \\ &= (\gamma|E_1\|E_2|)^2 E_s\cdot E_s^* \\ &= (\gamma|E_s\|E_1\|E_2|)^2\end{aligned} \tag{3-6}$$

which is again insensitive to the polarization of the input signal.

For FWM with a single pump in the polarization-diversity loop shown in Fig. 3.3 (d), the pump is equally split into two orthogonal parts, which are made to counter-propagate in the HNLF. Note that FWM occurs only between co-propagating lightwaves, we can obtain the generated idler as

$$\begin{aligned}E_{idler} &= \gamma E_{p\_//}(E_s^* E_{p\_//}) + \gamma E_{p\_\perp}(E_s^* E_{p\_\perp}) \\ &= \left(\gamma|E_s\|E_{p\_//}|^2 \sin\theta\cdot\hat{p}_{\_//} + \gamma|E_s\|E_{p\_\perp}|^2\cos\theta\cdot\hat{p}_{\_\perp}\right)e^{jt(2\omega_p-\omega_s)}\end{aligned} \tag{3-7}$$

Since the pump is equally split, the intensity of the vertical and horizontal parts should be the same. The power of idler is

$$\begin{aligned}|E_{idler}|^2 &= E_{idler}\cdot E_{idler}^* \\ &= (\gamma|E_s\|E_{p\_}|^2)^2(\sin^2\theta+\cos^2\theta) \\ &= (\gamma|E_s\|E_{p\_}|^2)^2 \\ |E_{p\_}| &= |E_{p\_//}| = |E_{p\_\perp}|\end{aligned} \tag{3-8}$$

In contrast to the dual-pump approaches where the idler generation is "insensitive" to the input signal polarization, the idler in a polarization-diversity loop is in principle independent of the signal polarization since no approximation is assumed. However, the stability of a loop structure may be difficult to maintain due to environmental disturbance in practical implementation.

3.1.2Polarization-Insensitive FWM in a Birefringent PCF

Polarization-insensitive FWM with a single pump can also be achieved in a linear structure, provided that the HNLF exhibits special characteristics other than high nonlinearity. As mentioned before, the HNLF can be a twisted one [7]. However, twisted fiber is not easy to fabricate. PCF is another kind of fiber that has much flexibility in the fiber properties owing to the variety in fiber structure design. Many of them have birefringence resulting from the asymmetric structure [8, 9]. Polarization-insensitive FWM using this kind of PCF was previously demonstrated in [10]. The theoretical model of partially degenerate FWM in this special fiber was reported in [11], where complicated nonlinear Schrodinger equation was used. Here we introduce another method to explain the principle of polarization-insensitivity of FWM in birefringent HNLF, which shows that the technique can be used for nondegenerate FWM or even multiple-pump FWM.

In our model, phase mismatch is critical in determining the FWM efficiency. Under the assumption of negligible pump depletion, nonlinear phase matching is insignificant since it mainly results from the pump and signal power, which are constant over the entire fiber.

As shown in Fig. 3.4, x and y are the two principal axes of the birefringent fiber. Both the signal and pump are split into x- and y-components. Parametric beating will occur

only between fields in the same polarization direction, while the beating will scatter fields in both directions. Combining the results from different parametric beating and scattering, the idler includes four components as

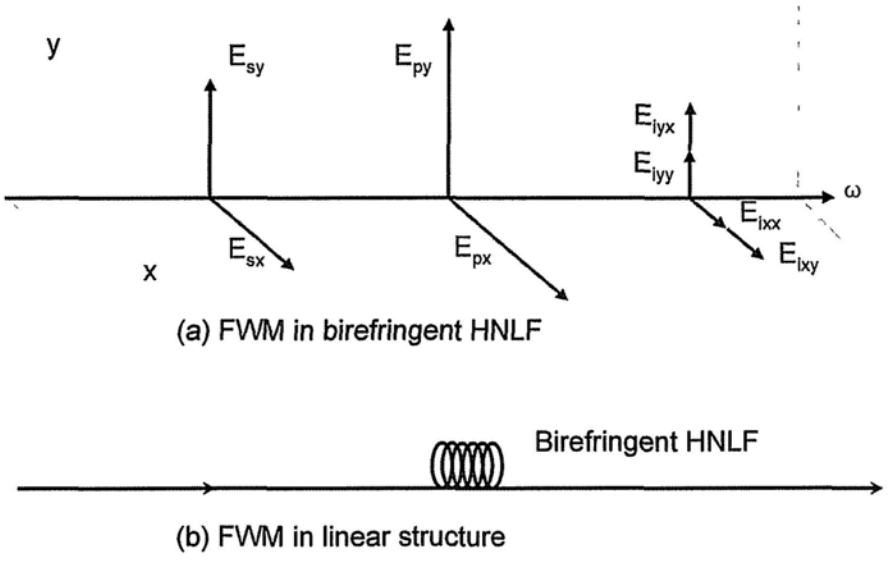

Fig. 3.4. Polarization-insensitive degenerate FWM in birefringent HNLF.

$$\begin{aligned} E_i &= (E_{ixx} + E_{ixy})\hat{x} + (E_{iyx} + E_{iyy})\hat{y} \\ &= \gamma((E_{px}E_{sx}^*)E_{px} + (E_{py}E_{sy}^*)E_{px})\hat{x} \\ &+ \gamma((E_{px}E_{sx}^*)E_{py} + (E_{py}E_{sy}^*)E_{py})\hat{y} \end{aligned} \tag{3-9}$$

where the second subscript in the idler fields indicates the direction of the generated field, while the third subscript indicates the direction of the beating fields. The four components have different phase mismatch factor. The ones with generated fields and beating fields in the same direction will only need to consider the chromatic dispersion, but those with generated fields and beating fields in different directions will take the birefringence into account as described in the following.

$$
\begin{aligned}
\Delta\beta(E_{ixx}) &= (2n_{px}\cdot\omega_p - n_{sx}\cdot\omega_s - n_{ix}\cdot\omega_i)\cdot L/c \\
\Delta\beta(E_{ixy}) &= (n_{py}\cdot\omega_p - n_{sy}\cdot\omega_s + n_{px}\cdot\omega_p - n_{ix}\cdot\omega_i)\cdot L/c \\
&= (2n_{px}\cdot\omega_p - n_{sx}\cdot\omega_s - n_{ix}\cdot\omega_i)\cdot L/c \\
&\quad + ((n_{py}-n_{px})\cdot\omega_p - (n_{sy}-n_{sx})\cdot\omega_s))\cdot L/c \\
&= \Delta\beta(E_{ixx}) + (\Delta n_p\cdot\omega_p - \Delta n_s\cdot\omega_s)\cdot L/c \\
\Delta\beta(E_{iyy}) &= (2n_{py}\cdot\omega_p - n_{sy}\cdot\omega_s - n_{iy}\cdot\omega_i)\cdot L/c \\
\Delta\beta(E_{iyx}) &= (n_{px}\cdot\omega_p - n_{sx}\cdot\omega_s + n_{py}\cdot\omega_p - n_{iy}\cdot\omega_i)\cdot L/c \\
&= \Delta\beta(E_{iyy}) - (\Delta n_p\cdot\omega_p - \Delta n_s\cdot\omega_s)\cdot L/c
\end{aligned}
\tag{3-10}
$$

where *n, L, and c* are the refractive index, fiber length, and light velocity, respectively. The additional phase-mismatch term for E_{ixy} and E_{iyx} is introduced by the birefringence. Since high-order PMD is usually not significant in a short fiber, we can further simplify the birefringence term as

$$
\begin{aligned}
\Delta\beta_{birefringence} &= (\Delta n_p\cdot\omega_p - \Delta n_s\cdot\omega_s)\cdot L/c \\
&= 2\pi L\cdot\left(\frac{\Delta n_p}{\lambda_p} - \frac{\Delta n_s}{\lambda_s}\right) \\
&\approx 2\pi L\cdot\Delta n\cdot\left(\frac{1}{\lambda_p} - \frac{1}{\lambda_s}\right) = 2\pi L\cdot\Delta n\cdot\frac{\lambda_s - \lambda_p}{\lambda_p\lambda_s} \\
\Delta n &= \Delta n_p \approx \Delta n_s
\end{aligned}
\tag{3-11}
$$

This result is similar to that obtained in [11], where a complicated derivation is used. When the birefringence is large enough to make the phase mismatch originated from chromatic dispersion negligible, the FWM efficiencies of E_{ixx} and E_{iyy} will be much larger than that of E_{ixy} and E_{iyx}. When the pump are equally split into its *x*- and *y*-component, the generated idler, which only contain two parts now, will be independent to polarization of the input signal since

$$\begin{aligned} |E_i|^2 &= E_i E_i^* \\ &= (E_{ixx}\hat{x} + E_{iyy}\hat{y})(E_{ixx}\hat{x} + E_{iyy}\hat{y})^* \\ &= \left(\gamma |E_s| \frac{|E_p|^2}{2}\right)^2 (\cos^2\theta + \sin^2\theta) \end{aligned} \tag{3-12}$$

To obtain large birefringence-induced phase mismatch, we can choose a fiber with high birefringence (Δn) or increase the fiber length (L). In either case, there is a non-zero minimum pump-probe (λ_s - λ_p) detuning (PPD) required by $\Delta\beta_{birefringence}$ for polarization-insensitive FWM.

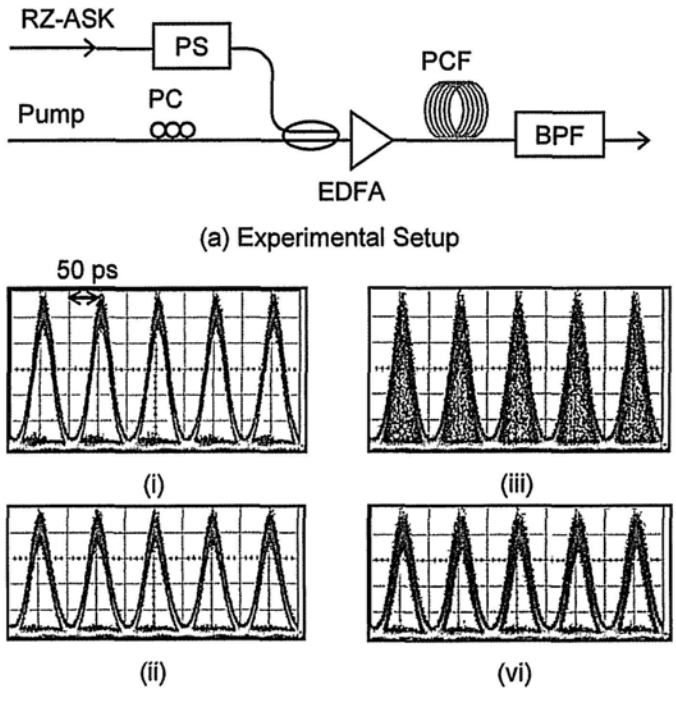

Fig. 3.5. Polarization insensitive wavelength conversion of 10-Gbit/s RZ-ASK signal based on FWM with single pump in a birefringence PCF. (i, ii): polarization-fixed input; (iii, vi): polarization-scrambled input; (i, iii): polarization of pump aligned to principal axes; (ii, vi): polarization of pump aligned 45° offset to principal axes. PS: polarization scrambler; PC: polarization controller; PCF: photonic crystal fiber; BPF: bandpass filter.

The theoretical prediction is verified by experiment for wavelength conversion of 10-Gbit/s RZ-amplitude shift keying (ASK) signals based on FWM with single pump in a birefringent PCF, as shown in Fig. 3.5. When the polarization of pump is aligned at 45° offset to the principal axes of the PCF, the eye remains widely opened for polarization-scrambled input signal. In the next section, the mechanism of polarization insensitivity will be expanded to the case of two-pump to achieve widely tunable wavelength conversion of DPSK signal.

3.2 Widely Tunable Wavelength Conversion of RZ-DPSK Signal

A large conversion bandwidth is an important merit of an optical wavelength converter. For a nonlinear medium, dual-parallel pump is an effective method to increase the conversion bandwidth of FWM [12]. In contrast to the dual-parallel or dual-orthogonal pump approach for polarization-insensitive FWM, the pump-pump wavelength detuning in [12] is required to be tunable in order to increase the conversion bandwidth. Thus, polarization-insensitive FWM cannot be simultaneously achieved. In our work, to demonstrate a wide conversion bandwidth and to simultaneously maintain the polarization-insensitivity of FWM, dual-pump FWM is used in a birefringent HNLF. The principle is similar to that described in section 3.1.2.

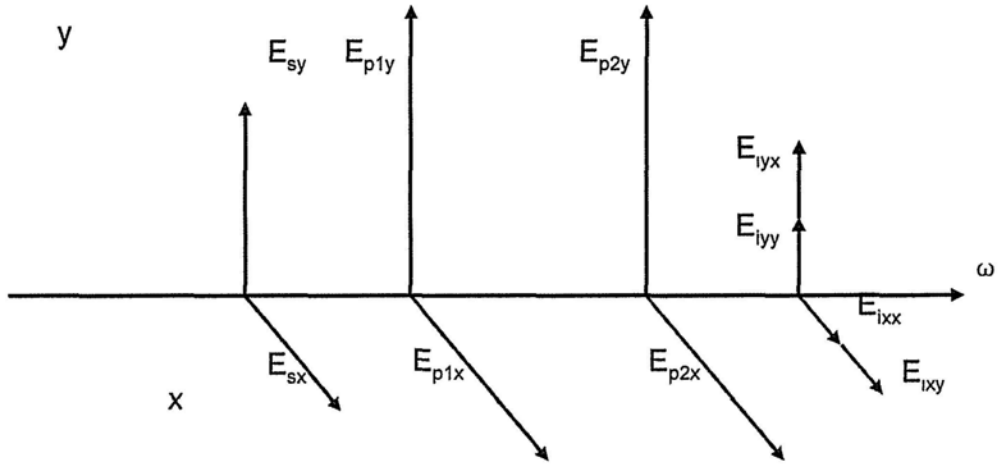

Fig. 3.6. Polarization-insensitive nondegenerate FWM in birefringent fiber.

As shown in Fig. 3.6, the field of the generated idler by nondegenerate FWM in a

birefringent fiber is

$$\begin{aligned} E_i &= (E_{ixx} + E_{ixy})\hat{x} + (E_{iyx} + E_{iyy})\hat{y} \\ &= \gamma((E_{p1x}E_{sx}^*)E_{p2x} + (E_{p1y}E_{sy}^*)E_{p2x})\hat{x} \\ &\quad + \gamma((E_{p1x}E_{sx}^*)E_{p2y} + (E_{p1y}E_{sy}^*)E_{p2y})\hat{y} \\ &= \gamma(E_{p1x}E_{sx}^*)E_{p2x}\cdot\hat{x} + \gamma(E_{p1y}E_{sy}^*)E_{p2y}\cdot\hat{y} \\ \Delta\beta_{birefringence} &= 2\pi L\cdot\Delta n\cdot(\frac{1}{\lambda_{p1}} - \frac{1}{\lambda_s}) \end{aligned} \tag{3-13}$$

When the two pumps are equally split between the two orthogonal principal axes of the birefringent fiber, the idler is insensitive to the polarization of the input signal.

$$\begin{aligned} |E_i|^2 &= \gamma^2((E_{p1x}E_{sx}^*)E_{p2x}\cdot\hat{x} + \gamma(E_{p1y}E_{sy}^*)E_{p2y}\cdot\hat{y})\cdot \\ &\quad ((E_{p1x}E_{sx}^*)E_{p2x}\cdot\hat{x} + \gamma(E_{p1y}E_{sy}^*)E_{p2y}\cdot\hat{y})^* \\ &= (\gamma|E_s|\frac{|E_{p1}||E_{p2}|}{2})^2(\cos^2\theta + \sin^2\theta) \end{aligned} \tag{3-15}$$

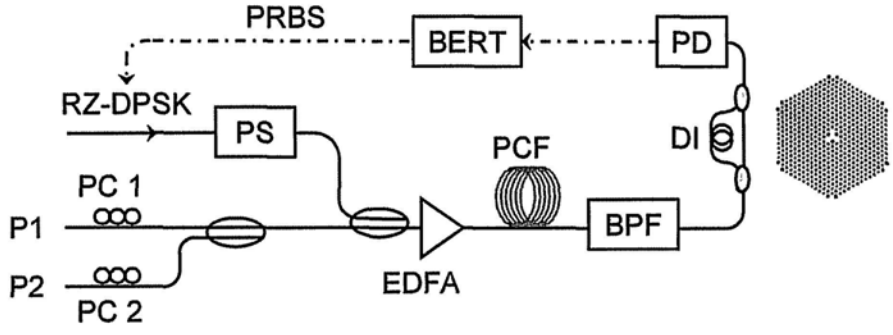

Fig. 3.7. Experimental setup to demonstrate polarization-insensitive, wideband wavelength conversion of RZ-DPSK signal based on FWM in birefringent PCF. PC: polarization controller; PS: polarization scrambler; BPF: optical bandpass filter; DI: delay interferometer; PD: photodetector. BERT: bit error ratio tester; Inset: cross-section of the birefringent PCF [8].

In this section, an experiment is carried out to demonstrate the validity of FWM in a birefringent PCF to achieve polarization-insensitive, wideband wavelength conversion of 10-Gbit/s RZ-DPSK signal. As shown in Fig. 3.7, the RZ-DPSK signal carries a PRBS, and its polarization is controlled by a polarization scrambler. The signal is combined with two CW pumps and together boosted by an EDFA to a total optical power of 26 dBm. The length of PCF is 64 m and no SBS occurs at this power level. The generated idler is filtered out by an optical filter and then sent to a fiber-based DI for demodulation. After photodetection, bit error ratio (BER) measurement is used to evaluate the conversion performance.

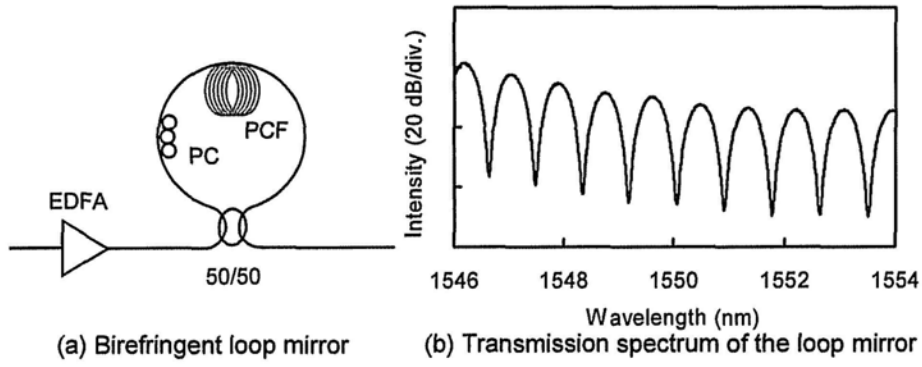

Fig. 3.8. (a) Birefringent loop mirror using PCF and (b) measured transmission spectrum of the loop mirror.

To measure the birefringence of the PCF, we construct a loop mirror using the PCF. As shown in Fig. 3.8 (a), the amplified spontaneous emission (ASE) of an EDFA is used as a wideband optical source. A periodical transmission spectrum is obtained at the output port as shown in Fig. 3.8 (b). The wavelength period is measured to be 0.86 nm, implying a birefringence of 4.37×10^{-5} near 1550 nm. Substituting this value

into equation (3-13), the phase mismatch caused by birefringence of the PCF is ~ 7.31 • $\Delta\lambda_{p1\text{-}s}$, where $\Delta\lambda_{p1\text{-}s}$ is wavelength detuning between signal and pump1. The PCF has a nonlinear coefficient of 11.2 W^{-1} km^{-1}, a dispersion coefficient of - 1.3 $ps{\cdot}nm^{-1}{\cdot}km^{-1}$ and a dispersion slope of ~ 0.001 $ps{\cdot}nm^{-2}{\cdot}km^{-1}$ at 1549.5 nm. The chromatic dispersion results in a maximum phase mismatch of 3.25 • $\Delta\lambda_{p1\text{-}s}$ using equation (3-15) (assuming $\lambda_{p2\text{-}s}$ = 50 nm, corresponding to a conversion bandwidth of 100 nm), where $\Delta\lambda_{p2\text{-}s}$ is wavelength detuning between signal and pump2. Thus, the phase mismatch caused by chromatic dispersion is much smaller than that caused by birefringence, fulfilling the assumption made in equation (3-13).

$$\begin{aligned}\Delta\beta &= L\cdot(\beta_{p1}+\beta_{p2}-\beta_s-\beta_i)\\ &= -DL\cdot\frac{2\pi c}{\lambda^2}\cdot\Delta\lambda_{p2-s}\cdot\Delta\lambda_{p1-s}\\ &= 0.065\cdot\Delta\lambda_{p2-s}\cdot\Delta\lambda_{p1-s}\end{aligned} \tag{3-15}$$

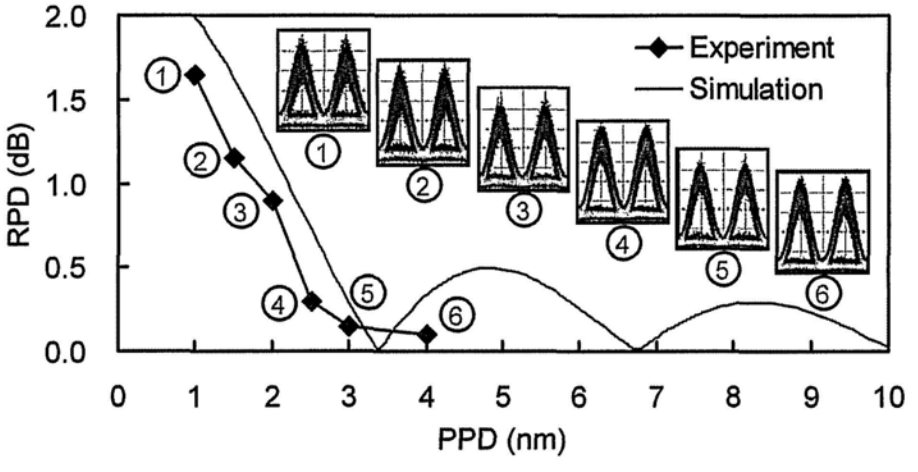

Fig. 3.9. Polarization dependence of FWM in birefringent PCF on different signal-to-pump1 wavelength detuning. RPD: residual polarization dependence; PPD: probe(signal)-to-pump1 detuning.

Using the equation (6) in the reference [11], the relation between PPD and polarization dependence of FWM could be calculated numerically. The simulation result is shown in Fig. 3.9, where the residual polarization dependence (RPD) is defined as the ratio of power variation to the average power of the converted RZ-DPSK signal. We also obtain the relation experimentally. In the experiment, the wavelength of RZ-DPSK signal is set at 1536.5 nm and its polarization state is changed by a polarization scrambler. The polarization scrambler is manually adjusted for the power measurement since the power meter cannot respond to the fast polarization variation in the automatic mode. By tuning the wavelength of pump1 away from the signal, the RPD drops dramatically. The experiment result shows the FWM is less sensitive to polarization than expected by the simulation result. This discrepancy may be caused by manual operation, which is hard to cover all the polarization states of signal. However, both the experiment and simulation shows a PPD larger than 3 nm is good enough to suppress the polarization dependence of FWM. Thus, the wavelength of pump1 is set to 1539.5 nm. The wavelength of the converted signal will be controlled only by tuning the wavelength of pump2.

Fig. 3.10 shows the FWM spectrum when pump2 is tuned to 1565.5 nm, reaching the gain edge of the EDFA. The ASE background is uneven and hence the OSNR of the converted RZ-DPSK signal will be degraded when it is located near the peak of the ASE noise at 1543 nm. Fig. 3.11 depicts fives pairs of measured eye diagrams when pump2 is set at different wavelengths, showing the polarization-insensitive

conversion and the influence of ASE noise across the spectrum. The converted signal is located exactly at the noise peak when pump2 is at 1540 nm. Thus, a relatively poor OSNR is obtained. With a gain-flattened EDFA, it is expected that improved conversion performance can be achieved continuously over the whole wavelength range. To verify this argument, we shift the whole wavelength mapping by 10 nm to a low ASE noise region. The wavelengths of the input RZ-DPSK signal, pump1, and pump2 are now set to 1546.5, 1549.5, and 1550 nm, respectively. A clear eye with large opening of the converted signal is obtained as depicted in Fig. 3.11 (e), compared to that without the 10-nm translation in Fig. 3.11 (d).

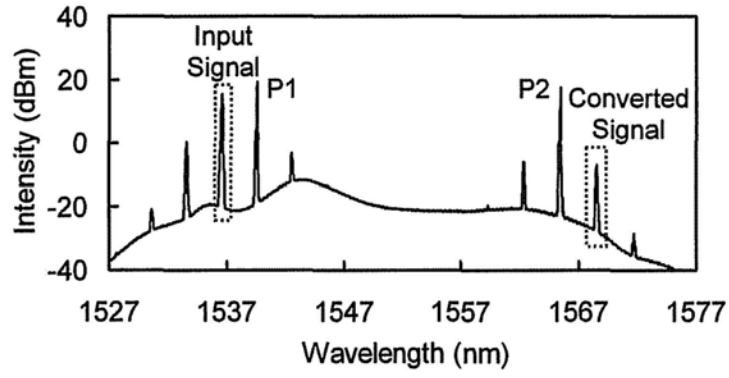

Fig. 3.10. FWM spectrum of polarization-insensitive RZ-DPSK wavelength conversion (pump2 is set at 1565.5 nm). The ASE peak is located at 1543 nm.

In Fig. 3.11, it is noted that the time jitter is slightly increased when the input signal is polarization-scrambled. This is caused by the ~ 9.3-ps differential group delay of the birefringent PCF. The jitter can in principle be compensated by adding a section of polarization maintaining fiber with a proper length, which should be orthogonally aligned to the PCF.

The measured conversion efficiency and the down-conversion bandwidth are shown in Fig. 3.12. The conversion efficiency is measured in a 1-nm step when pump2 is tuned from 1540 to 1567 nm. The actual FWM efficiency is ~ -21 dB for pump2 at 1567 nm. The variation of efficiency is smaller than 2.2 dB over the 27 nm down-conversion range. When the wavelengths of pump2 and the input signal are close, the beating between them becomes comparable to that between the input signal and pump1, hence increasing the conversion efficiency. Beyond 1567 nm, the gain edge of the EDFA, the conversion efficiency drops rapidly as pump2 can no longer be amplified. For comparison, the conversion efficiency of single-pump FWM in the same PCF is also shown in Fig. 3.12 with blue squares. The 3-dB conversion bandwidth is only ~14 nm.

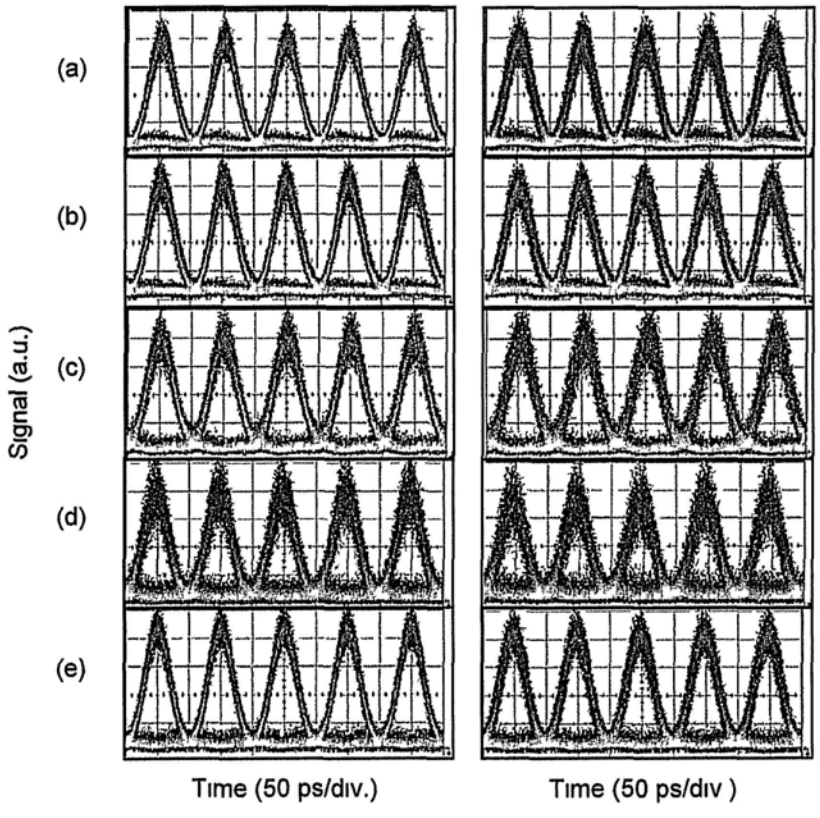

Fig. 3.11. Eye diagrams of the converted RZ-DPSK signals for polarization-fixed (left side) and polarization-scrambled (right side) input signals when pump2 is set to different wavelengths: (a) 1565 nm; (b) 1555 nm; (c) 1545 nm; (d) 1540 nm; (e) 1540+10 nm. For (e), the wavelengths of both pump 1 and input signal are also increased by 10 nm.

To further investigate the performance of wavelength conversion, we measure the bit-error ratio at different input polarizations and converted wavelengths. The results are shown in Fig. 3.13. The power penalty decreases by 1.8 dB due to the ASE noise variation when the wavelength of pump2 is increased from 1545 to 1565 nm. The maximum power penalty is 4.5 dB. The variation of the power penalties between different polarization states of the input is less than 0.3 dB, showing a large tolerance to polarization variation.

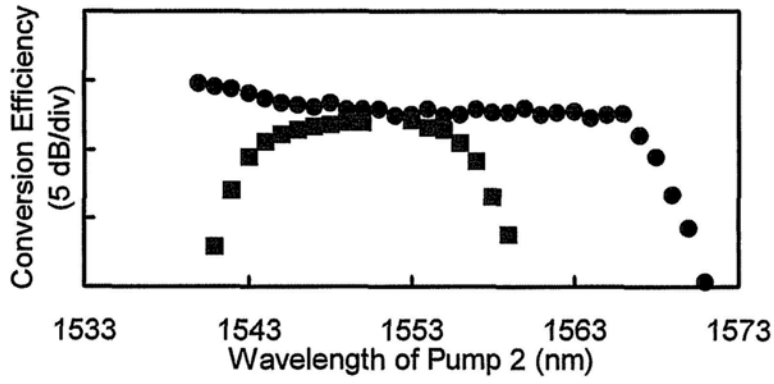

Fig. 3.12. Measured wavelength conversion efficiency for dual-pump (black dots) and single-pump (blue squares) FWM. Only the down-conversion part is shown for dual-pump FWM.

We have demonstrated polarization-insensitive, wideband wavelength conversion for RZ-DPSK signals using dual-pump FWM. The polarization-dependence is suppressed by one of the pumps using the PCF birefringence. The wavelength of the second pump is tuned to broaden the conversion bandwidth. A down-conversion bandwidth of 27 nm has been achieved for polarization-scrambled input signals. Error-free conversion is obtained with a maximum power penalty of 4.5 dB.

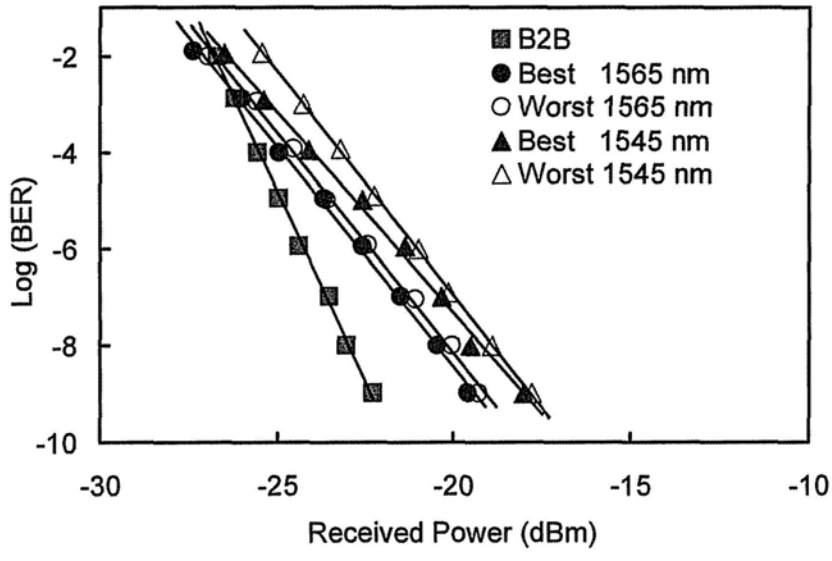

Fig. 3.13. BER measurement at different polarization states of the input signal and wavelengths of pump 2.

3.3 Polarization-Insensitive Multicasting of RZ-DPSK Signal

Wavelength multicast is an important functionality to distribute one data packet to different destinations in a WDM networks. Services like IPTV and video conference can be efficiently supported by this function. All-optical wavelength multicasting is desirable for the distribution of high bit-rate data packets in different modulation formats, bypassing the costly and speed-limited optical-electrical-optical conversion. For ASK format, wavelength multicasting can be achieved using techniques based on cross-absorption in electroabsorption modulator, cross gain modulation in SOA or optical parametric amplifier, FWM in SOA or highly nonlinear fiber, nonlinear polarization rotation in SOA, and self phase modulation in PCF [13-18]. Meanwhile, DSPK modulation format is expected to be widely implemented in next-generation optical communication networks. Similar to wavelength conversion of DPSK signal, wavelength multicasting of DPSK is more difficult to be achieved since only the phase-sensitive effects can be utilized to copy the phase information to new wavelengths, making FWM exclusively promising among the fiber nonlinear effects.

To satisfy the International Telecommunication Unit (ITU) grid in WDM system, it would be better for the generated multicast copies to be equally spaced. As shown in Fig. 3. 14, three pumps are equally spaced in wavelength and five equally-spaced copies are generated. However, this arrangement will cause crosstalk in copies which are generated from more than one parametric beating. Taking the copy 2 (C2) as an

example, it can be generated from two different parametric processes.

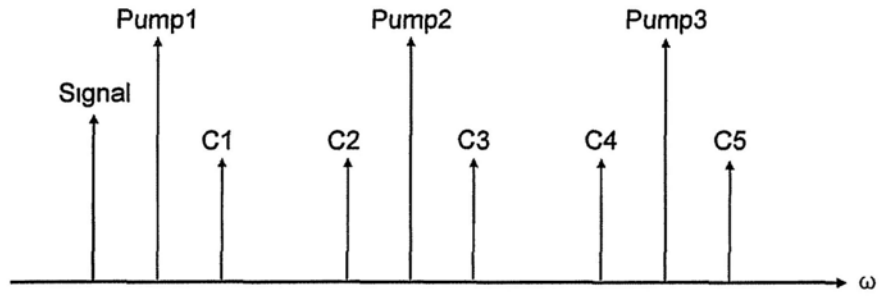

Fig. 3.14. Wavelength multicasting of DPSK signal with equally-spaced pumps.C1-5: five copies generated in wavelength multicasting.

$$E_{C2} = \gamma_1 E_s E_{p1}^* E_{p2} + \gamma_2 E_s E_{p2}^* E_{p3}$$
$$= \gamma_1 |E_s| |E_{p1}| |E_{p2}| e^{j t(\omega_s + \omega_{p2} - \omega_{p1})} + \gamma_1 |E_s| |E_{p2}| |E_{p3}| e^{j t(\omega_s + \omega_{p3} - \omega_{p2})} \quad (3\text{-}16)$$

Ideally, the frequency difference between pump1 and pump2 should be identical to that between pump2 and pump3. However, this cannot be true for free-running laser diodes without any facilities to lock their wavelengths. Therefore, the two components in C2 can occur at slightly different frequencies that are too close to be separated. This will lead to unstable optical beating in a photodector. Equally spaced pumps with orthogonally interleaved polarization have been used to overcome this problem [19], while it cannot be extended to cases with more than three pumps. Another method is to use copolarized pumps with unequal wavelength spacing [20]. This method will render some wavelength channels in ITU grid vacant. It however offers the advantage of removing the limitation on the number of pumps in principle and is also less restrictive on pump polarization.

As shown in Fig. 3.15, nine copies can be generated in wavelength multicasting using FWM with three unequally-spaced pumps. Here we just consider the parametric beating between signal-pump1 and signal-pump2. Pump3 is usually too far from the signal in wavelength (Taking the grid of 200 GHz as example, the wavelength spacing between signal and pump3 will be as large as 10.4 nm.) and the beating efficiency is too low to be significant. Even if the beating between signal-pump3 is significant, crosstalk would still not occur owing to the unequal wavelength spacing. Scattered by the signal-pump1 beating, five copies (C2-3, C7-8) are generated by the three pumps. The left four copies (C1, C5-6, and C9) are generated by scattering from signal-pump2 beating. Such an arrangement of pump wavelengths ensures that all the copies are generated from only one parametric beating. It also avoids the overlapping with idlers generated by pump-pump beatings (Cp).

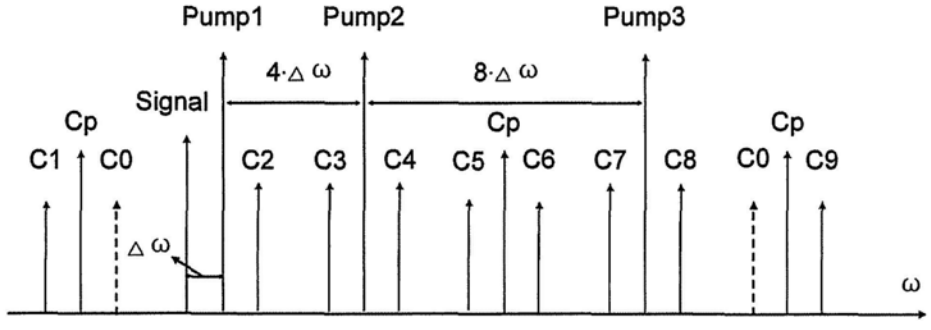

Fig. 3.15. Wavelength multicasting of DPSK signal with three unequally-spaced pumps. C1-9: nine copies generated in wavelength multicasting; C0: vacant channels; Cp: idlers from FWM between pumps.

For one more pump (pump4) added as shown in Fig. 3.16, it can be equally spaced from pump3 with the assumption that no beating between signal and pump3 is efficient. Four new copies (C10-13) will be obtained owing to this pump without introducing any crosstalk to the original copies. The number of vacant channels is kept to two as one original vacant channel is occupied by a new copy (C10) of the signal. Thus, this arrangement of pump wavelength does not limit the pump number in principle.

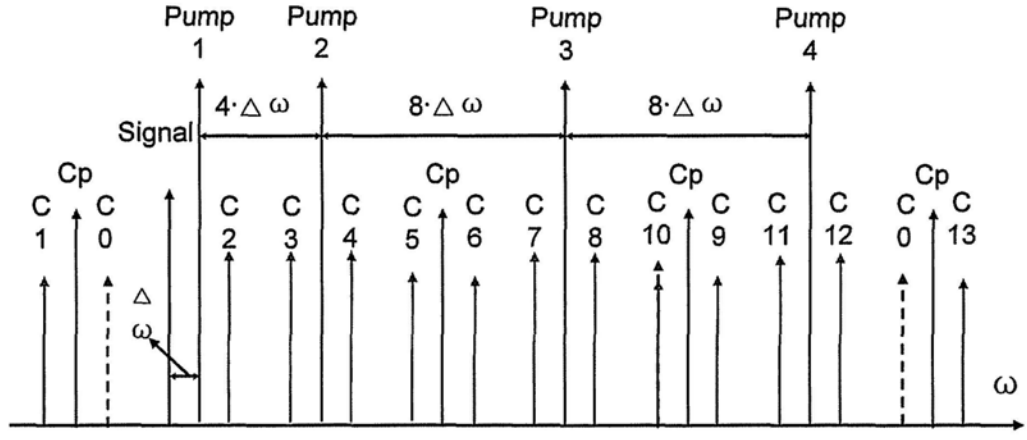

Fig. 3.16. Wavelength multicasting of DPSK signal with four unequally-spaced pumps. C1-9: nine copies generated in wavelength multicasting; C10-13: four additional copies generated owing to pump4; C0: vacant channels; Cp: idlers from FWM between pumps.

Since FWM has to be used, an issue for practical implementation of wavelength multicasting is the random polarization state of DPSK signal in the optical networks. This problem can be solved by FWM in a birefringent HNLF, which exhibits wide

FWM bandwidth [21]. To demonstrate its validity for wavelength multicasting, we use FWM with three unequally spaced pumps.

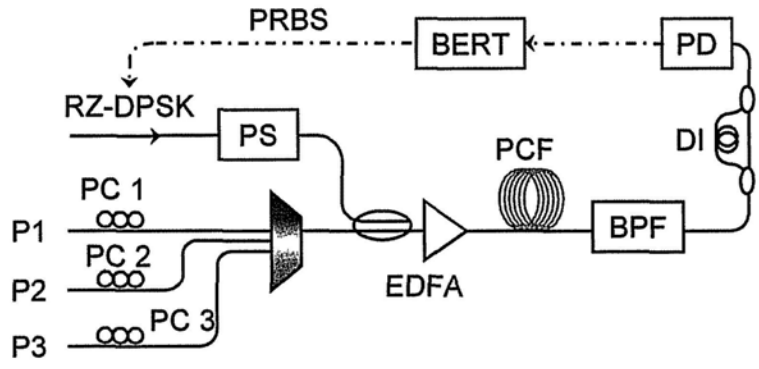

Fig. 3.17. Experimental setup of polarization-insensitive wavelength multicasting of DPSK signal using FWM in birefringent PCF.

Fig. 3.17 shows the setup to investigate polarization-insensitive DPSK wavelength multicasting in a birefringent PCF. A 10-Gbit/s RZ-DPSK signal at 1545.28 nm is combined with three CW pumps. The polarization of signal is controlled by a polarization scrambler. The same PCF as in section 3.2 is used and hence the minimum PPD should be larger than 3 nm to suppress the polarization dependence of FWM. This requirement makes the arrangement of pump wavelength in our experiment different from that shown in Fig. 3.15, since pump3 would be 39 nm away from signal and our EDFA cannot support such wideband amplification. However, this difference has no influence on the polarization-insensitive demonstration. In our experiment, the pumps have unequally spaced wavelengths at 1548.48 nm (P1 to signal: 3.2 nm), 1552.48 nm (P2 to P1: 4 nm) and 1557.28 nm (P3

to P2: 4.8 nm), conforming to a minimum PPD of 3.2 nm. The PPD can in principle be further reduced by increasing the fiber length or birefringence. With a power ratio of ~ 3 dB between each pump and the signal, the combined lightwaves are amplified to a total power of 25 dBm by an EDFA. To suppress the polarization dependence on input signal, all the pump polarizations are adjusted to be at 45 degrees to the principal axes of the PCF.

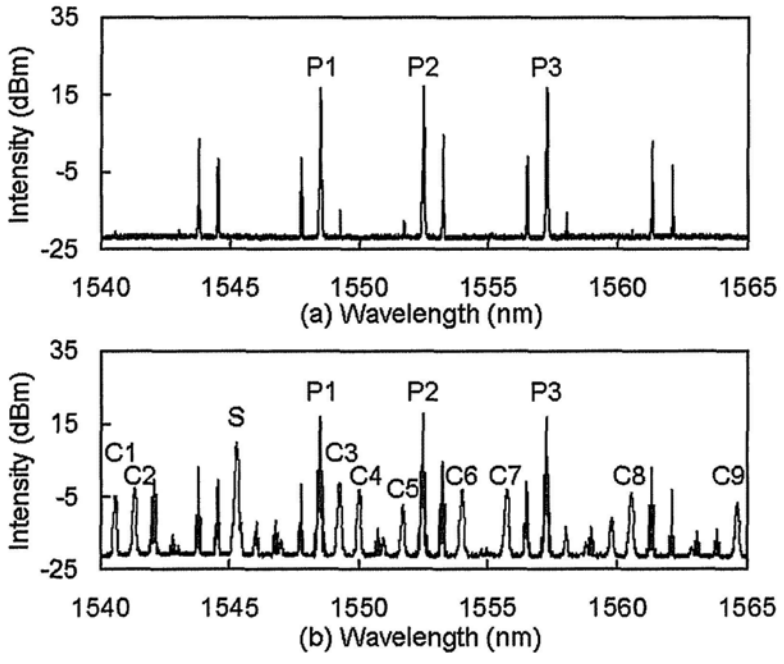

Fig. 3.18. FWM spectra for RZ-DPSK wavelength multicasting; (a) pump-pump beatings without input signal; (b) wavelength multicasting with input signal (the input signal and the multicast channels are marked and are shown in red).

The crosstalk from undesirable pump-to-pump beatings is minimized as shown by the spectra in Fig. 3.18. In Fig. 3.18 (a), the idlers generated by pure pump-pump beatings include seven strong first-order idlers and three weak second-order idlers.

Ideally, the multicast channels should not have spectral overlap with the first-order idlers. Fig. 3.18 (b) shows the spectrum for wavelength multicasting of 10-Gbit/s RZ-DPSK signal with nine multicast channels. None of the output channels overlaps with the first-order idlers, although C3 and C5 are degraded through overlapping with the second-order idlers. The nine multicast channels include eight channels generated by nondegenerate FWM (C1-4 and C6-9) and one channel generated by degenerate FWM of the signal and P1 (C5). The conversion efficiencies of the eight nondegenerate multicast channels, defined as the power ratios of the outputs to the input, are between -17.4 dB and -19.8 dB, while that of the degenerate one is -23.7 dB. The efficiencies of degenerate FWM between signal-P2 and signal-P3 are even much lower so that they are not useful for multicasting.

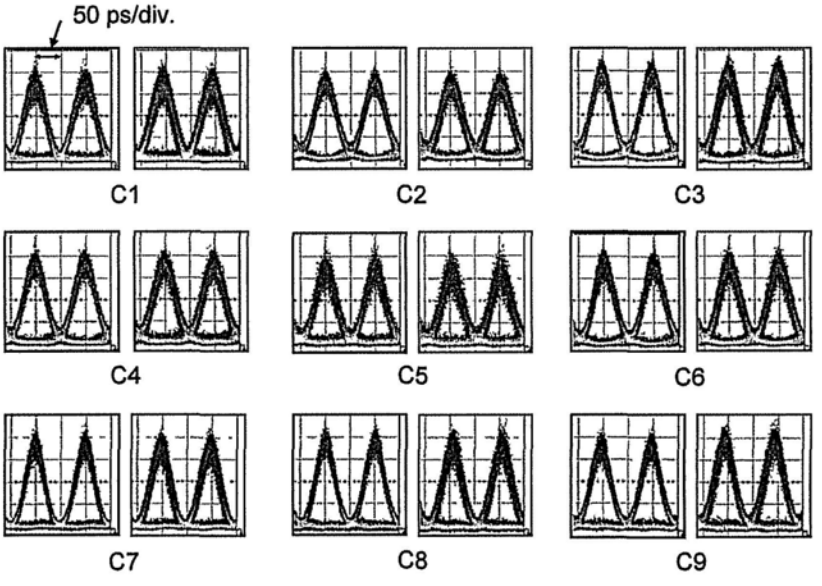

Fig. 3.19. Eye diagrams of the demodulated 10-Gbit/s RZ-DPSK multicast channels (in each pair, left: fixed polarization state of the input signal, right: time-varying polarization state of the input signal).

To measure the eye diagrams, the multicast RZ-DPSK signals are selected individually using a tunable optical bandpass filter and are demodulated with a fiber-based delay interferometer. Fig. 3.19 shows the open eye diagrams obtained for all the channels. In each pair, the left plot shows the output when the input polarization is fixed while the right plot corresponds to the case with time-varying input polarization generated with a polarization scrambler. Except for a time jitter of ~ 9 ps introduced by the birefringence of the PCF, the output eye diagrams obtained with a time-varying input polarization are almost as open as those with a fixed input polarization, confirming polarization-insensitive operation of our DPSK wavelength multicasting scheme. The jitter can in principle be compensated with another birefringent fiber following the setup, allowing operation with further increase in the signal data rate.

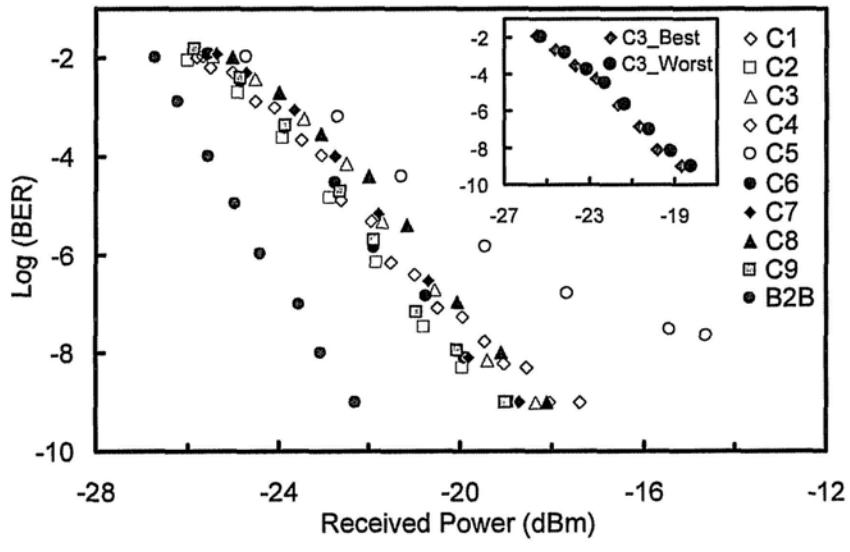

Fig. 3.20. BER measurements of the nine multicast channels (Inset: BER measurements of C3 at different polarization states of the input signal).

To further analyze the performance, BER of all the multicast channels are measured and the results are shown in Fig. 3.20. All the eight multicast channels generated from nondegenerate FWM achieve error free operation at the BER level of 10^{-9}, with the power penalty varying from 3.3 dB to 4.9 dB. However, C5 is produced from degenerate FWM and shows an error floor at the BER level of 10^{-8}. The observation can be explained by the relatively low FWM conversion efficiency in generating C5. The spectral overlap with a second-order idler of pump-pump beatings as shown in Fig. 3.18 also limits the performance. Without counting C5, the scheme yields a one-to-eight wavelength multicasting based on FWM with three pumps. As shown by the eye diagrams in Fig. 3.19, the degradation due to polarization-scrambling of the input signal is similar for all the multicast channels. To analyze the performance, we choose an arbitrary channel C3 and investigate the residual polarization dependence by measuring the BER when the input signal is set at different polarizations. The difference of the power penalties between the best and the worst cases is ~ 0.45 dB, thus further confirming the polarization-insensitive property of our scheme.

We have experimentally demonstrated polarization-insensitive, one-to-eight wavelength multicasting of a 10-Gbit/s RZ-DPSK signal based on FWM in a birefringent PCF using three unequally-spaced pumps. By choosing PPD larger than 3.2 nm and setting the pump polarizations 45 degrees to the principal axes, the polarization dependence of FWM is effectively suppressed. Open eye diagrams are obtained for all the multicast channels with both polarization-fixed and

polarization-scrambled inputs. The power penalty of the multicast channels ranges from 3.3 to 4.9 dB. The maximum variation of the power penalty at different input polarizations is ~ 0.45 dB, thus confirming polarization-insensitive operation of our scheme.

As shown in Fig. 3.18, the large PPD in unequally-spaced pump arrangement makes quite a few vacant wavelength channels in the ITU grid. To reduce the PPD to a level of 0.8 nm and to achieve the same wavelength arrangement shown in Fig. 3.15, we can use HNLF with a larger birefringence or fiber length. Such kind of fiber has been previously used in optical demultiplexing of data signals [22].

References

[1] M. P. Fok, J. A. Summers, M. L. Masanovic, C. Shu, and D. J. Blumenthal, "Tunable DPSK wavelength converter using an SOA-MZI monolithically integrated with a sampled-grating distributed Bragg reflector," in Proc. of CLEOE-IQEC 2007, Munich, Germany, paper CI1-5-TUE.

[2] M. Matsumoto, "A fiber-based all-optical 3R regenerator for DPSK signals," IEEE Photon. Technol. Lett., vol. 19, no. 5, pp. 273-275, Mar. 2007.

[3] S. H. Lee, K. K. Chow, and C. Shu, "All-optical ASK to DPSK format conversion using cross-phase modulation in a nonlinear photonic crystal fiber," in Proc. of CLEO/PR 2005, Tokyo, Japan, paper CFJ2-5.

[4] K. Inoue, "Polarization independent wavelength conversion using fiber four-wave mixing with two orthogonal pump lights of different frequencies," J. Lightw. Technol., vol. 12, no. 11, pp. 1916-1920, Nov. 1994.

[5] J. Ma, J. Yu, C. Yu, Z. Jia, X. Sang, Z. Zhou, T. Wang, and G. K. Chang, "Wavelength conversion based on four-wave mixing in high-nonlinear dispersion shifted fiber using a dual-pump configuration," J. Lightw. Technol., vol. 24, no. 7, pp. 2851-2858, Jul. 2006.

[6] T. Hasegawa, K. Inoue, and K. Oda, "Polarization independent frequency conversion by fiber four-wave mixing with a polarization diversity technique," IEEE Photon. Technol. Lett., vol. 5, no. 8, pp. 947-949, Aug. 1993.

[7] T. Tanemura, K. Katoh, and K. Kikuchi, "Polarization-insensitive nondegenerate four-wave mixing using circularly polarized pumps in twisted fiber," in Proc. of

CLEO/QELS 2005, Baltimore, MD, paper CWK1.

[8] K. P. Hansen, J. R. Folkenberg, C. Peucheret, and A. Bjarklev, "Full dispersion controlled triangular-core nonlinear photonic crystal fiber," in Proc. of OFC/NFOEC 2003, Atlanta, Georgia, paper PD02.

[9] D.-H. Kim and J. U. Kang, "Sagnac loop interferometer based on polarization maintaining photonic crystal fiber with reduced temperature sensitivity," Opt. Express, vol. 12, no. 19, pp. 4490-4495, Sep. 2004

[10] Z. Wang, N. Deng, C. Lin, and C.-K. Chan, "Polarization insensitive widely tunable wavelength conversion based on four-wave mixing using dispersion-flattened high-nonlinearity photonic crystal fiber with residual birefringence," in Proc of ECOC 2006, Cannes, France, Paper We3P18.

[11] W. Astar, A. S. Lenihan, and G. M. Carter, "Theoretical analysis of polarization-insensitive wavelength conversion by four-wave mixing in photonic crystal fiber," Electron Lett., vol. 43, no. 25, pp. 1419-1421, Dec. 2007.

[12] K. Inoue, "Tunable and selective wavelength conversion using fiber four-wave mixing with two pump lights," IEEE Photon. Technol. Lett., vol. 6, no. 12, pp. 1451-1453, Dec. 1994.

[13] K. Chow and C. Shu, "All-optical signal regeneration with wavelength multicasting at 6 × 10 Gbit/s using a single electroabsorption modulator," Opt. Express, vol. 12, no. 13, pp. 3050-3054, Jun. 2004.

[14] G. Contestabile, N. Calabretta, R. Proietti, and E. Ciaramella, "Double-stage cross-gain modulation in SOAs: An effective technique for WDM multicasting,"

IEEE Photon. Technol. Lett., vol. 18, no. 1, pp. 181-183, Jan. 2006.

[15]K. Wong, G. W. Lu, K. C. Lau, P. K. A. Wai, and L. K. Chen "All-optical wavelength conversion and multicasting by cross-gain modulation in a single-stage fiber optical parametric amplifier," in Proc. OFC, Anaheim, CA, March 2007, Paper OTuI4.

[16]Y. Wang, C. Yu, T. Luo, L. Yan, Z. Pan, and A. E. Willner, "Tunable all-optical wavelength conversion and wavelength multicasting using orthogonally polarized fiber FWM", J. Lightw. Technol., vol. 23, no. 10, pp. 3331-3338, Oct. 2005.

[17]G. Contestabile, N. Calabretta, M. Presi, and E. Ciaramella, "Signal and multicast wavelength conversion at 40 Gbit/s by means of fast nonlinear polarization switching in an SOA", IEEE Photon. Technol. Lett., vol. 17, no. 12, pp. 2652-2654, Dec. 2005.

[18]C. H. Kwok, S. H. Lee, K. K. Chow, C. Shu, C. Lin, and A. Bjarklev, "Polarization-insensitive all-optical wavelength multicasting by self phase-modulation in a photonic-crystal fiber," in Proc. CLEO, Long Beach, CA, May 2006, Paper CTuD4.

[19]M. P. Fok and C. Shu, "Multipump four-wave mixing in a photonic crystal fiber for 6 × 10 Gbit/s wavelength multicasting of DPSK signals," IEEE Photon. Technol. Lett., vol. 19, no. 15, pp. 1166-1168, Aug. 2007.

[20]G.-W. Lu, K. S. Abedin, and T. Miyazaki, "DPSK multicast using multiple-pump FWM in Bismuths highly nonlinear fiber with high multicast efficiency," Opt.

Express, vol. 16, no. 26, pp. 21964-21970, Dec. 2008.

[21] Y. Dai and C. Shu, "Widely tunable polarization-insensitive nondegenerate four-wave mixing wavelength conversion for DPSK signals," IEEE Photon. Technol. Lett., vol. 22, no. 15, pp. 1138-1140, Aug. 2010.

[22] H. Hu, et al, "Polarization-insensitive 640 Gbit/s demultiplexing based on four wave mixing in a polarization-maintaining fiber loop," J. Lightw. Technol., vol. 28, no. 12, pp. 1789-1795, Jun. 2010.

4 BIT-RATEVARIABLE DEMODULATION OF DPSK SIGNALS

DPSK modulation format is a strong candidate for long-haul and high-capacity optical communication owing to its high tolerance to optical nonlinear impairments [1]. With balanced detection, ~ 3-dB gain in receiver sensitivity can be also obtained over ASK. However, unlike the amplitude-modulated signals, the information of phase-modulated signals cannot be detected directly by a photodetector. Although coherent optical detection can retrieve the full information of a lightwave, including both phase and intensity, the complicated system and high cost limit its implementation in many cost-sensitive applications. Thus, conversion from phase-information to intensity-information is critical for successful information transmission using phase-modulated signals. This phase-to-intensity format conversion is called demodulation of phase-modulated signal. Except in optical receivers, demodulation can also be implemented in an optical network node where next hop may send the data to a sub-network in which amplitude-modulated signals are desired. Thus, it can be implemented as a modulation format conversion together with routing and switching function.

In this chapter, bit-rate tunable demodulation of DPSK signal is demonstrated using either a loop structure or a linear structure. Polarization-insensitive operation of a delay-asymmetric nonlinear loop mirror is first achieved using FWM with dual-orthogonal pumps in section 4.2. To enlarge the range of bit rates covered by the

loop mirror, FWM with dual-parallel pumps is used to enhance the wavelength conversion bandwidth in section 4.3. In section 4.4, bit-rate tunable demodulation is achieved in a linear structure using cascaded FWM.

4.1 Introduction to Delay-Asymmetric Nonlinear Loop Mirror

Different approaches have been proposed for demodulation of DPSK signals, based on either DI or discrimination filtering. For the DI approach, various kinds of optical delay have been used, including different lengths of optical fibers or waveguides [2], differential group delay [3, 4], and group velocity delay [5]. Discrimination filtering can be achieved using optical filters with very narrow linewidth, like fiber Bragg grating (FBG) [6] and silicon microring resonator [7].

4.1.1 Demodulation of DPSK Based on DI

DPSK modulation format uses phase change to represent information. As shown in Fig. 4.1 (a), if the data is bit "0", a π-phase change will be added to the optical carrier. For bit "1", no phase change will occur. This function can be achieved by a DPSK precoder in the electronic domain. In this way, a short bit sequence "0010100" is modulated to the optical carrier. However, if a photodetector is used to detect the DPSK signal before demodulation, a constant electrical signal carrying little information will be obtained, as the dash line in Fig. 4.1 (a). Fig. 4.1 (b) shows the structure of a fiber-based DI, which uses different fiber lengths to introduce a fixed relative delay between two copies of signals split from the DPSK input. The delay is designed to be one bit period of the DPSK signal. The two copies interfere with each other at the output, as shown in Fig. 4.1 (c). Out-of-phase interference generates a bit "0" and in-phase interference produces a bit "1". Thus, the demodulated DPSK

signal is an amplitude-modulated signal, which can be measured by a photodetector, and the obtained data sequence is exactly the same as that used for modulation.

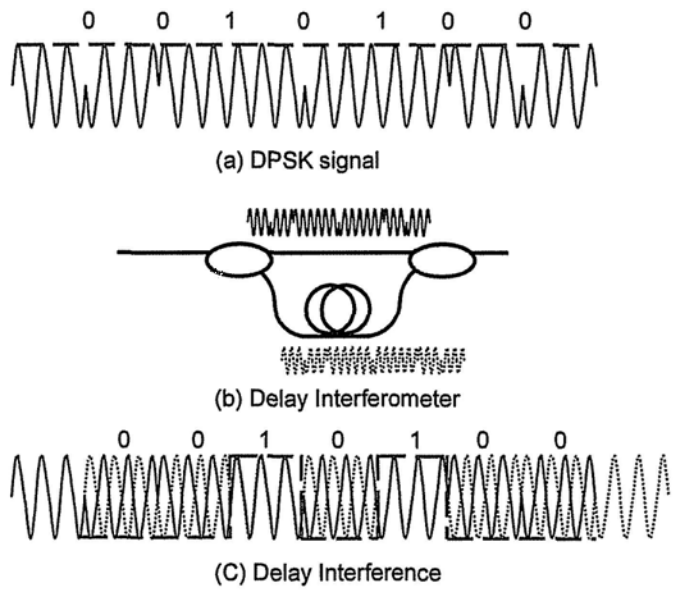

Fig. 4.1. Demodulation of DPSK using delay interferometer.

As mentioned, the delay introduced in the fiber-based DI is fixed, so the DI can only demodulate DPSK signal at a fixed bit rate. DI with variable delay for DPSK demodulation is important for several applications. 1), the transmission link is disturbed seriously so that error-correction coding is added to achieve error-free transmission and hence changing the bit-rate. 2), the delay time is optimized in order to increase the chromatic dispersion tolerance of the system [8]. 4), the delay time is tuned to perform multi-bit delay DSPK demodulation in an optically time-division-multiplexed (TDM) data stream, where a fine tuning of the delay time is also required to control the detrimental bit-delay mismatch [9]. To achieve variable

delay, slow light based on SBS [10] or fiber parametric process [11] and tunable wavelength conversion together with group velocity dispersion (GVD) [12] can be used. Since the optical wavelength conversion techniques are becoming mature, the latter one attracts increasing interest owing to its large delay range, high resolution, large bandwidth, and data format transparency.

4.1.2 Working Principle of DANLM

The delay-asymmetric nonlinear loop mirror (DANLM) [5] can serve as a DPSK demodulator. It is built with a DI structure that incorporates a tunable optical delay. The tunable delay is introduced by a technique based on wavelength conversion together with GVD. The principle is illustrated in Fig. 4.2. The input signal is first converted to another wavelength and then the converted signal propagates through a dispersive medium, like SMF or FBG. Due to the GVD, the velocity of the signal in the medium varies with the wavelength of converted signal. By changing the wavelength of the converted signal, the time delay in the medium will be changed. The wavelength of the signal can be converted back to the original one if necessary.

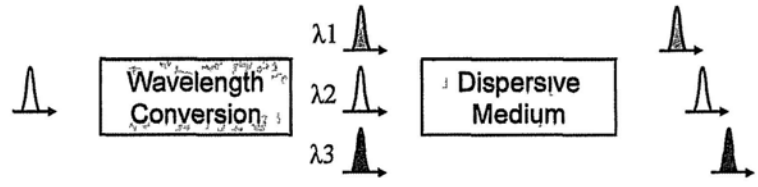

Fig. 4.2. (Color online) Tunable optical delay based on wavelength conversion together with GVD.

The structure of the DANLM and its equivalent DI structure are shown in Fig. 4.3. It is an optical loop mirror connected by a 3-dB coupler. The loop contains a nonlinear medium (PCF) and a dispersive medium (SMF) to perform wavelength conversion and to provide GVD, respectively. The input signal is split into a clockwise (CW) branch and a counter-clockwise (CCW) branch in the loop by the coupler. The CCW branch propagates through PCF first, so it is converted to another wavelength before entering the dispersive medium. Therefore, the time delay of the CCW signal is

determined by the converted wavelength. However, the CW branch sees the SMF first, so the delay is determined by the input signal wavelength. Although it is also converted to the same wavelength as the CCW branch in the PCF, the converted signal never has a chance to see the SMF. Therefore, a relative delay is introduced between the converted signals in the CW and CCW branches, which is given by

$$\Delta T = D \cdot L \cdot \left| \lambda_{input} - \lambda_{converted} \right| \tag{4-1}$$

where D and L are the dispersion coefficient and the length of the dispersive medium. As shown in equation (4-1), the delay can be tuned by changing the converted wavelength.

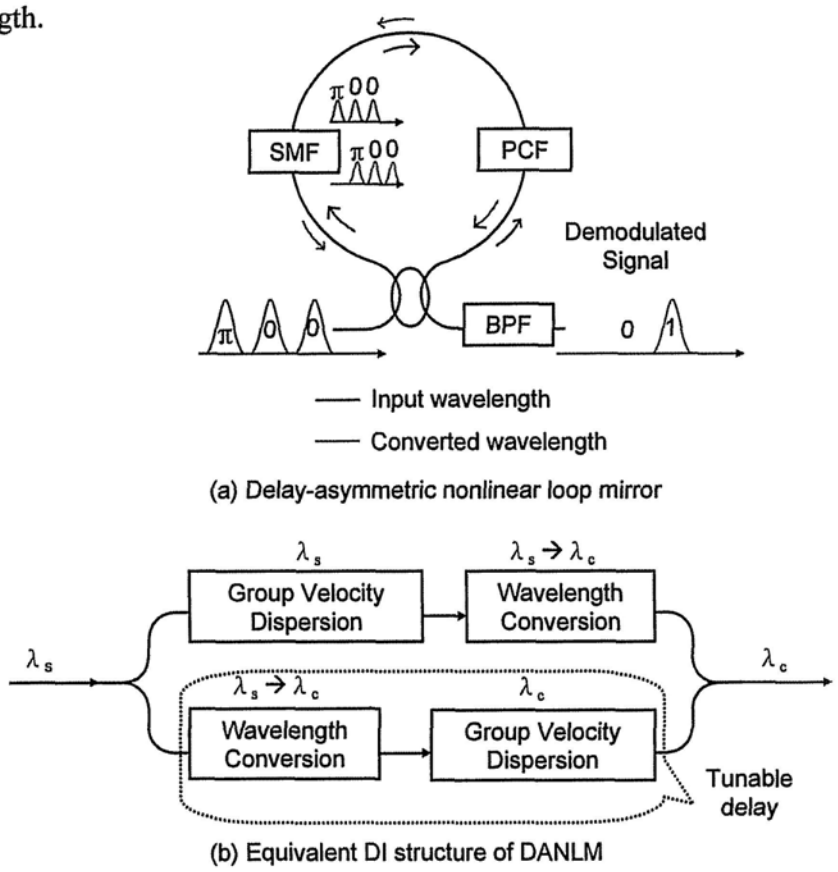

Fig. 4.3. (a) Structure of the delay-asymmetric nonlinear loop mirror and its equivalent DI structure. SMF: single mode fiber; PCF: photonic crystal fiber; BPF: bandpass filter.

The two converted signals are at exactly the same wavelength and interfere with each other when they encounter at the coupler. When the delay is set to one bit period, a phase-modulated signal will be demodulated. For input signals at different bit-rates, the delay can always be tuned to one bit period. Thus, a bit-rate tunable DPSK demodulator is achieved. Demodulation of 10 and 20-Gbit/s DPSK signals has been demonstrated in [5] using the DANLM.

4.2 Polarization-Insensitive Operation of DANLM

To process DPSK signal, the wavelength conversion process should preserve the optical phase, making FWM-based wavelength conversion a strong candidate. Again, the polarization dependence of FWM will be a concern. As discussed in section 2.1, we can use several approaches to solve this problem. The loop structure hinders the use of the polarization diversity technique. Also, FWM with dual-parallel pumps is not capable to support the wide conversion bandwidth required by the loop and birefringent HNLF is not commonly available, we thus use FWM with dual-orthogonal pumps to overcome the polarization dependence.

As shown in Fig. 4.4, the dual-orthogonal pumps are prepared by combining two CW lights with a polarization beam splitter (PBS). The polarization of the input DPSK signal is disturbed by a polarization scrambler. All the input lightwaves are combined together, fed into an EDFA to boost the total optical power to 27 dBm, and then launched into the DANLM. The loop mirror has a 600-m SMF and 64-m PCF, as the dispersive medium and nonlinear medium, respectively. The converted wavelength is filtered out by a bandpass filter, which is already a demodulated DPSK signal.

Fig. 4.5 shows the FWM spectrum of demodulation of 10-Gbit/s DPSK. The required delay for the demodulation is 100 ps. The 600-m SMF provides a total dispersion of 10 ps/nm, so the wavelength spacing between the input and converted signal should be 10 nm. The input signal locates at 1550 nm, and the two orthogonal pumps are at

1554.5 and 1555.5 nm, respectively, resulting in a converted wavelength at 1560 nm. There are another two copies of the input signal, which are generated from the degenerate FWM between signal-pump1 and signal-pump2, as indicated by C1 and C2 in Fig. 4.5. However, they are sensitive to the polarization of input signal.

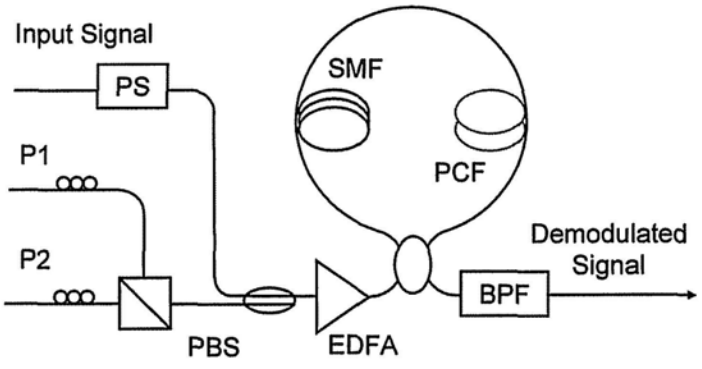

Fig. 4.4. Experimental setup of polarization-insensitive DANLM. PS: polarization scrambler; PBS: polarization beam splitter; SMF: single mode fiber; PCF: photonic crystal fiber; BPF: bandpass filter.

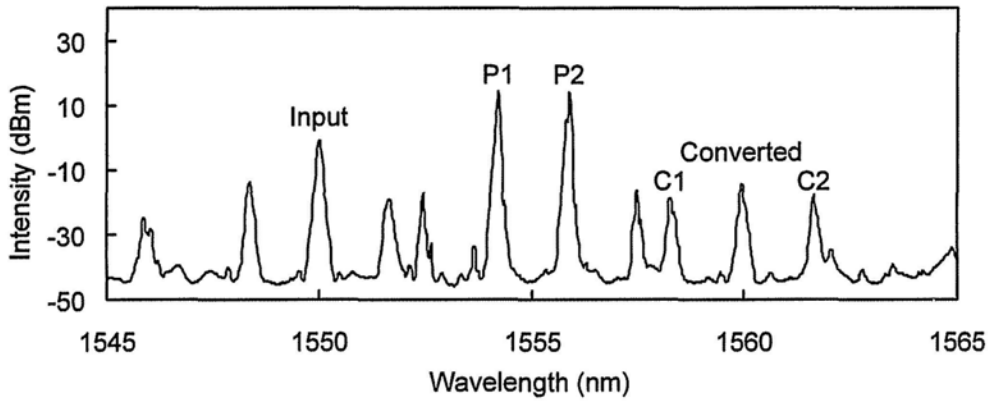

Fig. 4.5. Optical spectrum of polarization-insensitive FWM with dual-orthogonal pumps. P1: pump1; P2: pump2; C1, C2: converted wavelength from degenerate FWM between signal-P1 and signal-P2.

The converted signal is filtered out by an optical filter and sent to a photodetector for detection. The eye diagrams of the demodulated 10-Gbit/s RZ-DPSK signals are shown in Fig. 4.6., illustrating two different operations of DANLM. Fig. 4.6 (a, c) show the polarization-sensitive DANLM, which uses a single pump with wavelength at 1555 nm. The eye is completely closed when the polarization scrambler works. However, the polarization-insensitive DANLM can still produce a widely open eye except that a small time jitter is introduced by the birefringence of PCF, as shown in Fig. 4.6 (d).

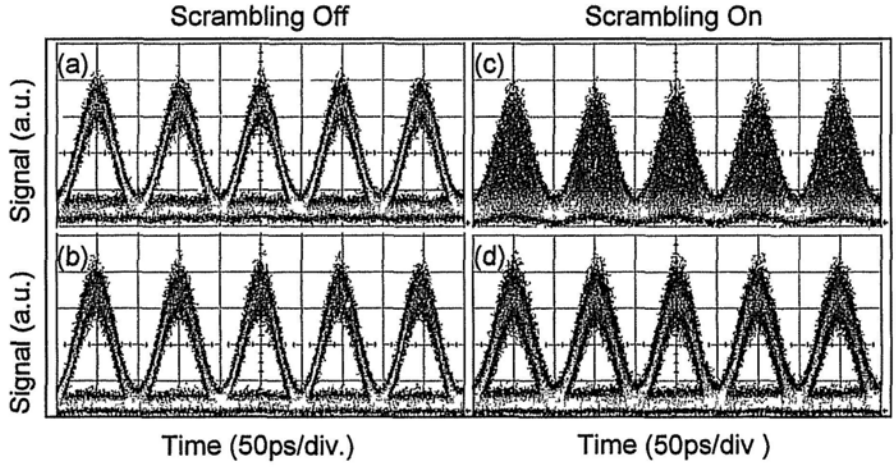

Fig. 4.6. Eye diagrams of demodulated 10-Gbit/s RZ-DPSK signal using (a, c): polarization-sensitive DANLM; (b, d): polarization-insensitive DANLM.

To demonstrate the capability of DANLM to demodulate of DPSK signal at tunable bit rates, the input signal is changed to 12.5 Gbit/s. To provide proper delay for the new data rate, we change the two pump wavelengths to 1553.5 and 1554.5 nm, respectively, which will convert the signal to a new wavelength at 1558 nm. The

8-nm wavelength spacing between the input signal and converted signal leads to 80-ps delay, exactly one bit period of the 12.5-Gbit/s signal. Similar results are obtained as shown in Fig. 4.7. As the pulse width in the 12.5-Gbit/s DPSK signal is smaller, the birefringence-caused time jitter will cause a relatively large degradation. The jitter can be minimized by using a nonlinear fiber without birefringence in the DANLM.

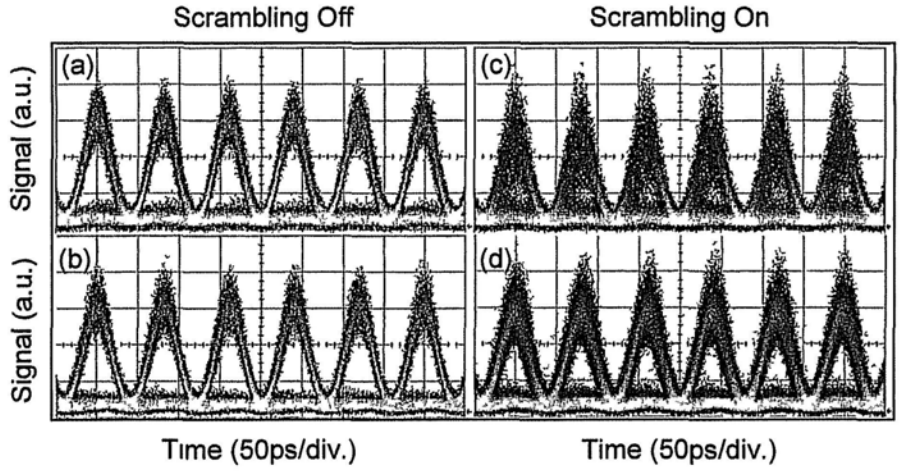

Fig. 4.7. Eye diagrams of demodulated 12.5-Gbit/s RZ-DPSK signal using (a, c): polarization-sensitive DANLM; (b, d): polarization-insensitive DANLM.

Fig. 4.8 shows the measured bit-error-rate (BER) performance at 10 Gbit/s. Error-free detection (BER < 10^{-9}) is obtained at a received power level of -20.6 dBm. To investigate the influence of polarization change on the system performance, the BER is first measured when PC_{in} is adjusted to yield a maximum output power. The BER is then measured again after PC_{in} is readjusted to yield a minimum output power. It is found that the receiver sensitivity changes by 0.8 dB at the error-free

detection level.

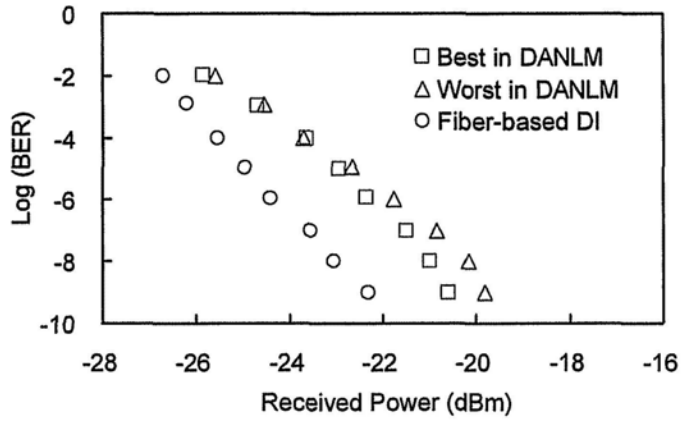

Fig. 4.8. BER measurement of the 10-Gbit/s DPSK signal demodulated by polarization-insensitive DANLM.

In conclusion, a polarization-insensitive DANLM has been demonstrated for variable bit-rate DPSK demodulation. The operating principle is based on non-degenerate FWM with dual orthogonal pumps. The eye diagrams of the demodulated DPSK signals remain widely opened when the polarization of the input signal is fast varied. The variation of the output power is suppressed to less than 0.35 dB for signals at both 10 Gbit/s and 12.5 Gbit/s. A small time jitter is observed due to the birefringence in the PCF and a power penalty of 0.8 dB is incurred.

4.3 Wideband Operation of DANLM

As mentioned in section 4.1.1, the technique based on wavelength conversion together with GVD is relatively simple in generating a large tunable delay. This is also one advantage of DANLM over other bit-rate tunable demodulator [3]. In principle, the delay can be enlarged by increasing the total dispersion or the wavelength conversion bandwidth. However, large dispersion will cause signal distortion and hence a compensation technology is required [13]. In contrast, a large conversion bandwidth brings little degradation to the signal quality. To enhance the bandwidth of FWM-based wavelength conversion, the dual-parallel pump scheme has been demonstrated to be effective [14]. The enhancement can be explained by a smaller phase-mismatch.

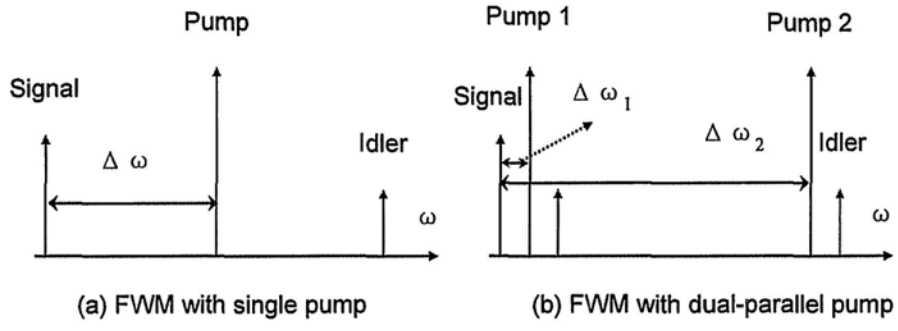

Fig. 4.9. (a) FWM with signal pump and (b) bandwidth-enhanced FWM with dual-parallel pump.

Fig. 4.9 illustrates the frequency mapping of FWM with single pump or dual-parallel pumps. The frequency spacing between the input signals and the generated idlers are the same. Thus, we have

$$2\Delta\omega = \Delta\omega_1 + \Delta\omega_2 \tag{4-2}$$

Assuming the two FWM occur in the same nonlinear medium, they will see the same dispersion characteristics. The phase-mismatch for FWM with single pump is

$$\begin{aligned}\Delta\beta_{single-pump} &= (2\beta_p - \beta_s - \beta_i)\cdot L \\ &= -\beta_2 \cdot \Delta\omega^2 \cdot L\end{aligned} \tag{4-3}$$

where β_2 is GVD parameter and L is the length of nonlinear medium.

Similarly, the phase-mismatch for FWM with dual-parallel pump is

$$\begin{aligned}\Delta\beta_{dual-pump} &= (\beta_{p1} + \beta_{p2} - \beta_s - \beta_i)\cdot L \\ &= -\beta_2 \cdot \Delta\omega_1 \cdot \Delta\omega_2 \cdot L\end{aligned} \tag{4-4}$$

From equation (4-2), we know

$$\begin{aligned}\frac{\Delta\beta_{single-pump}}{\Delta\beta_{dual-pump}} &= \frac{(\Delta\omega_1 + \Delta\omega_2)^2}{4\Delta\omega_1\Delta\omega_2} \\ &= \frac{1}{2} + \frac{1}{4}\left(\frac{\Delta\omega_1}{\Delta\omega_2} + \frac{\Delta\omega_2}{\Delta\omega_1}\right) \geq 1\end{aligned} \tag{4-5}$$

This ratio is always larger than 1 and will increase dramatically with the conversion bandwidth, explaining the bandwidth enhancement of FWM with dual-parallel pumps.

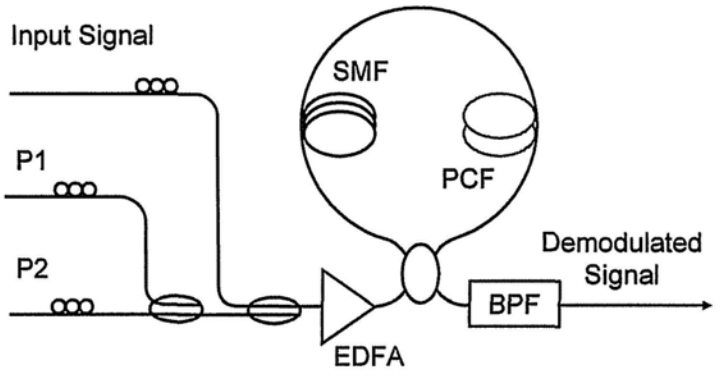

Fig. 4.10. Experimental setup of the dual-parallel pumped DANLM. P1: pump1; P2: pump2; SMF: single mode fiber; PCF: photonic crystal fiber; BPF: optical bandpass filter.

Using this technique, DANLM can demodulate DPSK signals over larger bit-rate range. As shown in Fig. 4.10, the input DPSK signal is combined with two CW pumps with couplers. The wavelength of signal and pump1 are fixed at 1534.6 and 1536.2 nm, respectively. The optical delay is controlled by tuning the wavelength of pump2. The length of SMF is also 600 m, providing a dispersion of 10 ps/nm. First, pump2 is set at 1543.0 nm, converting the signal to a new wavelength at 1544.6 nm. The 10-nm wavelength spacing produces 100-ps delay in the DANLM and an input signal at 10-Gbit/s can be demodulated. Then, pump2 is tuned to 1566.3 nm, which generates the new wavelength at 1567.9 nm, producing a delay of 333 ps for the demodulation of 3-Gbit/s DPSK signal.

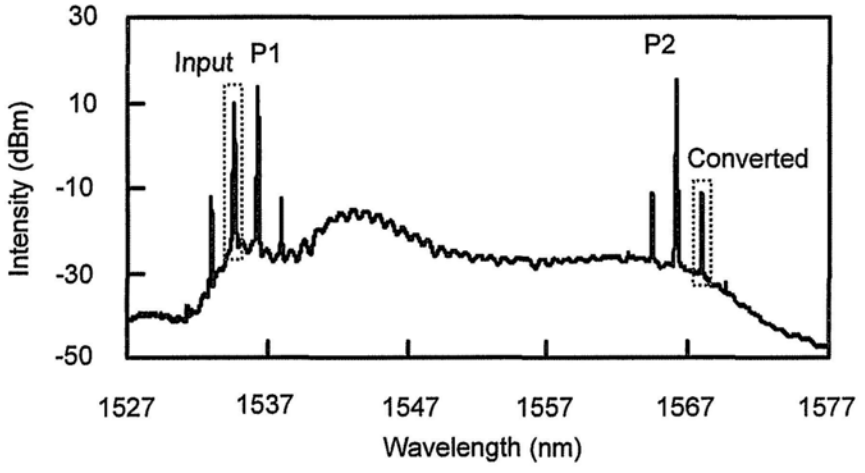

Fig. 4.11. Spectrum of FWM with dual-parallel pumps to produce 333-ps optical delay.

The demodulated eye diagrams are shown in Fig. 4.12. Wide open eyes are obtained for both cases. With the 10-ps/nm GVD used in the DANLM, a delay resolution of

0.1 ps can be achieved provided that the wavelength resolution of pump2 is 0.01 nm, which is readily available for most commercial tunable lasers. Such a fine resolution can guarantee DPSK demodulation at 'continuously' tunable bit-rate from 3 to 10 Gbit/s.

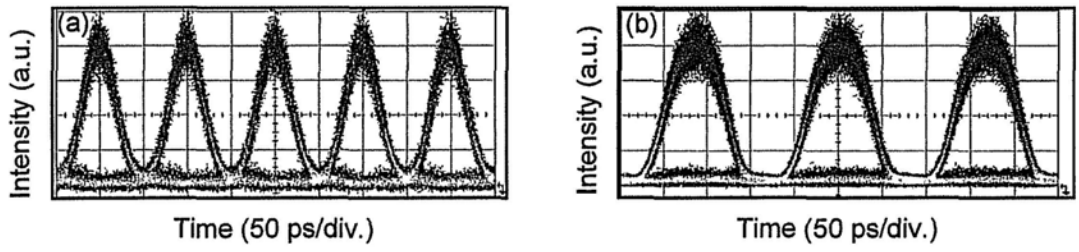

Fig. 4.12. Eye diagrams of demodulated 10-Gbit/s (a) and 3-Gbit/s (b) DPSK signals.

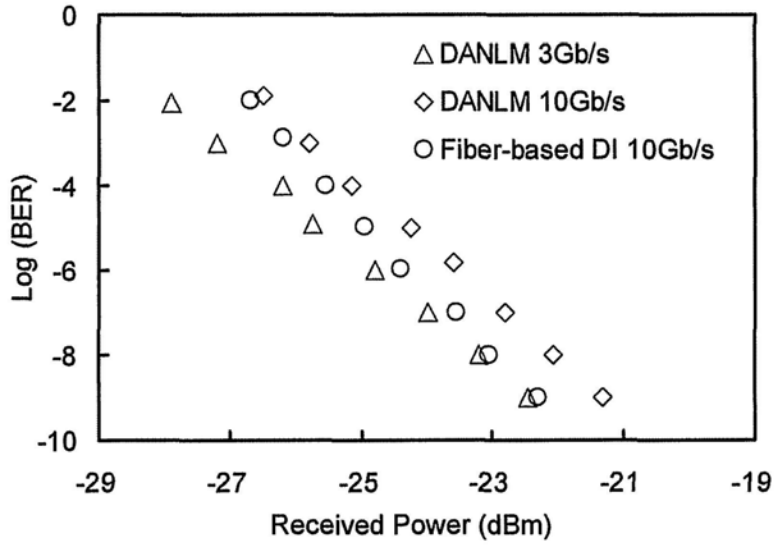

Fig. 4.13. BER measurements of DPSK demodulation with the conventional DI and the DANLM.

The BER is measured to evaluate the performance of demodulation. We depict in Fig.

4.13 the BER performance for demodulation with a conventional fiber-based DI at 10 Gbit/s and our DANLM at both 3 and 10 Gbit/s. The power penalty of demodulation with the DANLM at 10 Gbit/s as compared to the DI is 1 dB at a BER level of 10^{-9}.

We have demonstrated the demodulation of RZ-DPSK signals at 3 and 10 Gbit/s by a dual-pumped DANLM. The variable 1-bit delay is generated by FWM-based wavelength conversion and GVD. FWM with two pumps is used to extend the conversion bandwidth, thus achieving widely tunable bit rates. The power penalty is only 1 dB compared to a conventional fixed bit-rate demodulator at 10 Gbit/s.

Until now, the demonstrated DPSK demodulation schemes can be divided into three main categories according to their work principles. The first one is to use the delay introduced by different physical paths, like the delay-line interferometer (DLI). The second one is to use the delay introduced by different optical paths in the same physical paths. The difference of optical paths can be caused by PMD, CD, or mode dispersion. The third category utilizes optical discrimination filtering, including passive filters like FBG and silicon micro-ring (MR), or active filters like SBS.

Our DANLM belongs to the second category. Compared with approaches using passive devices, the apparent advantage is bit-rate tunability. Although the one based on MR can also work over a wide bit-rate band, it works only for signals at several fixed wavelengths and is difficult to generate demodulated signals suitable for

balanced detection. Compared with the other active approach based on SBS, the difference lays on the possibility to work with balanced detection. The SBS approach can only provide a demodulated signal for signal-ended detection. The main limitation of DANLM is its complicated system architecture and subsequently large footprint. We expect the emergence of highly efficient nonlinear medium and dispersive medium to solve this. In the end, the features of existing DPSK demodulation schemes are summarized in Table A. There is no perfect one, but DLI can be the most practical one for demodulation at fixed bit rate.

Table A: Comparison of various DPSK demodulation schemes

Demodulators	Bit-rate Variability	Polarization Independence	Wavelength Variability	Balanced Detection	System Architecture	Insertion Loss
DLI [2]	*Fixed*	*Yes*	*Wideband*	*Yes*	*Simple*	*Low*
PMD [4]	*Fixed*	*Yes*	*Wideband*	*Yes*	*Moderate*	*Low*
CD (DANLM)	*Tunable*	*Possible*	*Tunable*	*Yes*	*Complex*	*N/A*
MD [15]	*Fixed*	*Possible*	*Wideband*	*Possible*	*Simple*	*High*
FBG [6]	*Fixed*	*Possible*	*Fixed*	*Possible*	*Simple*	*Moderate*
MR [7]	*Wideband*	*Possible*	*Fixed*	*Possible*	*Simple*	*High*
SBS [16]	*Tunable*	*Possible*	*Tunable*	*No*	*Complex*	*N/A*

DLI: delay-line interferometer
PMD: polarization mode dispersion; CD: chromatic dispersion; MD: mode dispersion
MR: micro-ring; FBG: fiber Bragg grating; SBS: stimulated Brillouin scattering

4.4 Bit-Rate Variable Demodulator in Linear Structure

DANLM is a delay-tunable DI working for DPSK demodulation over a large bit-rate tunable range. However, the bulkiness of the DANLM can be a concern in some applications. Compact devices to provide GVD and nonlinearity are desired. Nonlinear optical effects have been demonstrated in SOA [17], periodically poled lithium niobate [18], silicon waveguide [19], and chalcogenide glass [20]. They are all candidates to replace HNLF with a length of tens to hundreds of meters. As for the dispersive medium, chirped FBG can provide tens of ps/nm dispersion over a fiber segment as short as several centimeters. Chirped FBG works in a reflection manner which is different from that of other dispersive medium like SMF, so it cannot be implemented in a loop structure. To utilize chirped FBG, we propose a novel linear structure to realize bit-rate tunable DPSK demodulator in this section.

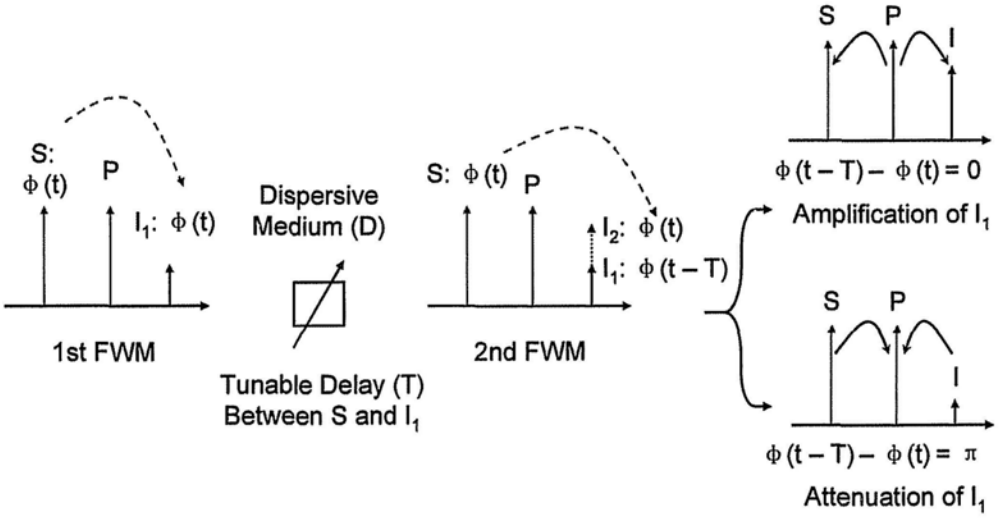

Fig. 4.14. Principle of DPSK demodulation based on cascaded FWM. S: signal; P: pump; I: idler.

Fig. 4.14 illustrates the scheme of DPSK demodulation in a linear structure, which is based on cascaded FWM. The principle is similar to that of phase sensitive amplification [21]. The first FWM generates idler 1 which is then automatically phase-locked to the signal and the pump. The phase of idler 1 is determined by the signal phase and pump phase as

$$\varphi_{idler1} = 2\varphi_{pump} - \varphi_{signal} \tag{4-6}$$

All the three lights are launched into a dispersive medium to introduce relative delay since they are at different wavelengths. The pump is a CW light with a linewidth of ~ 1 MHz, so it is not necessary to consider its group delay compared to the phase-modulated signal and idler. The delay between the signal and the idler can be calculated using the equation (4-1). After a delay time T is introduced between the signal and idler 1, the second FWM is initiated to amplify or to attenuate the idler 1 through the interference between idler 1 and idler 2. The amplification or attenuation is determined by the phase difference between the signal, the pump, and idler 1 in the second FWM,

$$\begin{aligned} \Delta\varphi &= 2\varphi_{pump} - \varphi_{signal}(t) - \varphi_{idler1}(t-T) \\ &= \varphi_{signal}(t-T) - \varphi_{signal}(t) \end{aligned} \tag{4-7}$$

where the 0-phase and π-phase difference correspond to amplification and attenuation of idler 1, respectively.

The delay time T is generated based on a combination of wavelength conversion and dispersion. For a given dispersion coefficient, T is determined by the wavelength shift between the signal and idler 1, which is adjustable by tuning the pump

wavelength. If T is set to one bit period of a DPSK signal, the idler power after the cascaded FWM processes will depend on the phase difference between two neighboring bits in the data sequence, converting the phase modulation to intensity modulation. In our experiment, the delay time T is introduced in a chirped FBG with a 20-ps/nm dispersion. By tuning the pump wavelength of FWM, one-bit delay can always be generated for DPSK signals at variable bit-rates to achieve the demodulation. Moreover, additional 0-phase or π-phase shift can be introduced between the signal and idler 1, thus switching the output between ODB and AMI formats that appear respectively at the constructive and destructive ports of a conventional fixed-delay DI.

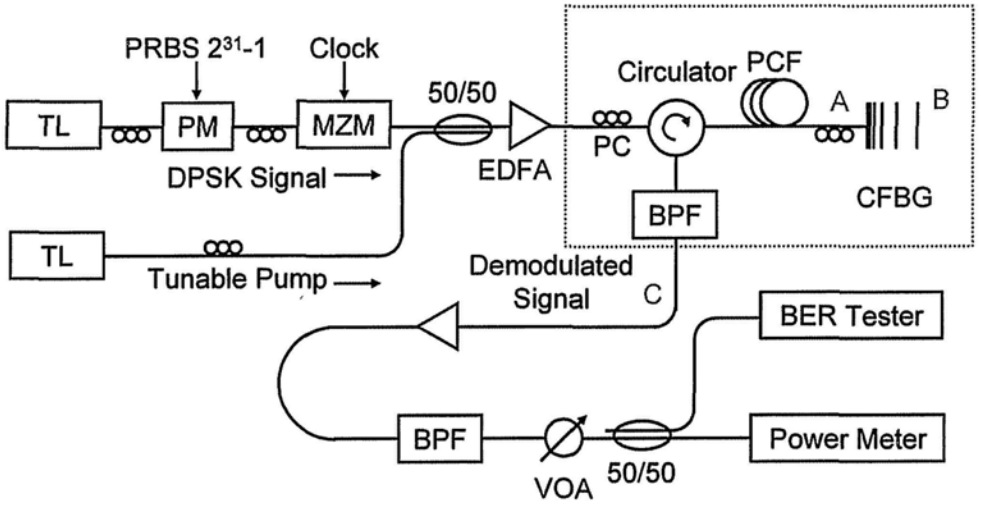

Fig. 4.15. Setup of the bit-rate variable demodulator. TL: tunable laser; PM: phase modulator; MZM: Mach-Zehnder modulator; EDFA: erbium-doped fiber amplifier; PC: polarization controller; BPF: optical bandpass filter; PCF: photonic crystal fiber; CFBG: chirped fiber Bragg grating; BER: bit error ratio. Demodulator is shown in the dot-line rectangle area.

Fig. 4.15 shows the experimental setup of the linear-structure bit-rate variable DPSK demodulator. The FWM-based wavelength conversion is performed in a 41-m PCF. The PCF is placed between two polarization controllers to overcome polarization change caused by the PCF birefringence. Following the PCF, a chirped FBG provides a flattened dispersion of 20 ps/nm and a reflectance of 99% over the range of 1535 to 1565 nm. An optical circulator and a bandpass filter with a 3-dB bandwidth of 0.6 nm are used to extract the idler output. It should be noted that we can perform the cascaded FWM in a single nonlinear medium owing to the reflection working manner of chirped FBG, which is helpful to reduce the cost.

We will demonstrate the demodulation of both NRZ- and RZ-DPSK signals. In addition to a tunable laser and a phase modulator driven by a PRBS (2^{31}-1), a MZM driven by a clock is also included in the DPSK transmitter. When a NRZ-DPSK signal is used as the input, the MZM will be turned off. The DPSK signal is combined with a wavelength tunable CW pump before they are amplified by an EDFA to a total power of ~ 26 dBm. The first stage of FWM takes place when the signal and the pump propagate through the PCF towards the chirped FBG. After the reflection from the chirped FBG, the pump, the signal, and the generated idler 1 will travel through the PCF again in the opposite direction. Owing to the high reflectance of the chirped FBG, the optical power loss results mainly from the splice between the PCF and the chirped FBG. The loss is ~ 2.5 dB in our setup such that the second stage of FWM is still effective. Idler 1 experiences a tunable delay with reference to

the signal in the chirped FBG according to its wavelength, which is controlled by the CW pump wavelength. When the delay is set to one bit period of the corresponding data rate, the phase difference between two neighboring bits of the DPSK signal will determine an amplification or attenuation of idler 1, resulting in DPSK demodulation at variable bit-rates.

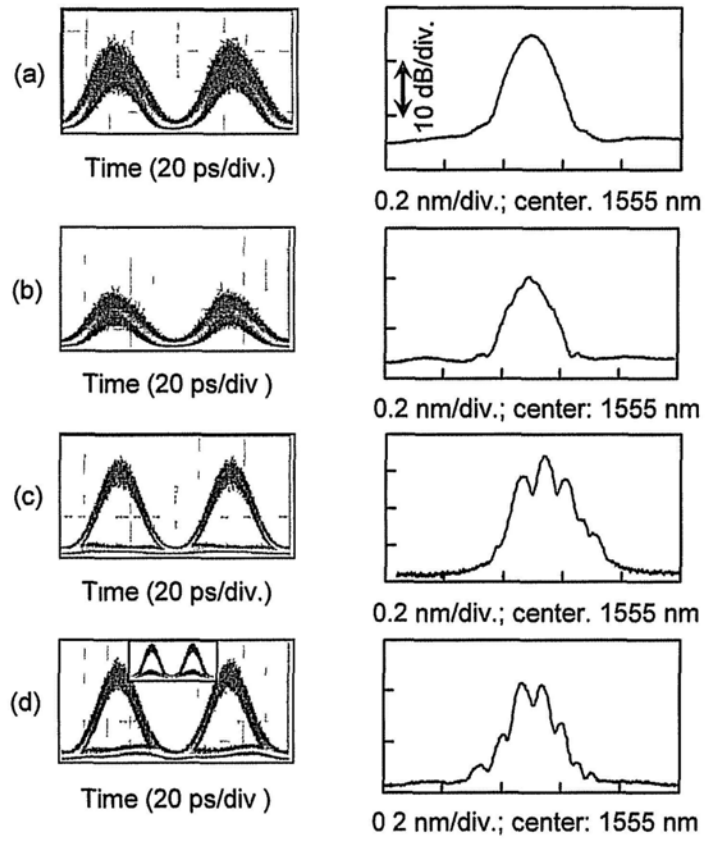

Fig. 4.16. Eye diagrams and optical spectra of the idlers centered at 1555 nm. (a) after the first FWM, (b) behind the chirped FBG, (c) after the second FWM with 0-phase shift, and (d) after the second FWM with π-phase shift. The measurement positions correspond to points A, B, and C in Fig. 4.15. Inset: incomplete depletion of idler 1.

To verify the demodulation principle, Fig. 4.16 shows the eye diagrams and spectra of the idlers obtained from 10-Gbit/s RZ-DPSK signal measured at three different positions in the setup, indicated as A, B, and C in Fig. 4.15. These are the idlers obtained after the first stage of FWM, behind the chirped FBG, and after the second stage of FWM, respectively. At points A and B, both the eye diagrams and the spectra agree with those of a DPSK signal without demodulation [22], implying that demodulation is achieved neither by a single FWM process nor by discrimination filtering with the chirped FBG. Only after two stages of FWM, the phase modulation is converted to intensity modulation. By slightly tuning the CW pump wavelength, an additional phase shift of 0 or π can be introduced to generate an output in DB format or AMI format, respectively, as shown in Fig. 4.16 (c) and (d). The wavelength resolution of our CW pump is 0.001 nm, corresponding to a minimum phase shift of ~ 0.05π for a 20-ps/nm dispersion. To introduce a π-phase shift, the pump wavelength should be shifted by 0.02 nm to yield a 0.04-nm shift of the idler wavelength.

It is worth mentioning that the splicing loss between the PCF and the chirped FBG results in a difference of the signal powers in the two stages of FWM, possibly leading to incomplete depletion of idler 1 and hence a degraded extinction ratio (ER) of the demodulated signal, as shown in the inset of Fig. 4.16. We experimentally find that the ER can be improved by changing the signal-to-pump power ratio to a positive value of ~ 3 dB, unlike the usual case where the ratio is negative to keep the

signal weaker than the pump. With the adjustment, the residual power of bit 0 in idler 1 is reduced, as shown in the other two eye diagrams in Fig. 4.16. One also notices a finite signal distortion of AMI format compared to DB format. It can be explained by the discrete control of phase shift resulted from discrete wavelength tuning of the pump laser. When the phase shift is aligned to be 0 for the DB format, it may be difficult to tune it exactly to π to generate AMI format. The problem can be mitigated using a smaller dispersion to provide a finer tuning at a given tuning resolution of the pump wavelength.

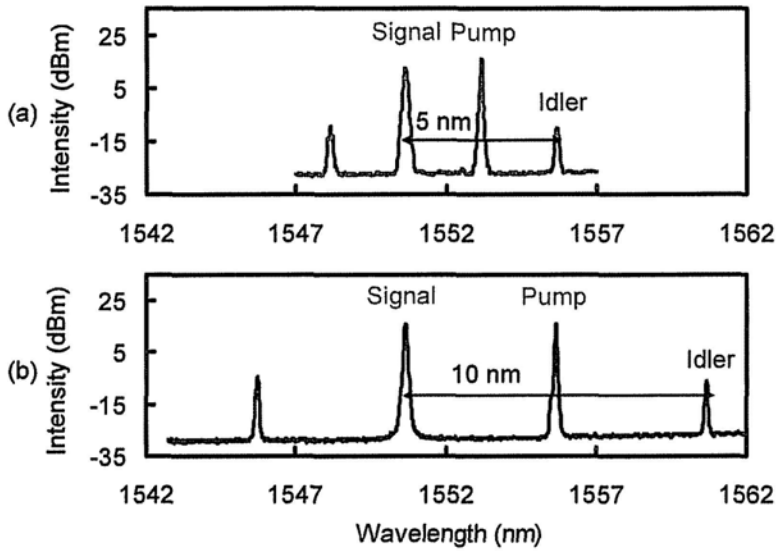

Fig. 4.17. FWM spectra in the demodulation of (a) 10-Gbit/s and (b) 5-Gbit/s DPSK signals.

To demodulate DPSK signals at different bit rates, we tune the wavelength of the CW pump to introduce a proper delay between the signal and idler 1. Fig. 4.17 (a) and (b) show the experimental FWM spectra in the demodulations of 10-Gbit/s and 5-Gbit/s

signals, respectively. The FWM efficiency, defined as the power ratio of the generated idler to the input signal, is ~ -22 dB. For 10-Gbit/s signal, the wavelength shift between the signal and idler is 5 nm, thus providing a 100-ps delay with the 20-ps/nm dispersion in the chirped FBG. For 5-Gbit/s signal, a 10-nm wavelength shift provides a 200-ps delay.

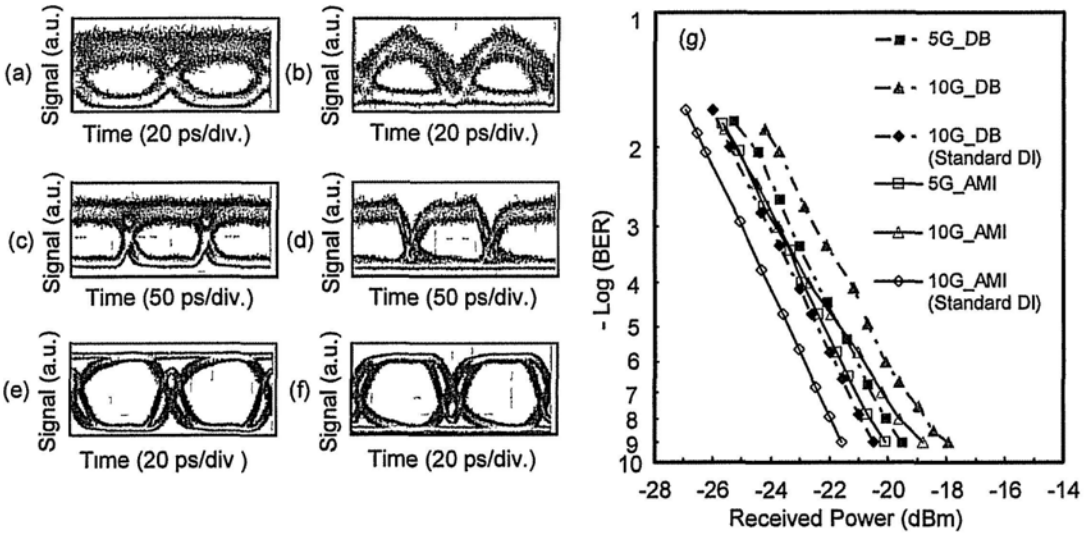

Fig. 4.18. Demodulated NRZ-DPSK signals. Bit-rate variable demodulator: (a) 10-Gbit/s DB, (b) 10-Gbit/s AMI, (c) 5-Gbit/s DB, (d) 5-Gbit/s AMI; Standard DI: (e) 10-Gbit/s DB, (f) 10-Gbit/s AMI; and (g) BER measurement of the demodulated signals.

For NRZ-DPSK signals, the demodulated signals are shown in Fig. 4.18, including 10-Gbit/s DB, 10-Gbit/s AMI, 5-Gbit/s DB and 5-Gbit/s AMI as indicated in (a)-(d). For all cases, clear eyes are obtained, demonstrating the capability of our demodulator to operate at widely variable bit rates. For comparison, the eye diagrams

of demodulated 10-Gbit/s NRZ-DPSK signals obtained from a standard fiber-based Mach-Zehnder DI with a fixed-delay of ~ 100 ps are also shown in Fig. 4.18 (e) and (f). The BER of the six signals measured with a 10-GHz single-ended photodetector are shown in Fig. 4.18 (g). In general, the NRZ-AMI format has a higher receiver sensitivity compared to NRZ-DB format due to a difference in the pulse shape caused by transient phase modulation at the rising edge and falling edge. For 10-Gbit/s NRZ-DPSK signal, the standard DI exhibits 2.5 and 2.8 dB improvement in the receiver sensitivities over our bit-rate variable demodulator for DB and AMI formats, respectively. The difference can be explained by the occurrence of ASE noise in the EDFA and signal degradation in FWM in the bit-rate variable scheme. The additional 0.3 dB degradation of AMI may result from the discrete phase tuning as mentioned above.

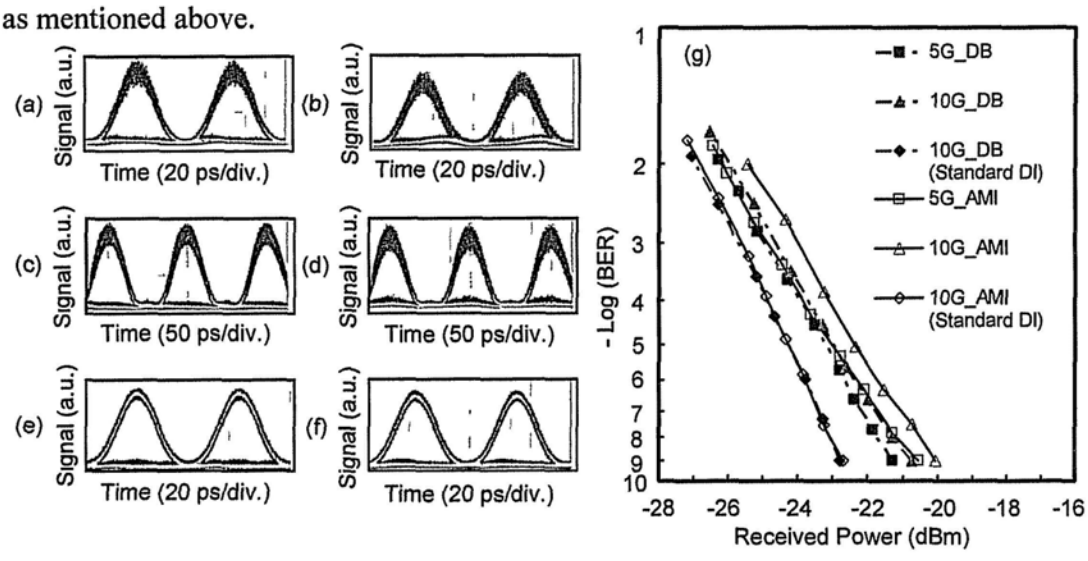

Fig. 4.19. Demodulated RZ-DPSK signals. Bit-rate variable demodulator: (a) 10-Gbit/s DB, (b) 10-Gbit/s AMI, (c) 5-Gbit/s DB, (d) 5-Gbit/s AMI; Standard DI: (e) 10-Gbit/s DB, (f) 10-Gbit/s AMI; and (g) BER measurement of the demodulated signals.

The results of RZ-DPSK signals with a duty cycle of ~ 50% are also shown in Fig. 4.19 (a) - (g). For the standard DI, DB and AMI formats show almost identical receiver sensitivities. For variable bit-rate demodulation, however, RZ-AMI has a smaller tolerance to discrete phase tuning compared to NRZ-AMI, resulting in an additional degradation of 0.7 dB with reference to RZ-DB.

For further miniaturization of our setup, integrated devices can be used to replace the fiber components. A chirped vertical grating based on SOI technology has been demonstrated in [23], providing a 7.0×10^5 ps/nm/km dispersion with an acceptable level of reflectance. Combining with a silicon nano-waveguide [19], both the functionalities of wavelength conversion and dispersion can be possibly integrated into a tiny silicon chip.

In conclusion, a bit-rate variable DPSK demodulator is demonstrated in a straight-line structure. The setup exploits a process similar to phase sensitive amplification using cascaded FWM in a 41-m PCF separated by a tunable optical delay. The delay is obtained from wavelength conversion followed by dispersion in a chirped fiber Bragg grating. By tuning the delay, NRZ-DPSK and RZ-DPSK signals at 10 Gbit/s and 5 Gbit/s are demodulated with error-free performances. The switching between DB and AMI formats is also achieved by the fine control of the delay.

References

[1] A. H. Gnauck and P. J. Winzer, "Optical phase-shift-keyed transmission," J. Lightw. Technol., vo. 23, no. 1, pp. 115-130, Jan. 2005.

[2] K. Voigt, L. Zimmermann, G. Winzer, T. Mitze, J. Bruns, K. Petermann, B. Huttl, and C. Schuber, "Performance of 40-Gbit/s DPSK demodulator in SOI-technology," IEEE Photon. Technol. Lett., vol. 20, no. 8, pp. 614-616, Apr. 2008

[3] L. Christen, Y. Lize, S. Nuccio, A. Willner, and L. Paraschis, "Variable rate, multi-format receiver design for 10 to 40 Gbit/s DPSK and OOK formats," Opt. Express, vol. 16, no. 6, pp. 3828-3833, Mar. 2008.

[4] C. W. Chow and H. K. Tsang, "Polarization-independent DPSK demodulation using a birefringent fiber loop," IEEE Photon. Technol. Lett., vol. 17, no. 6, pp. 1313-1315, Jun. 2005.

[5] M. P. Fok and C. Shu, "Delay-asymmetric nonlinear loop mirror for DPSK demodulation," Opt. Lett., vol. 33, no. 23, pp. 2845-2847, Dec. 2008.

[6] G. Davide, G. Gianluca, L. Paolo, L. Stefano, J. Davide, G. Andrea, and B. Michele, "Demonstration of differential phase-shift keying demodulation at 10 Gbit/s optimal fiber Bragg grating filters," Opt. Lett., vol. 33, no. 13, pp. 1512-1514, Jul. 2008.

[7] L. Xu, C. Li, C. Wong, and H. K. Tsang, "Optical differential-phase-shift-keying demodulation using a silicon microring resonator," IEEE Photon. Technol. Lett., vol. 21, no. 5, pp. 295-297, Mar. 2009.

[8] Y. K. Lizé, L. Christen, X. Wu, J.-Y. Yang, S. Nuccio, T. Wu, A. E. Willner, and R. Kashyap, "Free spectral range optimization of return-to-zero differential

phase shift keyed demodulation in the presence of chromatic dispersion," Opt. Express, vol. 15, no. 11, pp. 6817-6822, May. 2007.

[9] Y. K. Lize, L. Christen, M. Nazarathy, Y. Atzmon, S. Nuccio, P. Saghari, Robert G., J.-Y. Yang, R. Kashyap, A. E. Willner, and L. Paraschis, "Tolerances and receiver sensitivity penalties of multibit delay differential-phase shift-keying demodulation," IEEE Photon. Technol. Lett., vol. 19, no. 23, pp. 1874-1876, Dec. 2007.

[10] K. Y. Song, M. G. Herraez, and L. Thevenaz, "Observation of pulse delaying and advancement in optical fibers using stimulated Brillouin scattering," Opt. Express, vol. 13, no. 1, pp. 82-88, Jan. 2005.

[11] L. Yi, W. Hu, Y. Su, M. Gao, and L. Leng, "Design and system demonstration of a tunable slow-light delay line based on fiber parametric process," IEEE Photon. Technol. Lett., vol. 18, no. 24, pp. 2575-2577, Dec. 2006

[12] E. Myslivets, N. Alic, J. R. Windmiller, R. M. Jopson, and S. Radic, "400-ns continuously tunable delay of 10-Gbit/s intensity modulated optical signal," IEEE Photon. Technol. Lett., vol. 21, no. 4, pp. 251-253, Feb. 2009.

[13] L. Christen, O. F. Yilmaz, S. Nuccio, X. Wu, I. Fazal, A. E. Willner, C. Langrock, and M. M. Fejer, "Tunable 105 ns optical delay for 80 Gbit/s RZ-DQPSK, 40 Gbit/s RZ-DPSK, and 40 Gbit/s RZ-OOK signals using wavelength conversion and chromatic dispersion," Opt. Lett., vol. 34, no. 4, pp. 542-543, Feb. 2009.

[14] K. Inoue, "Tunable and selective wavelength conversion using fiber four-wave mixing with two pump lights," IEEE Photon. Technol. Lett., vol. 6, no. 12, pp.

1451-1453, Dec. 1994.

[15]J. Du, Y. Dai, G. K. P. Lei, W. Tong, and C. Shu, "Photonic crystal fiber based Mach-Zehnder interferometer for DPSK signal demodulation," Opt. Express, vol. 18, no. 8, pp. 7917-7922, Mar. 2010

[16]L. Yi, Y. Jaouen, W. Hu, J. Zhou, Y. Su, and E. Pincemin, "Simultaneous demodulation and slow light of differential phase-shift keying signals using stimulated-Brillouin-scattering-based optical filtering in fiber," Opt. Lett., vol. 32, no. 21, pp. 3182-3184, Nov. 2007.

[17]A. Mecozzi, et al., "Optical spectral inversion without frequency shift by four-wave mixing using two pumps with orthogonal polarization," IEEE Photon. Technol. Lett., vol. 10, no. 3, pp. 355-357, Mar. 1998.

[18]P. Martelli, et al., "All-optical wavelength conversion of a 100-Gbit/s polarization-multiplexed signal," Opt. Express, vol. 17, no. 20, pp. 17758-17763, Sep. 2009.

[19]N. Ophir, et al., "Continuous wavelength conversion of 40-Gbit/s data over 100 nm using dispersion-engineered silicon waveguide," IEEE Photon. Technol. Lett., vol. 23, no. 2, pp. 73-75, Jan. 2011.

[20]M. D. Pelusi, F. Luan, S. Madden, D.-Y. Choi, D. A. Bulla, B. Luther-Davies, and B. J. Eggleton, "Wavelength conversion of high-speed phase and intensity modulated signals using a highly nonlinear chalcogenide glass chip," IEEE Photon. Technol. Lett., vol. 22, no. 1, pp. 3- 5, Jan. 2010.

[21]K. Croussore and G. Li, "Phase regeneration of NRZ-DPSK signals based on

symmetric-pump phase sensitive amplification," IEEE Photon. Technol. Lett., vol. 19, no. 11, pp. 864-866, Jun. 2007.

[22]P. J. Winzer and R.-J. Essiambre, "Advanced modulation formats for high-capacity optical transport networks," J. Lightw. Technol., vol. 24, no. 12, pp. 4711-4728, Dec. 2006.

[23]D. T. H. Tan, et al., "Chip-scale dispersion engineering using chirped vertical gratings," Opt. Lett. 33, 3013-3015 (2008).

5 BIT-RATE VARIABLE CLOCK RECOVERY OF NRZ-DPSK SIGNALS

Clock recovery is a fundamental building block for optical processing such as logic operation, time-division demultiplexing, pulse format conversion, and 3R regeneration. It is required in optical network nodes to prepare data packets for their next hop, like to add or drop tributaries in optical time division multiplexing (OTDM) system, to convert NRZ signal to RZ signal, or to converted amplitude-modulated signal to phase-modulated signal [1]. It can also be implemented in middle of a transmission link to achieve retiming.

For a RZ-ASK signal, different clock recovery approaches have been demonstrated using electro-optical phase-locking loop [2], SOA-based ring laser or self-pulsing distributed feedback laser with injection-locking [3, 4], Fabry-Perot filter [5], and SBS loop [6, 7]. These approaches are also readily used for clock recovery of NRZ-ASK signal with an additional preprocessing element to convert NRZ signal to pseudo-return-to-zero signal [8, 9].

Clock recovery for DPSK signal is also important as the format has demonstrated superior transmission performance and improved receiver sensitivity with balanced detection. For RZ-DPSK format, the data signal itself is almost a clock with possibly time jitter introduced during the transmission. Most approaches applicable to RZ-ASK signal can be directly used for RZ-DPSK signal. However, for NRZ-DPSK

signal generated either with a phase modulator (PM) or a MZM, only very weak clock tones, if any, can be found. A preprocessing step is thus required before the clock recovery to regenerate or to enhance the clock tones [10, 11]. Although clock recovery of MZM-generated NRZ-DPSK signal can be achieved directly by using a self-pulsating distributed Bragg reflector laser [12], the PM-generated NRZ-DPSK signal will require some preprocessing. Examples of preprocessing include demodulation using DI [11, 13], narrow band optical filtering [10], and phase-modulation to intensity-modulation conversion using chromatic dispersion [14]. Following the preprocessing, the recovery circuit can be built using a Fabry-Perot filter [10] or SOA ring laser [11, 13, 14].

In this chapter, bit-rate variable clock recovery of NRZ-DPSK signal is demonstrated. The clock recovery schemes combine different preprocessing methods and bit-rate transparent clock extraction based SBS loop. In section 5.1, the working principle of SBS loop for clock extraction is introduced. In section 5.2, combining with a preprocessing using fiber-based DI, a wideband clock recovery circuit for NRZ-DPSK signal is demonstrated. In section 5.3, the DI is replaced by DANLM to achieve a bit-rate tunable NRZ-DPSK clock recovery circuit.

5.1 Bit-Rate Transparent Clock Recovery Using SBS Loop

Most of the demonstrated approaches on clock recovery work at fixed bit rate or a limited range of bit rates, although bit-rate tunable processing can offer a high flexibility in optical network management. A few examples of bit-rate variable clock recovery schemes includes clock recovery for RZ-ASK signal using SBS loop [6], clock recovery for NRZ-ASK signal using SOA-based preprocessing and a compact self-pulsating laser with a small tunable range of bit-rates [15] or using a Gaussian filter together with an optimal clock recovery unit with enhanced operation range [16]. All techniques assume some prior knowledge about the bit rate of the signal except the one based on SBS loop, making it outstanding in some circumstances where the data rate is completely unknown. Its validity for ASK signal has been demonstrated and it would be useful to extend this function to DPSK signal.

The structure of SBS loop for clock recovery is shown in Fig. 5.1 (a), which works as an active filter. Fig. 5.1 (b) explains its working principle. It utilizes the strong clock tones in the optical spectrum of a phase-constant RZ-ASK signal, and exclusively amplifies the clock tones compared to the information-bearing components. After that, the signal will become an optical clock.

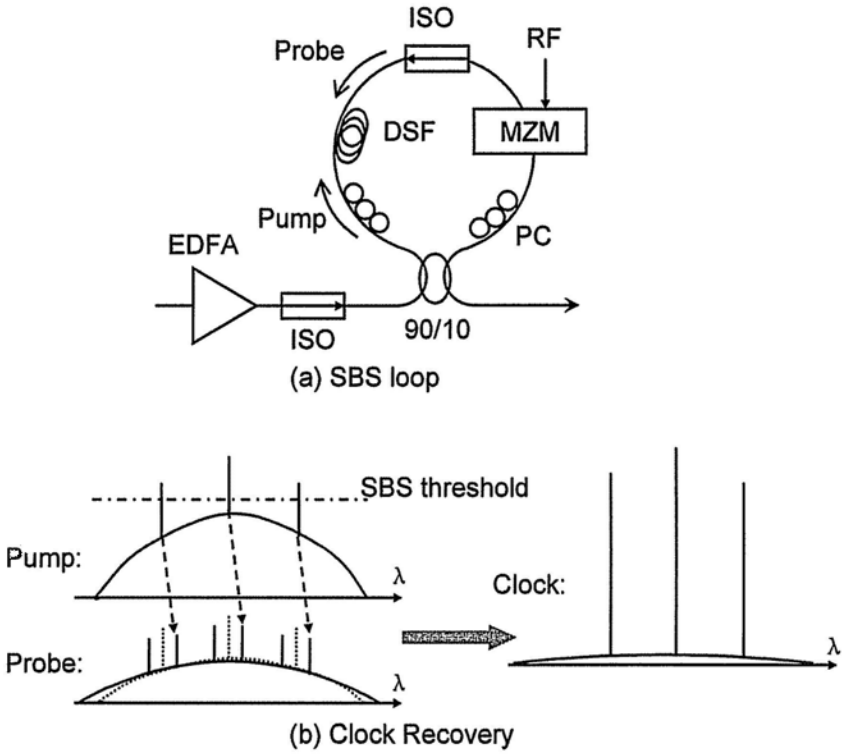

Fig. 5.1. SBS loop for clock recovery; (a) SBS loop; (b) working principle of clock recovery. ISO: optical isolator; DSF: dispersion shifted fiber; MZM: Mach-Zehnder modulator; PC: polarization controller. The probe is generated from the carrier-suppressed modulation of original signal. Dash line: spectrum before modulation; solid line: spectrum after modulation.

The exclusive amplification can be achieved in the SBS loop. The input signal is first split to two branches with large power ratio (for example, ~ 10 dB in Fig 5.1 (b)). The stronger branch is the pump for SBS process. The smaller branch needs to be modulated in addition by a MZM with bias at null point, and the carrier-suppressed modulation will generate two copies of the original signal: one is red-shifted and the other is blue-shifted. The red-shifted copy is the probe for SBS process by setting the

modulation frequency equal to Stokes shift of Brillouin scattering. When the pump and probe counter-propagates with each other in a nonlinear medium, like dispersion shifted fiber (DSF), with a proper power control to make only the power of clock tones in pump reach the SBS threshold, the clock tones in probe will be amplified by the SBS process. Since the gain bandwidth of SBS is ~ 20 MHz, only the clock tones will be amplified. The amplified probe is no other than a recovered optical clock signal.

5.2 Wideband Clock Recovery of NRZ-DPSK Signal Using Fiber-Based DI

As mention in last section, a NRZ-DPSK signal has no clock tones due to its constant intensity and hence preprocessing is required to generate and enhance the clock tones. The essential idea of preprocessing is to convert the phase modulation to intensity modulation in a RZ format. An effective method to achieve this function is demodulation of NRZ-DPSK signal using DI with a delay less than one bit. Since the "less-than" requirement on the delay is quite lax, a DI is possible to work over a wide bit-rate range to generate clock tones. Moreover, if an optical circuit can recover clocks over a compatible bit-rate range, the combination of the two produces a possibility to construct a wideband clock recovery unit. In this section, the SBS loop will work together with a fiber-based DI to demonstrate such a clock recovery unit.

As shown in Fig. 5.2, a fiber-based DI is used as demodulator for NRZ-DPSK signal at different bit rates. The delay of DI is smaller than one bit period of the maximum bit rate, so the output at the destructive port of DI is in a RZ format, which discloses the clock information of the original NRZ-DPSK signal. For different bit rates, the ratios between delay of DI and one bit period are changing, leading to varying duty cycles of the obtained RZ signals. The influence of duty-cycle variation on clock recovery performance is interesting to look at.

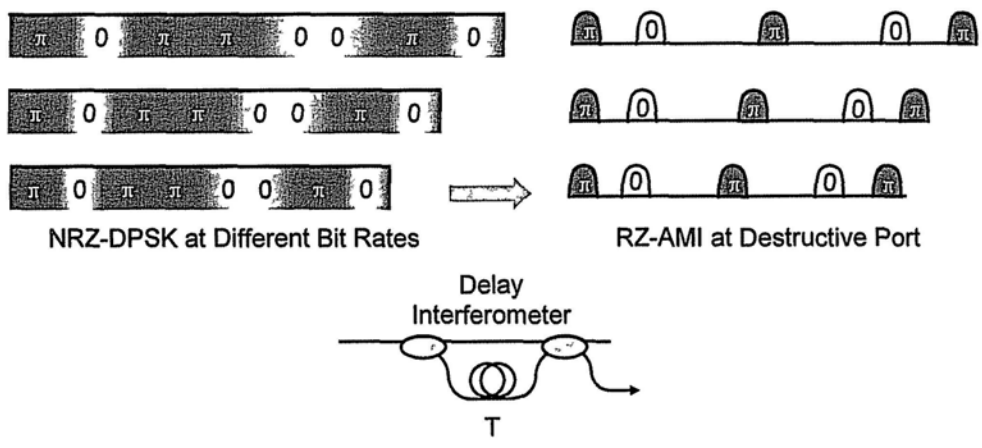

Fig. 5.2. RZ format generation using a DI. AMI: alternate mark inversion.

One should note that the obtained RZ signals are still not ready for clock recovery using SBS loop since the loop requires strong optical clock tones to distinguish them from other weaker information-bearing spectral components. The obtained signals, although in a RZ format, have varying optical phase since they are also in an AMI format [17], which strongly weakens the optical clock tones. To enhance the optical clock tones, the phase variation of the RZ signals must be erased to generate phase-constant RZ-ASK signals. The phase erasure can be implemented using phase insensitive processes, like XPM and XGM, to extract only the intensity information of the RZ-AMI signals. In proposed scheme, the phase erasure is implemented using XPM in a nonlinear polarization rotation (NPR) format [18] since it can provide an excellent extinction ratio of modulation over a large range of bit rates.

Fig. 5.3 shows all the stages in the wideband clock recovery circuit. In the circuit, the signal starts from a NRZ-DPSK signal, evolves step by step with each step to

enhance its optical clock tones, and becomes a clock signal at the output of the circuit. In principle, the NPR-based phase erasure and SBS-loop-based clock recovery can work at bit rates from several Gbit/s to hundreds of Gbit/s. The fiber-based DI is the bottleneck of the clock recovery unit. In our experiment, the capability of DI with a fixed delay of 50 ps will be investigated.

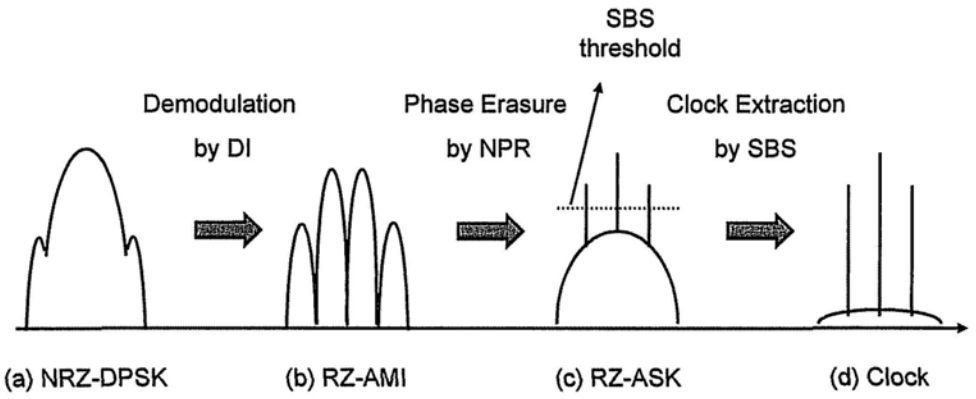

Fig. 5.3. Signal evolution in the wideband clock recovery circuit. DI: delay interferometer; NPR: nonlinear polarization rotation; SBS: stimulated Brillouin scattering.

The experimental setup is shown in Fig. 5.4. A PM-generated NRZ-DPSK signal at the wavelength of 1549.3 nm is fed into the standard DI for demodulation. To investigate the influence of input OSNR on clock recovery performance, an ASE noise is used to contaminate the NRZ-DPSK signal before the DI. It is turned on only when we characterize the OSNR response of our circuit. The OSNR is modified by changing the noise power with a variable optical attenuator (VOA). After the DI, a RZ-AMI signal is obtained at the destructive port (see point "b" in Fig. 5.4). The

AMI signal and a CW probe at the wavelength of 1552.4 nm are combined together, amplified to a total power of ~ 17 dBm, and fed into a 1-km HNLF to perform the NPR. The polarization of AMI signal is adjusted to 45 degrees to that of the probe, and the polarization-rotated probe is selected by a polarization beam splitter. The residual AMI signal is rejected by an optical bandpass filter and a RZ-ASK signal with constant phase is obtained (see point "c" in Fig. 5.4). The RZ-ASK signal is amplified to ~ 28 dBm and launched into a SBS loop. The SBS loop is composed by a 90/10 coupler, an 11-km DSF, an optical isolator, and a MZM. The coupler splits the RZ-ASK signal into a 10% branch and a 90% branch with the larger one ready for working as the SBS pump. The smaller branch is modulated by the MZM, which is biased at the null point and driven by a sinusoidal signal at the frequency of 10.511 GHz, equal to the Stokes shift of Brillouin scattering in the DSF. The modulation generates a red-shifted copy, which is the SBS probe. The probe counter-propagates with the SBS pump in the DSF, and its clock tones are amplified through SBS gain as the intensity of optical clock tones of the pump is higher than the SBS threshold. The information-bearing components, however, are intact because the intensity of their pump does not reach the SBS threshold. The amplified probe (see point "d" in Fig. 5.4) is a recovered clock signal. The clock is further fed into a SOA (Kamelian, model OPA-20-N-C-FA) to suppress its amplitude noise using gain saturation effect (see point "e" in Fig. 5.4). The recovered clock is detected and analyzed by wideband oscilloscope and RF spectrum analyzer.

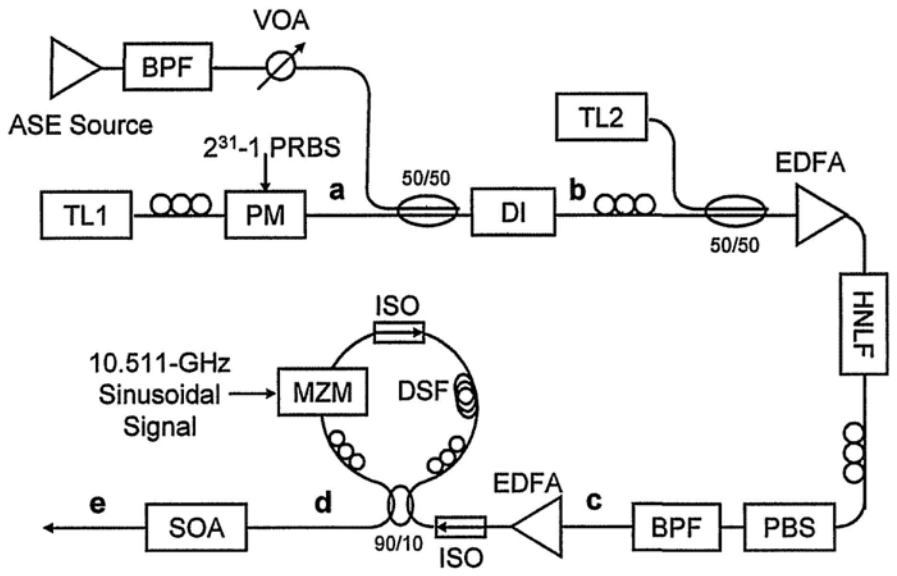

Fig. 5.4. Experimental setup of wideband clock recovery circuit. ASE: amplified spontaneous emission; BPF: bandpass filter; VOA: variable optical attenuator; TL: tunable laser; PM: phase modulator; DI: delay interferometer; HNLF: highly nonlinear fiber; PBS: polarization beam splitter; ISO: optical isolator; DSF: dispersion shifted fiber; MZM: Mach-Zehnder modulator; SOA: semiconductor optical amplifier.

Fig. 5.5 shows the optical spectrum and waveform evolution in our setup, taking the 10-Gbit/s NRZ-DPSK as an example. The monitored positions are the points a-e indicated in Fig. 5.4. Starting from a NRZ-DPSK signal, clock tones are first obtained by demodulating the signal in the DI. After erasing the phase variation of RZ-AMI signal, strong optical clock tones is generated in RZ-ASK signal. The optical clock tones are amplified in the SBS loop and in the time domain, the clock is recovered. It seems that only three optical clock tones have higher intensity than

information-bear components in Fig. 5.5 (c). However, we can find that six clock tones have been amplified in Fig. 5.5 (d). The discrepancy ensues from the limited resolution of optical spectrum analyzer (0.01 nm). The amplitude noise of recovered clock is suppressed by gain saturation effect of the SOA and the spectrum in Fig. 5.5 (e) broadens a little owing to self phase modulation and intra four-wave mixing in the SOA.

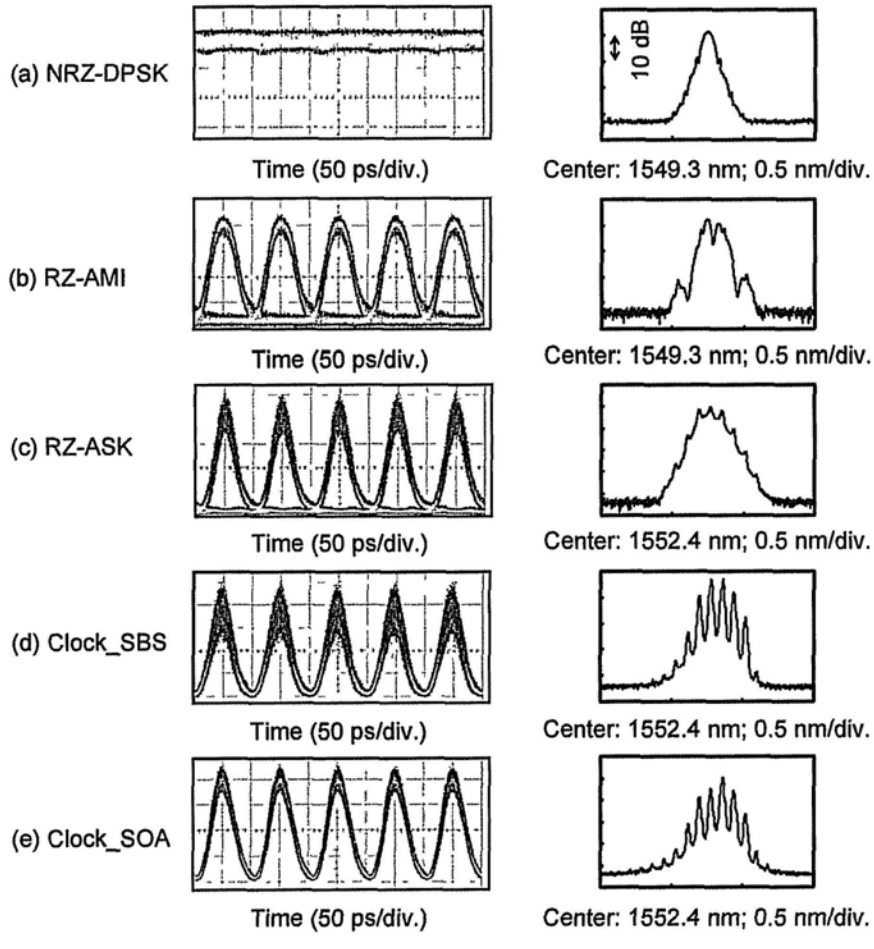

Fig. 5.5. Optical spectrum and waveform evolution in clock recovery of 10-Gbit/s NRZ-DPSK.

After detected by a 32-GHz photodetector, the clock signal is characterized in a RF spectrum analyzer. Fig. 5.6 plots the RF spectrum and single sideband (SSB) phase noise of the recovered 10-GHz clock. The intensity ratio of clock tones to information-bearing components increases to 48 dB for the recovered clock signal. By integrating the phase noise power from 10 Hz to 1 MHz (five decades is the maximum range available in our analyzer), the rms time jitter of the recovered 10-GHz clock is evaluated to be 465 fs.

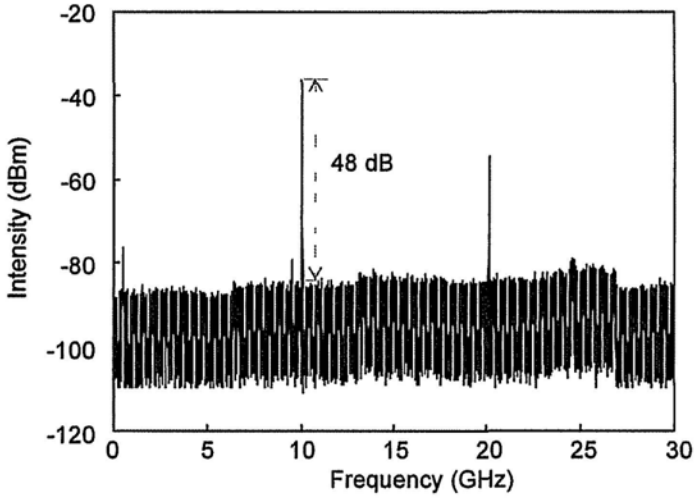

(a) RF spectrum

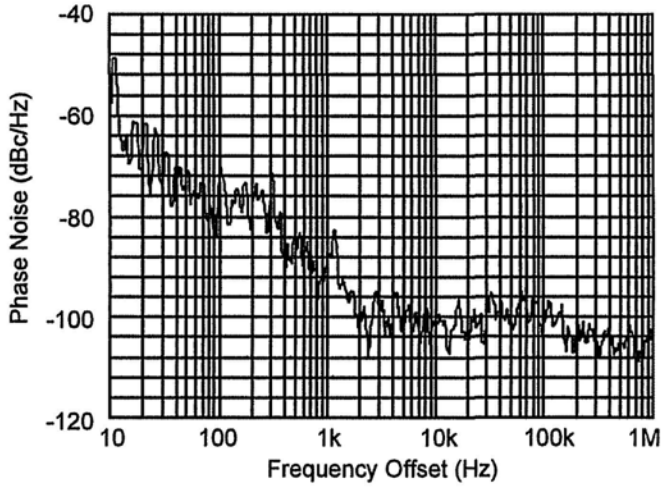

(b) SSB Phase Noise

Fig. 5.6. RF spectrum (a) and SSB phase noise (b) of the recovered 10-GHz clock. SSB: single sideband.

To demonstrate the wide bit-rate range that our circuit covers, Fig. 5.7 shows the accumulated diagrams of recovered clock at bit rate varying from 7.5 to 15 Gbit/s. The pattern of NRZ-DPSK signal is a PRBS with length of 2^{31}-1 and the accumulating time is ~ 10 seconds. The input RZ-AMI signals are also shown in the left side, with time jitter increasing with bit rates.

Fig. 5.8 shows the rms time jitter of the recovered clock at different bit rates, ranging from 409 to 743 fs. The jitter fluctuation is less than 250 fs over the bit-rate range from 7.5 to 15 Gbit/s. The increase of time jitter at lower bit rates may result from the power reduction of the RZ-AMI signal. The reduction is due to the fixed power of NRZ-DPSK signal at the input of DI and smaller duty cycle of RZ-AMI signal at lower bit rates. If we readjust the power to optimize the NPR performance, the increase can be mitigated and the time jitter at 7.5 Gbit/s can be reduced to ~ 620 fs. The bit-rate variation also leads to the change of time jitter of RZ-AMI signal. The jitter varies between 2.4 and 4.9 ps over the bit-rate range. It should be mentioned that different from the time jitter of recovered clock, which is calculated using the SSB phase noise, the time jitter of RZ-AMI signal is directly measured by the wideband oscilloscope since it is at the level of several ps. The time jitter of recovered clock is found insensitive to the jitter variation of RZ-AMI signal, especially compared with the sensitivity to the NPR performance, which is mainly determined by the power ratio of RZ-AMI signal to CW probe. For example, although the time jitter of RZ-AMI signal at 15 Gbit/s is as large as 4.9 ps, we can

still optimize the time jitter of recovered clock to ~ 500 fs by readjusting the power of the RZ-AMI signal, close to the performance at 13 Gbit/s with a RZ-AMI time jitter of 2.9 ps.

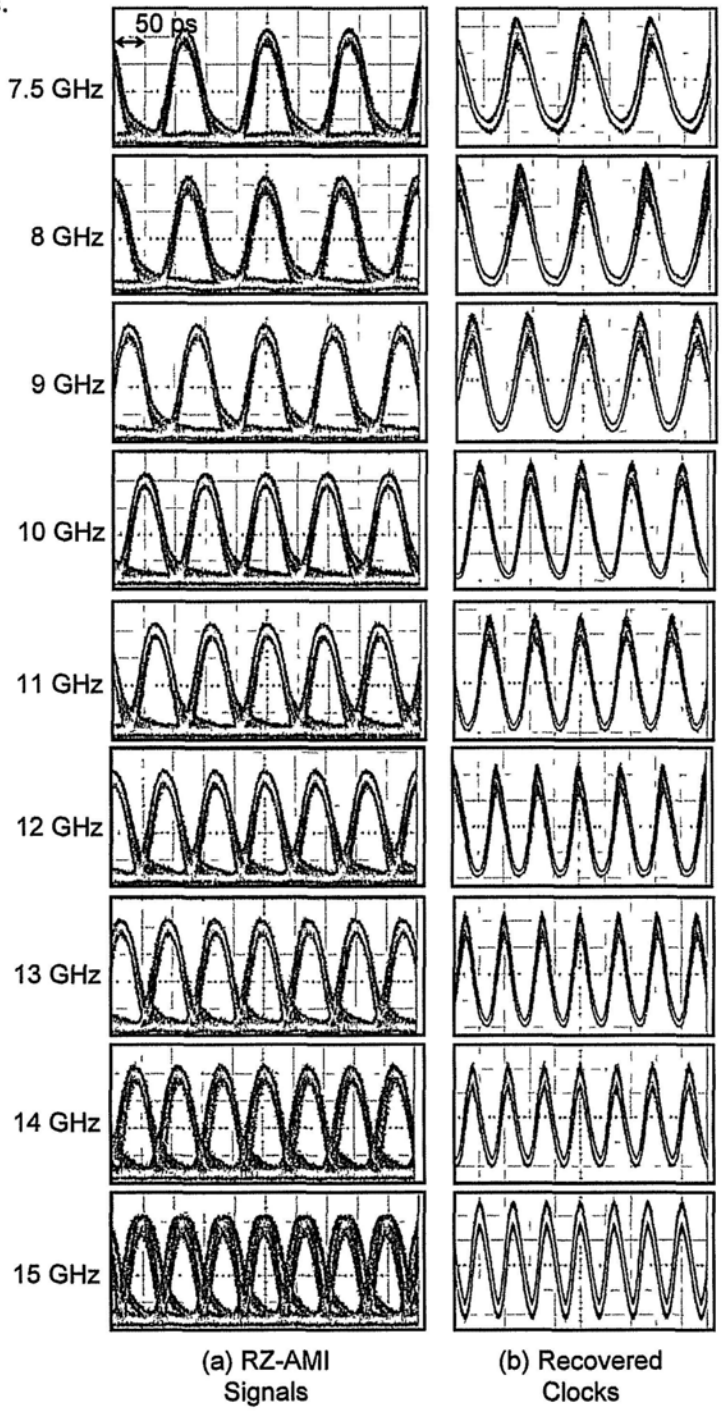

Fig. 5.7. (a) Input RZ-AMI signals after DI and (b) recovered clocks of NRZ-DPSK signals after SOA with bit-rate varying from 7.5 to 15 Gbit/s.

To investigate the influence of input OSNR on clock recovery performance, we fix the bit rate at 10 Gbit/s and turn on the ASE noise source. The OSNR varies from 40 dB to 10 dB by changing the noise power. The time jitter decreases with the OSNR and is less than 1 ps when the OSNR is larger than 14 dB, as shown in Fig. 5.9. However, it increases quickly when the noise it too large. Large noise disturbs NPR performance, which is essential to generate optical clock tones.

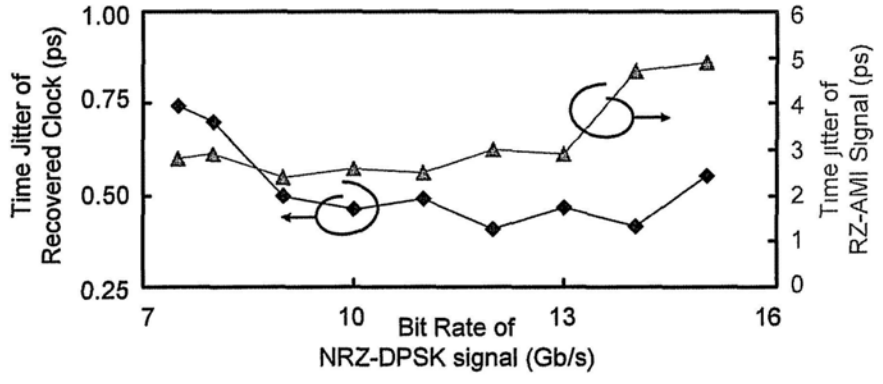

Fig. 5.8. RMS Time jitters of RZ-AMI signals and recovered clocks at different bit rates.

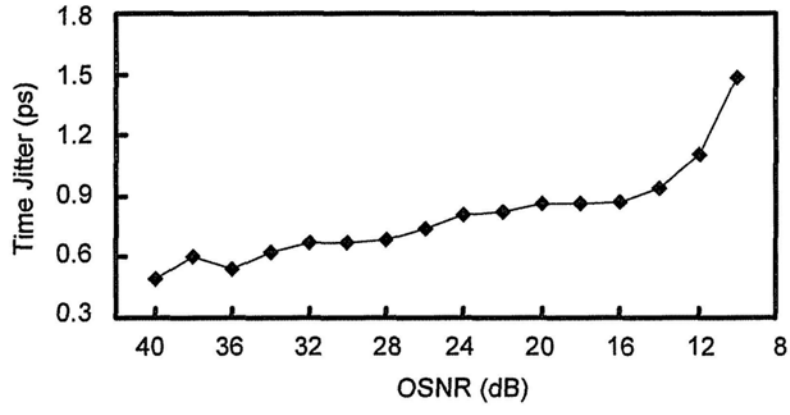

Fig. 5.9. Time jitter of recovered clock of 10-Gbit/s NRZ-DPSK signal at different input OSNR.

In conclusion, a wideband clock recovery circuit for NRZ-DPSK signal is demonstrated. The circuit utilizes a wideband NRZ-DPSK to RZ-AMI demodulation in a standard DI and bit-rate transparent phase erasure by NPR, clock recovery by SBS loop and amplitude noise suppression by SOA. Without any adjustment, clock of NRZ-DPSK signal at bit rate varying from 7.5 to 15 Gbit/s is recovered, with a rms time jitter between 409 and 743 fs over the bit rate range. The influence of both the input time jitter and OSNR is investigated, and the performance of NPR is found to be dominating in the circuit.

5.3 Bit-Rate Tunable Clock Recovery of NRZ-DPSK Signal Using DANLM

The bandwidth of NRZ-DPSK preprocessing using fiber-based DI is limited due to that the delay is fixed. Therefore, if the delay-fixed DI is replaced by a delay-tunable one, the bit-rate range covered by the clock recovery circuit would be enlarged. As discussed in chapter 3, DANLM is such a kind of DI. In this section, we use DANLM to process NRZ-DPSK signal and try to make the clock recovery circuit work over a larger range of bit rates.

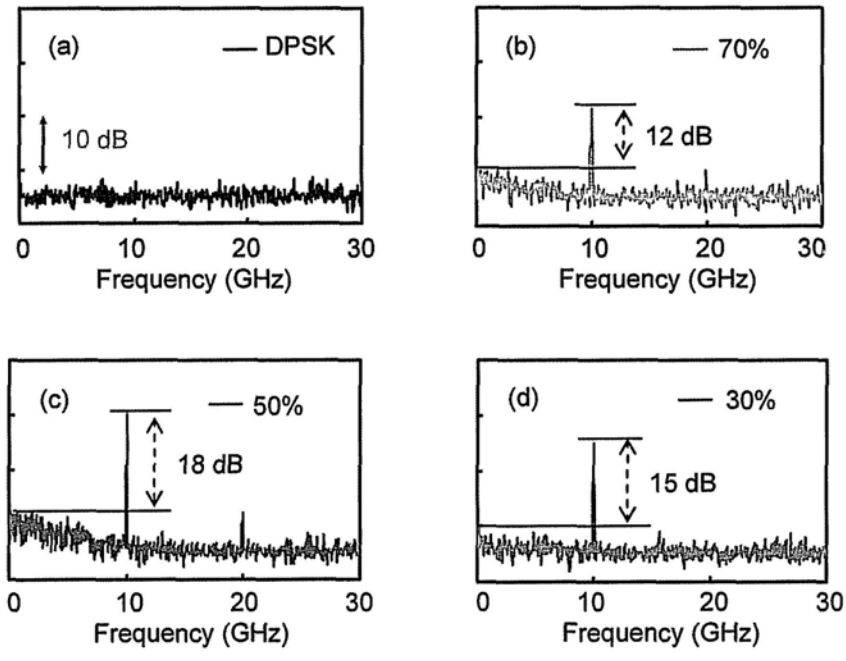

Fig. 5.10. RF spectra of (a) input NRZ-DPSK signal and (b)-(d) output RZ-AMI signals at different duty cycles.

The SBS loop needs to distinguish the clock tones from information-bearing components, so the power difference between them is desired to be as large as

possible. Since the DANLM can provide a tunable delay, we can change the delay to find a RZ-AMI signal with optimized duty cycle to produce a largest difference between clock tones and information-bearing components. Fig. 5.10 shows the measured RF spectra of 10-Gbit/s RZ-AMI signal with duty cycles of 70, 50, and 30%, and the 50% duty cycle is found to provide the largest intensity difference of 18 dB. So the delay in the DANLM is tuned to half a bit period at different bit rates to prepare RZ-AMI signals with 50% duty cycle for the SBS loop. In our setup with dispersion of 10 ps/nm, this means to maintain a relation between the pump-signal wavelength detuning ($\Delta\lambda$ nm) and bit rate (B Gbit/s) of NRZ-DPSK signal of $\Delta\lambda \cdot B = 25$.

The experimental setup is shown in Fig. 5.11, which is quite similar to the one in section 5.2 except that DANLM replaces the fiber-based DI. A PM-generated NRZ-DPSK signal at 1549.5 nm is first combined with a CW pump. The total power is boosted to ~ 26 dBm by an EDFA. The combined light waves are then directed to the DANLM, consisting of 600-m SMF and 64-m PCF as the dispersive and nonlinear media, respectively. The SMF provides a dispersion of ~ 10 ps/nm and the PCF has a nonlinear coefficient of 11 (W•km)-1 at ~ 1550 nm. The DANLM is polarization sensitive in this experiment but it can be implemented in a polarization-insensitive scheme [19]. Its output is a demodulated DPSK signal in the RZ-AMI format with duty cycle of 50%. The RZ-AMI signal is then combined with a CW probe at 1552.4 nm to perform the NPR, and the obtained phase-constant

RZ-ASK signal is launched into a SBS loop for clock recovery. The clock with a power level of ~ 6.5 dBm is further directed to a SOA (Kamelian, model OPA-20-N-C-FA) to suppress its amplitude noise using the gain saturation effect. The SOA is biased at 47 mA. Finally, we demonstrate the use of the recovered clocks in bit-rate variable conversion of NRZ-DPSK signal to RZ-DPSK signal by FWM in a HNLF.

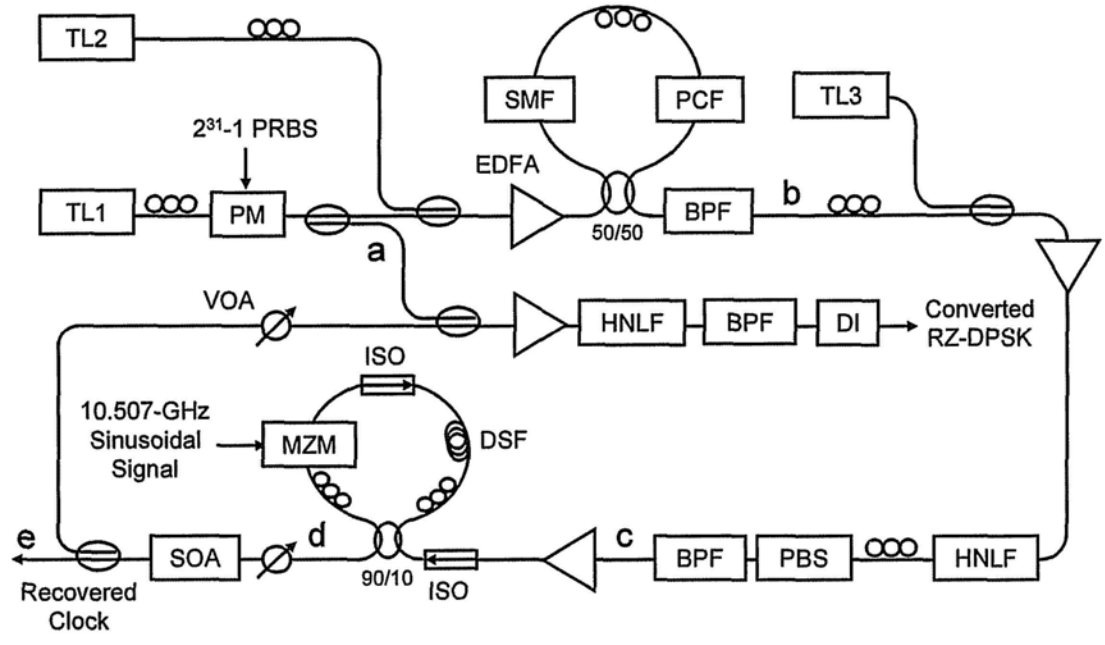

Fig. 5.11. Experimental setup of the bit-rate tunable clock recovery circuit for NRZ-DPSK signal. TL: tunable laser; PM: phase modulator; SMF: single mode fiber; PCF: photonic crystal fiber; BPF: bandpass filter; HNLF: highly nonlinear fiber; PBS: polarization beam splitter; ISO: isolator; DSF: dispersion shifted fiber; MZM: Mach-Zehnder modulator; SOA: semiconductor optical amplifier; VOA: variable optical attenuator; DI: delay interferometer.

Fig. 5.12 shows the measured optical spectrum and waveform evolution at 10-Gbit/s. The monitored positions are the points a-e indicated in Fig. 5.11. Starting from a NRZ-DPSK signal, clock tones are first obtained by demodulation with a half-bit delay of 50 ps using 2.5 nm wavelength detuning. After erasing the phase variation in the RZ-AMI signal, strong optical clock tones are generated in the RZ-ASK signal. The clock tones are amplified in the SBS loop for clock recovery. Although only three clock tones appear to have intensities higher than the information-bearing components in Fig. 5.12 (c), amplification of five clock tones is actually observed as shown in Fig. 5.12 (d). The discrepancy is caused by the limited resolution of 0.01 nm of the optical spectrum analyzer. Finally, the amplitude noise of the recovered clock is suppressed in the SOA and more clock tones appear in Fig. 5.12 (e) owing to intraband four-wave mixing effect.

Clock recovery of NRZ-DPSK signal with bit rate from 4 to 15 Gbit/s is achieved by tuning the wavelength of TL2 from 1555.75 to 1551.17 nm. The profiles of the recovered clocks shown in Fig. 5.13 are measured using the accumulated mode of the oscilloscope. The NRZ-DPSK signal is a 2^{31}-1 PRBS and the accumulating time is ~ 10 s. At low bit rates, the wavelength detuning in the DANLM is large, resulting in a weak conversion efficiency and degraded demodulation performance. Hence, the recovered clock exhibits a higher noise level and a slight distortion. The upper limit of the bit rate in this work is restricted by our phase modulator. However, if the operation is above 40 Gbit/s, one may need to explore other techniques like

fiber-based optical power limiter [20] to replace the SOA that has a finite recovery time.

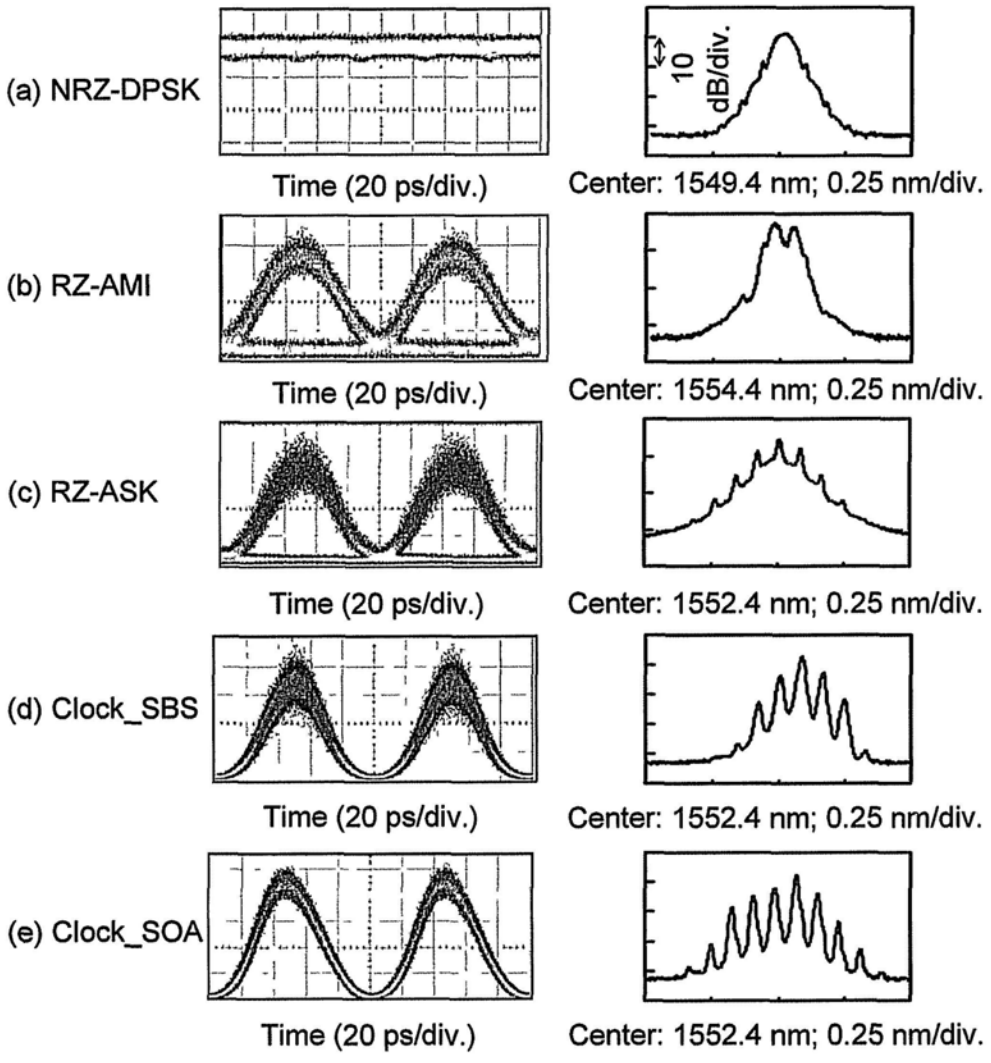

Fig. 5.12. Optical spectrum and waveform evolution in the clock recovery of 10-Gbit/s NRZ-DPSK.

To quantitatively evaluate the clock recovery performance, the clock signal is analyzed using an RF spectrum analyzer (Agilent 8564EC). Fig. 5.14 (a) shows the spectrum of the 10-GHz recovered clock. The intensity ratio of the main clock tone

to information-bearing components is increased from 18 (shown in Fig. 5.10 (c)) to 42 dB. The SSB phase noise spectrum of the 10-GHz clock is shown in Fig. 5.14 (b). By integrating the phase noise power from 10 Hz to 1 MHz carrier offset, the rms time jitter of the recovered 10-GHz clock is evaluated to be ~ 667 fs. The data at other bit rates are plotted in Fig. 5.14 (c). The variation of the intensity ratio is less than 4 dB and the jitter of the recovered clocks ranges from 0.5 to 1.8 ps over the entire bit-rate range. The jitter variation is less than 200 fs at high bit rates but increases rapidly at low bit rates. The reason is because the wavelength detuning in the DANLM increases with the inverse of the bit rate. For example, from 15 to 10 Gbit/s, the detuning increase only by 0.83 nm, compared to 3.47 nm from 9 to 4 Gbit/s. The jitter variation may be further suppressed by adopting a HNLF with a wider wavelength conversion bandwidth inside the DANLM.

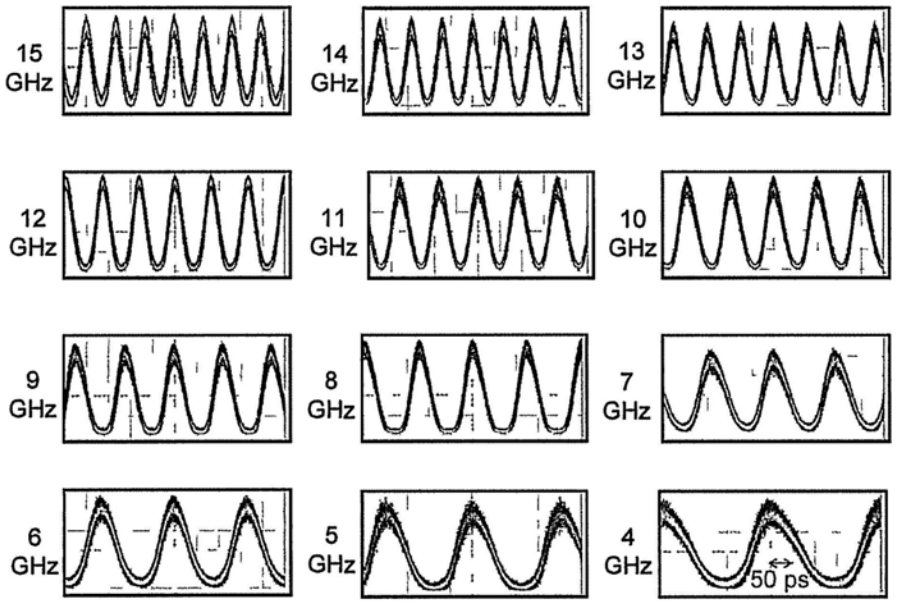

Fig 5.13 Recovered clocks of NRZ-DPSK signals with bit-rates varying from 4 to 15 Gbit/s.

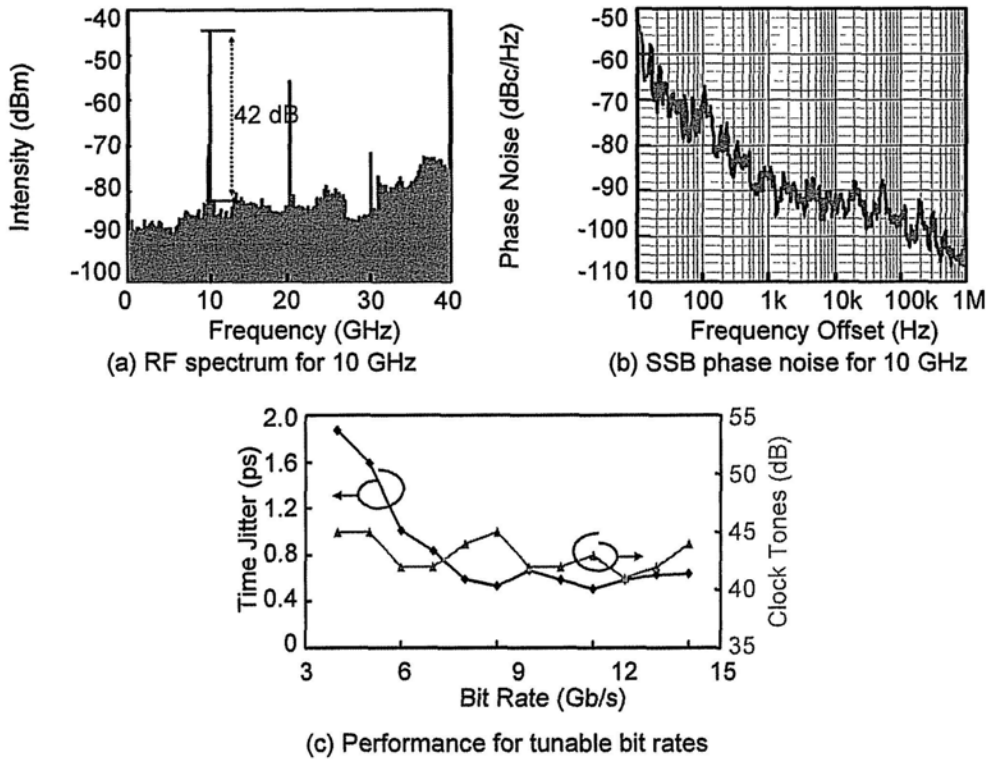

Fig. 5.14 (a) RF spectrum and (b) SSB phase noise of the recovered 10-GHz clock; (c) Time jitters of the recovered clocks and intensity ratios of clock tones to information-bearing components at different bit rates.

Using the recovered clock as a pump, NRZ- to RZ-DPSK conversion can be achieved based on FWM with the original NRZ-DPSK signal. We demonstrate the conversion at 5 and 10 Gbit/s. Fig. 5.15 shows the BER performance and corresponding eye diagrams. Compared with the NRZ formats, the RZ formats show higher receiver sensitivity. At 10 Gbit/s, although the converted RZ-DPSK signal is noisier than the RZ-DPSK signal generated from pulse carving of NRZ-DPSK signal, the error-free power penalty is only 0.4 dB owing to its smaller duty cycle. For

5-Gbit/s DPSK signal, the penalty increases to 1 dB due to larger noise of the recovered 5-GHz clock.

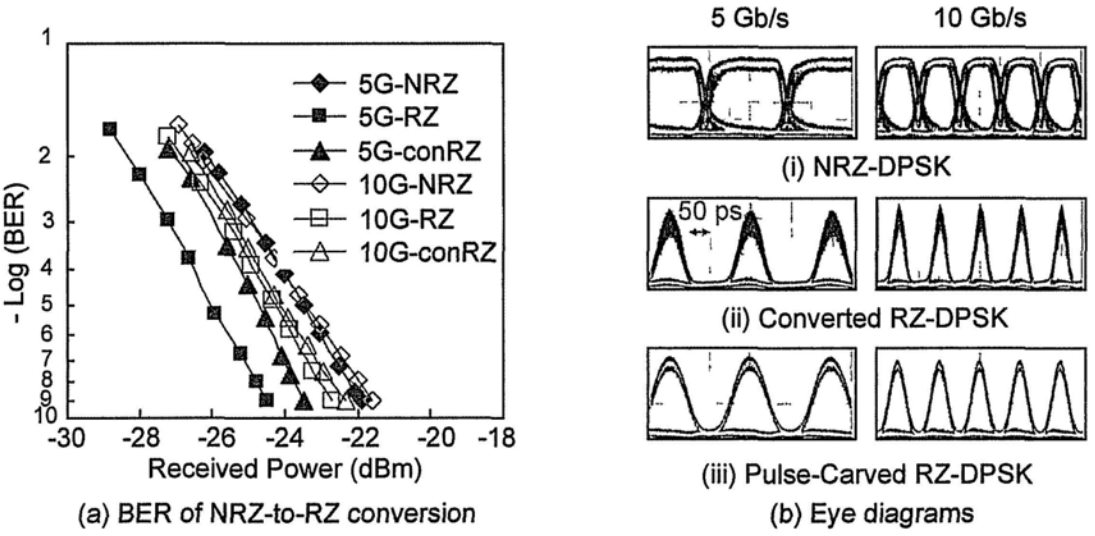

Fig. 5.15 (a) Bit-error ratio and (b) eye diagrams of original NRZ-DPSK, RZ-DPSK converted by FWM, and RZ-DPSK pulse-carved by intensity modulator

We demonstrate a continuously bit-rate tunable clock recovery scheme for NRZ-DPSK signal. The setup consists of four key processing functions: bit-rate tunable demodulation by DANLM, bit-rate transparent phase erasure by NPR, clock recovery by SBS loop, and wideband amplitude noise suppression by SOA. Optical clocks are recovered at bit rates ranging from 4 to 15 Gbit/s. The rms time jitters of the recovered clocks are evaluated by integration of the SSB phase noise and are found to vary from 0.5 to 1.8 ps. The recovered clocks are used for NRZ-DPSK to RZ-DPSK format conversion based on FWM at variable bit rates with <1 dB penalties.

Table B: Comparison of various clock recovery schemes of NRZ-DPSK signal

NRZ-DPSK Clock Recovery		Bit-rate Variability	Wavelength Variability	System Architecture	Modulator Limitation	Time Jitter (fs)
Preprocessing	Clock recovery					
DI [11]	SOA ring laser	*Fixed*	*Tunable*	*Moderate*	*NO*	*800*
Birefringent loop mirror [13]	SOA ring laser	*Fixed*	*Tunable*	*Moderate*	*NO*	*750*
SMF [14]	SOA ring laser	*Fixed*	*Tunable*	*Moderate*	*NO*	*718*
TMF [21]	SOA ring laser	*Fixed*	*Tunable*	*Moderate*	*NO*	*<1600*
N/A	Self-pulsating DBR laser diode [12]	*Fixed*	*Wideband*	*Simple*	*MZM only*	*760*
FBG [10]	FP filter	*Fixed*	*Fixed*	*Moderate*	*NO*	*710*
DI+NPR	SBS loop	*Wideband*	*Wideband*	*Moderate*	*NO*	*500*
DANLM+NPR	SBS loop	*Tunable*	*Tunable*	*Complex*	*NO*	*580*

DI: delay interferometer; SOA: semiconductor amplifier; SMF: single mode fiber; TMF: two-mode fiber; DBR: distribute Bragg reflection; FBG: fiber Bragg grating; FP: Fabry-Perot; NPR: nonlinear polarization rotation; DANLM: delay asymmetric nonlinear loop mirror

In the end, we summarize the features of existing clock recovery schemes of NRZ-DPSK signal in Table B. In reference [12], a compact device is demonstrated to recover clock without preprocessing stage. The approach is limited to NRZ-DPSK signal generated with MZM, which has some clock tones due to the intensity dips. However, for MZM with larger bandwidth, the clock tones are probably too weak to be enhanced using the approach. Generally, all the other schemes require a preprocessing to generate some clock tones, and then use another circuit to recover the clock.

DI, FBG, and two-mode fiber are compact compared with other preprocessing devices. However, FBG only works for DPSK signal at a fixed wavelength. DANLM

has a complicated structure, but it can work at tunable bit rates over a wide range. The clock recovery circuits can be divided into two kinds: SOA ring laser or FP filter. The SBS loop is actually an active FP filter with a capability of bit-rate transparent clock recovery. This feature distinguishes it from the others. To utilize SBS loop, we need to erase the phase variation of the preprocessed signal to enhance the SBS effect. NPR is used in our work for this purpose. One may note that NPR causes a polarization dependence problem to the whole circuit. This problem can be solved by replacing NPR with polarization-insensitive XPM.

In conclusion, our approaches based on DANLM/DI-NPR-SBS have a unique feature of bit-rate variability over the others. In particular, the DI one can work for DPSK signals over a wide band of bit rates and wavelengths without any tuning, no matter the signals are generated by which kind of modulator. The system is also comparable with most of the others in the aspect of complexity.

References

[1] C. Schmidt-Langhorst, R. Ludwig, M. Galili, B. Huettl, F. Futami, S. Watanabe, C. Schubert, "160 Gbit/s all-optical OOK to DPSK in-line format conversion," in Proc. of ECOC 2006, Cannes, France, paper Th4.3.5.

[2] C. Boerner, V. Marembert, S. Ferber, C. Schubert, C. Schmidt-Langhorst, R. Ludwig, and H. G. Weber, "320 Gbit/s clock recovery with electro-optical PLL using a bidirectionally operated electroabsorption modulator as phase comparator," in Proc. of OFC/NFOEC 2003, Atlanta, GA, paper OTuO3.

[3] K. Vlachos, G. Theophilopoulos, A. Hatziefremidis, and H. Avramopoulos, "30 Gbps, broadly tunable, all-optical clock recovery circuit," in Proc. of OFC/NFOEC 2000, Baltimore, ML, paper ThP2-1.

[4] Y. Li, C. Kim, G. Li, Y. Kaneko, R. L. Jungerman, and O. Buccafusca, "Wavelength and polarization insensitive all-optical clock recovery from 96-Gbit/s data by using a two-section gain-coupled DFB laser," IEEE Photon. Technol. Lett., vol. 15, no. 4, pp. 590-592, Apr. 2003.

[5] G. Contestabile, A. D' Errico, M. Presi, and E. Ciaramella, "40-GHz all-optical clock extraction using a semiconductor-assisted Fabry-Perot filter," IEEE Photon. Technol. Lett., vol. 16, no. 11, pp. 2523-2525, Nov. 2004.

[6] D. L. Butler, J. S. Wey, M. W. Chbat, G. L. Burdge, and J. Goldhar, "Optical clock recovery from a data stream of an arbitrary bit-rate by use of stimulated Brillouin scattering," Opt. Lett., vol. 20, no. 6, pp. 560-562, Mar. 1995.

[7] X. Zhou, H. H. M. Shalaby, C. Lu, T. H. Cheng, and P. Ye, "A performance analysis of all-optical clock extraction circuit based on stimulated Brillouin scattering," J. Lightw. Technol., vol. 18, no. 10, pp. 1453-1466, Oct. 2000.

[8] W. W. Tang, M. P. Fok, and C. Shu, "All-optical clock recovery from NRZ data using a NRZ-to-PRZ converter constructed with a polarization-maintaining fiber loop mirror filter," in Proc. of CELO/PR 2005, Tokyo, Japan, paper CThM1-2.

[9] Y. Yu, X. Zhang, E. Zhou, and D. Huang, "All-optical clock recovery from NRZ signals at different bit rates via preprocessing by an optical filter," IEEE Photon. Technol. Lett., vol. 19, no. 24, pp. 2039-2041, Dec. 2007.

[10] G. Contestabile, M. Presi, N. Calabretta, and E. Ciaramella, "All-optical clock recovery for NRZ-DPSK signals," IEEE Photon. Technol. Lett., vol. 18, no. 23, pp. 2544-2546, Dec. 2006.

[11] Y. Yu, X. Zhang, and D. Huang, "All-optical clock recovery from NRZ-DPSK signal," IEEE Photon. Technol. Lett., vol. 18, no. 22, pp. 2356-2358, Nov. 2006.

[12] X. Tang, J. C. Cartledge, A. Shen, F. V. Dijk, and G.-H. Duan, "All-optical clock recovery for 40-Gbit/s MZM-generated NRZ-DPSK signals using a self-pulsating DBR laser," IEEE Photon. Technol. Lett., vol. 20, no. 17, pp. 1443-1445, Sep. 2008.

[13] F. Wang, Y. Yu, X. Huang, and X. Zhang, "All-optical clock recovery of 20 Gbit/s NRZ-DPSK signals using polarization-maintaining fiber loop mirror filter and semiconductor optical amplifier fiber ring laser," Opt. Commun., vol. 282, pp. 2292-2296, Feb. 2009.

[14] S. Fu, M. Tang, W.-D. Zhong, Y. J. Wen, and P. Shum, "All-optical NRZ-DPSK clock recovery using chromatic-dispersion-induced clock tone," IEEE Photon. Technol. Lett., vol. 19, no. 12, pp. 925-927, Jun. 2007.

[15] J. Slovak, C. Bornholdt, J. Kreissl, S. Bauer, M. Biletzke, M. Schlak, and B. Sartorius, "Bit rate and wavelength transparent all-optical clock recovery scheme for NRZ-coded PRBS signal," IEEE Photon. Technol. Lett., vol. 18, no. 7, pp. 844-846, Apr. 2006.

[16] Y. Yu, X. Zhang, E. Zhou, and D. Huang, "All-optical clock recovery from NRZ signals at different bit rates via preprocessing by an optical filter," IEEE Photon. Technol. Lett., vol. 19, no. 24, pp. 2039-2041, Dec. 2007.

[17] P. J. Winzer and R.-J. Essiambre, "Advanced modulation formats for high-capacity optical transport networks," J. Lightw. Technol., vol. 24, no. 12, pp. 4711-4728, Dec. 2006.

[18] C. H. Kwok, C. W. Chow, H. K. Tsang, and C. Lin, "Nonlinear polarization rotation in a dispersion-flattened photonic-crystal fiber for ultrawideband (>100 nm) all-optical wavelength conversion of 10 Gbit/s nonreturn-to-zero signals," Opt. Lett., vol. 31, no. 12, pp. 1782-1784, Jun. 2006.

[19] Y. H. Dai, M. P. Fok, and C. Shu, "Polarization-insensitive delay-asymmetric nonlinear loop mirror for variable bit-rate DPSK demodulation," in Proc. of OFC/NFOEC 2009, San Diego, CA, paper OThM3.

[20] Ch. Kouloumentas, A. Tzanakaki, and I. Tomkos, "Clock recovery at 160 Gbit/s and beyond, using a fiber-based optical power limiter," IEEE Photon. Technol. Lett., vol. 18, no. 22, pp. 2365-2367, Nov. 2006.

[21] S.-W. Jeon, T.-Y. Kim, W.-B. Kwon, and C.-S. Park, "All-optical clock extraction from 10-Gbit/s NRZ-DPSK data using modal interference in a two-mode fiber," Opt. Commun., vol. 283, pp. 522-527, Oct. 2010.

6 DELAYED INTERFERENCE OF PSK SIGNAL TO GENERATE UWB SIGNALS

As the frequency and bandwidth of microwave signal grows to satisfy increasing demand of wireless information service, many functions in microwave systems are complex or even not directly possible in the electronic domain. On the other hand, optical fibers provide extremely large bandwidth as well as very low loss, attracting the radiofrequency engineers to process their signals in the optic domain. The mature of direct-modulated lasers, external modulators, and photodetectors with large bandwidth enables high efficiency and low distortion of conversion between microwave signal and optical signal, and finally the worlds, radiofrequency engineering and optoelectronics, are combined together as microwave photonics [1].

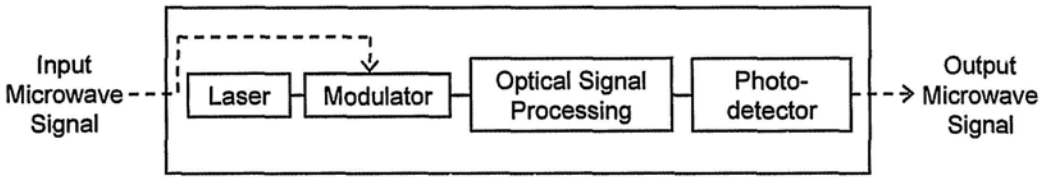

Fig. 6.1. Microwave signal processing using microwave photonic technology.

As shown in Fig. 6.1, in microwave photonics, the microwave signal is first converted to optical signal using direct modulation or external modulation. The optical signal is then flexibly processed in optical system and converted back to microwave signal using photodetector. Functions like true time delay [2], filtering [3], analog-to-digital conversion [4], millimeter wave generation [5], arbitrary waveform

generation [6], as well as UWB signal generation [7] can be implemented in this kind of structure.

In this chapter, photonic generation of UWB signal using delayed interference of phase-modulated signals is demonstrated. Section 6.1 reviews different approaches of photonic generation of UWB signals. In section 6.2, monocycle pulse is generated using a fiber-based DI to perform the delayed interference of a $\pi/2$ PSK signal, which is generated by a phase modulator.

6.1 Introduction to Photonic Generation of UWB Signal

It is well known that radiofrequency is a rare resource in modern society. As shown in the United States Frequency Allocation Chart [8], the radiofrequency from 9 kHz to 300 GHz has already been allocated to different wireless applications. For new wireless services demanded in the 4G wireless system, radiofrequency engineers have to rely on even higher frequency. However, high frequency will result in harsh requirements on system design and increase the cost. UWB technology proposes a novel point of view to solve today's problem in spectrum management. It tries to use the radiofrequency occupied by other wireless applications and introduce slight disturbance to these applications. This idea can be realized by distributing the signal power of the new application over a wide frequency band, and then in each band of original wireless applications, the signal power from the new application is too small to cause significant degradation on their quality of service [9]. UWB technology has received legal adoption of United States and Federal Communications Commission (FCC) has allocated a band from 3.1 to 10.6 GHz for the technology [10], as shown in Fig. 6.2. The maximum power density over the band is regulated to less than – 41.3 dBm/MHz in order to protect the original wireless applications from disturbance. FCC also gives a strict definition of a UWB device as "any device where the fractional bandwidth is greater than 0.25 or occupies 1.5 GHz or more of spectrum" [10]. The fractional bandwidth is

$$B_{fr} = 2\frac{f_H - f_L}{f_H + f_L} \tag{6-1}$$

where f_H and f_L is the upper and lower frequencies of the -10 dB emission point.

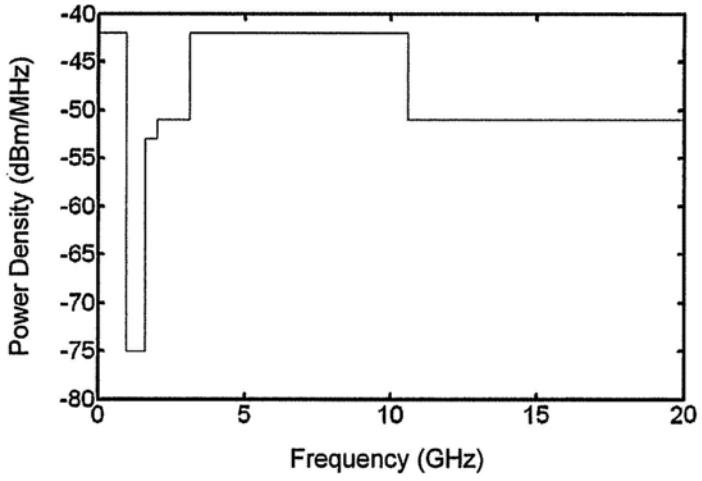

Fig. 6.2. Band of UWB technology regulated by FCC.

Based on this definition, even if the bit rate carried by a UWB signal is tens of Mb/s, the bandwidth of devices to process the signal should be over 1.5 GHz. On one hand, this feature makes UWB system easy to upgrade to bit rate as high as Gbit/s. On the other hand, this requirement may not be cost-effective for electronic devices, while potentially not harsh for optoelectronic devices, making photonic generation and processing of UWB signal attractive. One more reason for UWB signal generation in optic domain is to increase the transmission distance. As mentioned, the UWB technology cannot affect the normal operation of original wireless applications, so the power of the UWB signal is regulated to less than - 41.3 dBm/MHz by FCC. Such a low power cannot afford the large loss of wireless signal in free space, so the transmission distance of UWB signal is limited to ~ 10 meters. To cover large area,

the combination of UWB wired and wireless links is proposed and UWB-over-fiber [11] is a promising technology since the signal is confined in fiber to avoid interference with other wireless signals and the loss in fiber is quite low. UWB-over-fiber requires UWB pulse in optical form. It can be achieved by generating a UWB signal in electric domain and then modulating the signal on a CW light. However, electrical generation of UWB signal is not easy due to the wide bandwidth. Therefore, direct photonic generation of UWB signal has attracted much interest recently.

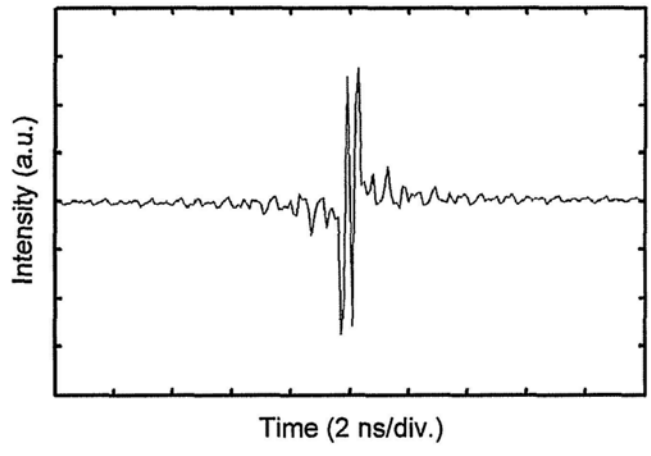

Fig. 6.3. UWB impulse with spectrum precisely compliant with FCC definition.

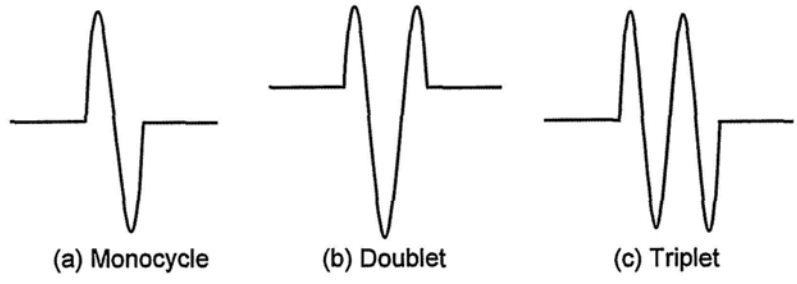

Fig. 6.4. Three kinds of UWB signal waveforms.

Fig. 6.3 shows the UWB impulse with spectrum precisely compliant with FCC definition. It is obtained by performing inverse Fourier transform of the spectrum shown in Fig. 6.2. Although it is not necessary for every UWB signal to cover the entire frequency range from 3.1 to 10.6 GHz, the intensity waveform in Fig. 6.3 discloses that a UWB signal ought to be a few-cycle or even monocycle pulse. In practice, the common UWB signals used in wireless applications are monocycle, doublet and triplet pulse, as shown in Fig. 6.4. The essential idea of photonic generation of UWB signal is to shape the optical waveform into one of the three or other UWB waveforms.

Many photonic approaches have been demonstrated. A comprehensive review [7] has divided these techniques into three main categories: 1) phase-modulation to intensity-modulation conversion, 2) processing with a photonic microwave delay-line filter, and 3) optical spectral shaping and frequency-to-time mapping.

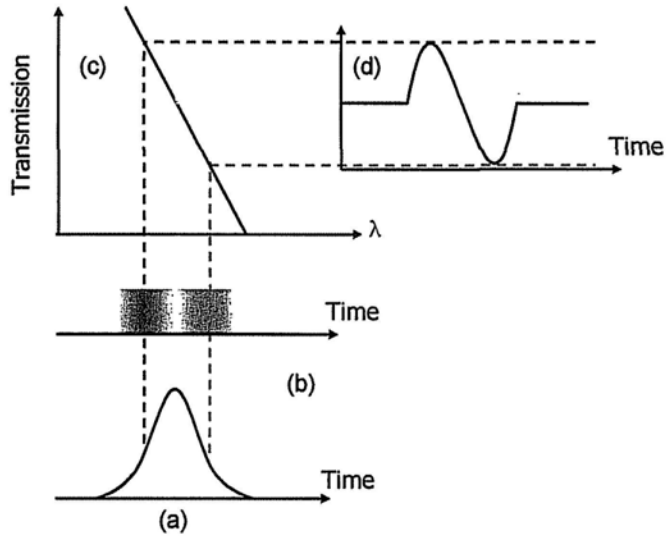

Fig. 6.5. (color online) UWB generation based on phase-modulation to intensity-modulation conversion.

Fig. 6.5 illustrates the principle of the first category of photonic UWB generation. A CW light is first phase-modulated by an electrical pulse signal as shown in Fig. 6.5 (a) and a chirped light will be generated (Fig. 6.5 (b)). The chirped light is then processed by an optical frequency discriminator, which has a linear transmission curve as shown in Fig. 6.5 (c). Since transmission coefficient varies with wavelength, the wavelength chirp in the CW light is converted to a monocycle shape of intensity (Fig. 6.5 (d)). Using this approach, if the frequency discriminator is not discriminative enough, the electrical pulse signal must be amplified to a high power to introduce large chirp for the CW light. For example, if the discriminator needs a wavelength difference of +/- 0.1 nm to generate a monocycle pulse and a phase modulator with π phase shift voltage of V_π is used to introduce the chirp, rough estimation is $2V_\pi$ voltage required by the electrical signal with a pulse width of ~ 100 ps. Another problem in this approach is the wavelength of CW light must locate at the center of the linear region of the frequency discriminator, not applicable to generate UWB signal at multiple wavelengths which is useful in a WDM system. An example of this kind of approach is generation of monocycle pulse demonstrated by Li et al. [12], who used analog phase modulation in a phase modulator to introduce sufficient amount of frequency chirp and adopted a Sagnac loop mirror as the optical frequency discriminator. They also demonstrated the convenience to implement bi-phase modulation of monocycle pulse by modulating the birefringence inside the loop mirror.

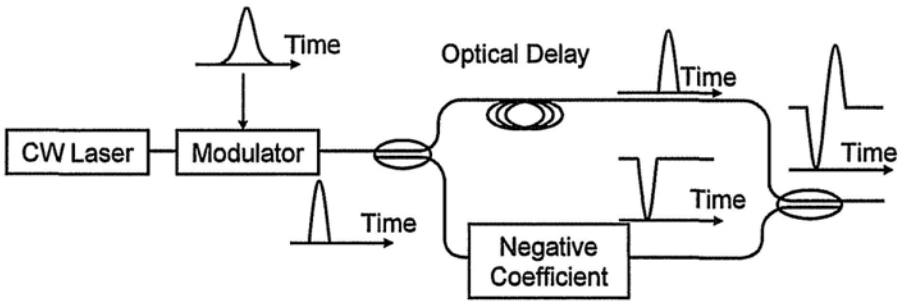

Fig. 6.6. UWB generation based on photonic microwave delay-line filter.

The second type of photonic generation of UWB waveform is shown in Fig. 6.6. First, we obtain an optical pulse by modulating the intensity of a CW light, or we can use a pulsed laser source [13]. The optical pulse is then split into two paths. One will experience a proper optical delay, and the other will be inverted by an optoelectronic device with negative tap coefficient. Devices of this kind can be a SOA or OPA utilizing XGM [14, 15] or a balanced photodetector [16]. The two branches are added together incoherently at the output and a monocycle pulse is generated. The challenge of this approach is how to obtain the negative coefficient with power consumption and cost. Attention is also paid to avoid the coherent addition of the two branches.

The third category of photonic generation of UWB waveform requires a wideband optical source. The spectrum of the light is shaped into UWB waveform by optical filters and mapped to time domain by dispersive medium. Due to the high cost of wideband optical source, complication of spectral shaping and dispersion sensitivity

of the waveform, this approach is not frequently used.

Except the three, photonic generation of UWB based on injection-locking is also demonstrated [17], and complicated UWB waveform with excellent spectral features can be obtained. This approach needs to further explore implementation of flexible data modulation.

6.2 Monocycle Pulse Generation Using Fiber-Based DI

Photonic UWB generators those are capable to generate multiple UWB waveforms, easy to implement data modulation, applicable to multiple optical wavelengths, implementable with few active devices to reduce power consumption and cost, and integrable are desirable. The generated UWB signal should also be tolerant to dispersion in the transmission fiber. In this section, we propose a novel approach to generate UWB monocycle pulse in the optical domain using passive optical devices. The system consists of a phase modulator (PM) together with a fiber-based DI. Digital phase modulation is used and only a moderate $\pi/2$ phase shift is required to generate the UWB pulse using the delayed interference. Destructive interference provides an efficient method to generate negative coefficient. Although only one kind UWB waveforms can be generated, it is convenient for pulse position modulation, suitable for multiple wavelengths, and potentially integrable. In addition, the generated monocycle exhibits a high tolerance to dispersion in the transmission fiber.

The principle of our approach is illustrated in Fig. 6.7. A $\pi/2$-PSK signal is first generated by a PM. Note that there is a transient phase during the transition from 0 to $\pi/2$, as well as from $\pi/2$ to 0. The $\pi/2$-PSK signal is then launched into a DI and is split into two arms. A time delay (ΔT) and a phase shift ($\Delta\varphi$) is introduced in one arm, as shown in Fig. 6.7 (a). The phase shift $\Delta\varphi$ in the DI is set to $\pi/2$. After propagation in the DI, the two $\pi/2$-PSK signals interfere with each other at the constructive port. As shown in Fig. 6.7 (b), in the first stage I, the two signals interfere with a $\pi/2$ phase

difference and a moderate optical power is obtained. Following that, the phase difference changes to 0 and the two signals interfere constructively, leading to a maximum output power. In the third stage III, the phase difference changes to π and the two signals interfere destructively, resulting in a minimum output power. In the IV (last) stage, the phase difference returns to $\pi/2$ and the same power as that in stage I is obtained. Therefore, the delayed interference output of the $\pi/2$-PSK signal is a monocycle pulse. If the phase shift is set to - $\pi/2$, a polarity-reversed monocycle pulse will be obtained.

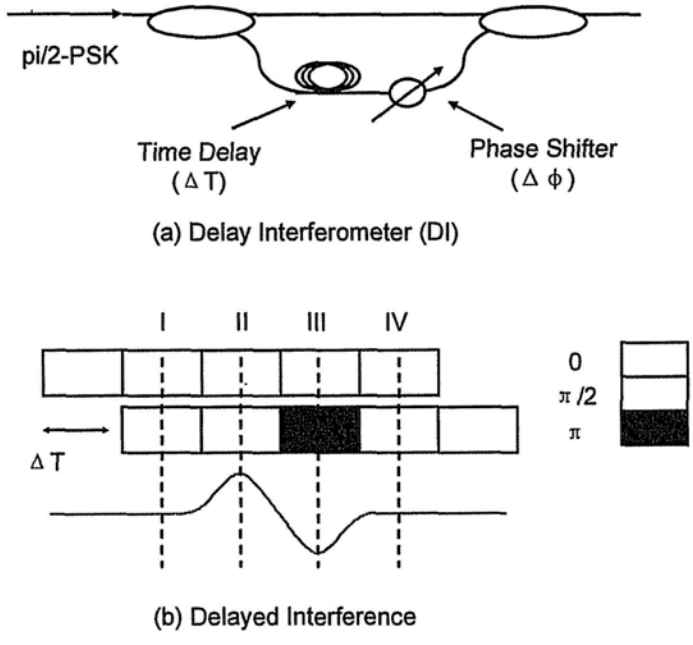

Fig. 6.7. Principle of UWB monocycle pulse generation based on delayed interference of $\pi/2$ PSK signal.

To verify the proposed approach, we use a fiber-based DI providing a relative time delay of 50 ps. The phase shift can be adjusted by slightly heating the fiber. The

experimental setup is shown in Fig. 6.8.

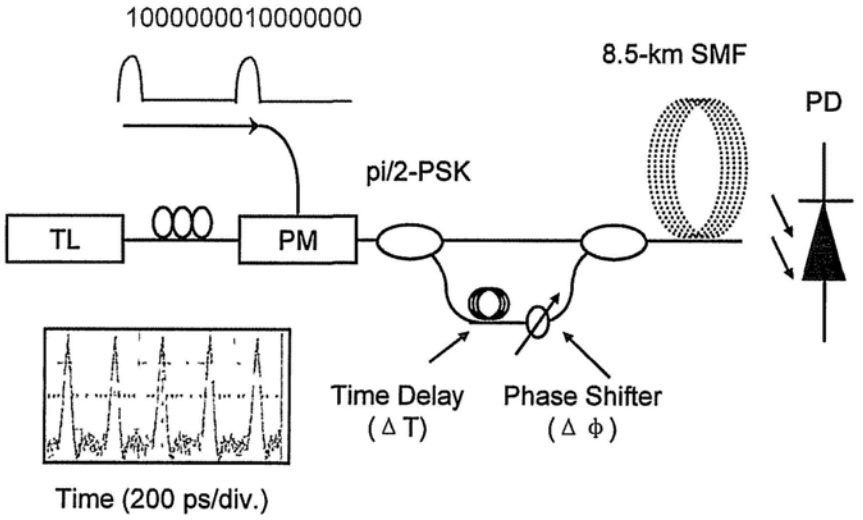

Fig. 6.8. Experimental setup. TL: tunable laser; PM: phase modulator; PD: photodetector; SMF: single mode fiber. Inset shows the input electrical waveform.

A CW tunable laser (TL) is used as the light source, providing an optical power of 3 dBm at a wavelength of 1550 nm. The output is modulated by a PM that has a V_π of 8.3 V. Here, we just need a $\pi/2$ phase shift in the PM. The electrical modulation sequence applied to the PM is provided by a bit pattern generator (BPG) with a fixed pattern "1000 0000" at a bit-rate of 20-Gbit/s, i.e. a pulse train with a repetition rate of 2.5 GHz, as shown in the inset of Fig. 6.8. The full width at half maximum (FWHM) of the electrical pulse is 70 ps. The generated $\pi/2$-PSK signal with an optical power of - 1.3 dBm is then launched into the DI for UWB monocycle pulse generation. The $\pi/2$ phase shift between the two arms in the DI can be controlled by a heater or alternatively, by slightly tuning the optical wavelength. The use of a heater eliminates the limitation on the operating wavelength. The generated optical pulse is

obtained at the constructive port of the DI. The measured optical power is - 4.5 dBm, indicating a 3.2-dB insertion loss of the generator. The loss results mainly from the loss of optical power at the destructive port of the DI, where another monocycle pulse train with a reversed polarity is produced. The signal can also be used to carry information if an additional data modulator is added in the setup. The generated UWB monocycle signal is measured by a photodetector (Agilent 83440D) with a bandwidth of 30 GHz and a conversion gain of 32.5 V/W.

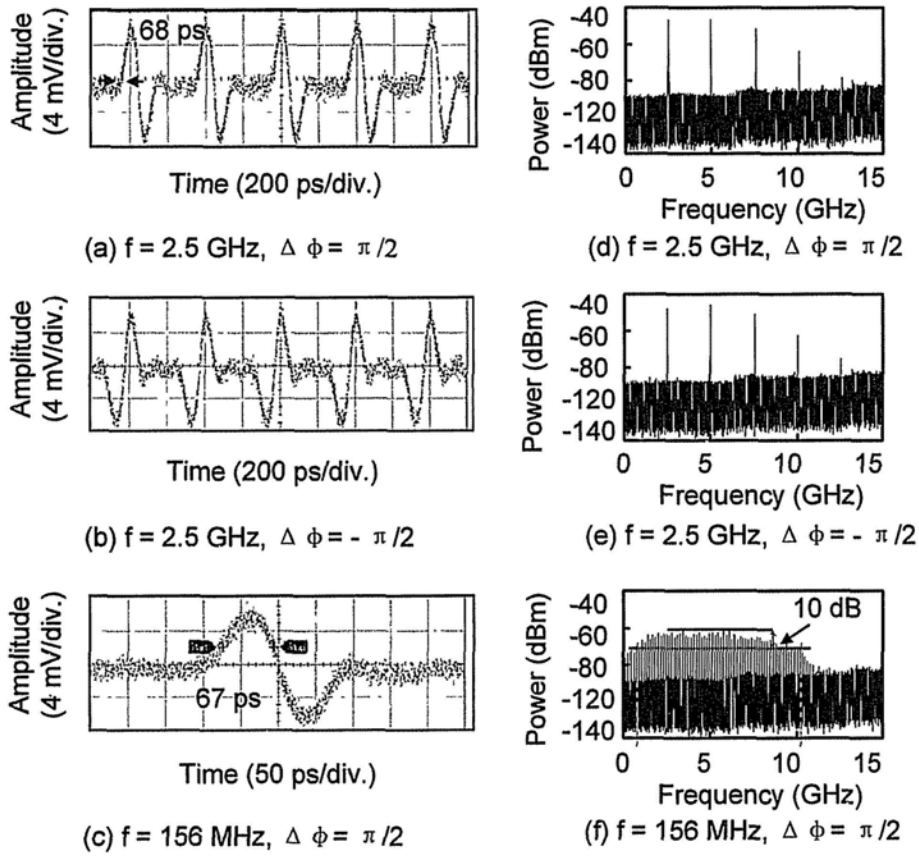

Fig. 6.9. (a) - (c) Generated UWB monocycle waveforms and (d) - (f) corresponding RF spectra. f: repetition rate; Δφ: phase shift between two arms in the DI.

The obtained monocycle pulses and their RF spectra are shown in Fig. 6.9. A pair of UWB pulses with opposite polarities is achieved by switching the relative phase shift between $\pi/2$ and - $\pi/2$. The FWHM of the monocycle pulses are ~ 68 ps. Since the repetition rate of 2.5 GHz is too high for disclosing the details of the RF spectrum, we change the fixed pattern to "100....00" (one "1" out of 128 bits) to reduce the repetition rate to 156.25 MHz, as shown in Fig. 6.9 (c) and (f). The FWHM of the pulse is 67 ps and is almost the same as that of the 2.5-GHz repetition rate. The spectrum shown in Fig. 6.9 (f) has a central frequency of 5.6 GHz and a 10-dB bandwidth of 9.4 GHz, corresponding to a fractional bandwidth of ~ 168% for the generated monocycle pulse.

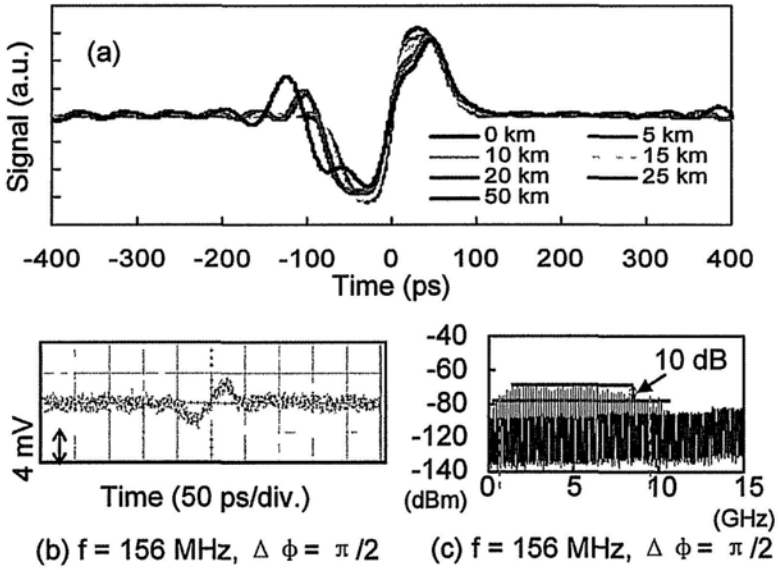

Fig. 6.10. (Color online) (a) Simulated monocycle waveforms after transmission in a SMF of different lengths. (b) measured waveform and (c) measured RF spectrum after transmission in an 8.5-km SMF.

To investigate the dispersion tolerance, simulation is performed on the monocycle waveform after its transmission in a standard SMF of different lengths. The electrical driving signal is assumed to be a Gaussian pulse train and the fiber dispersion parameter is set to – 22.13 ps^2/km. One should note that the frequency chirp is non-uniform across the optical pulses. The simulation result is shown in Fig. 6.10 (a). The waveform distortion is negligible within 10 km and is still acceptable after 25 km propagation. By adding a dispersion compensation module, the transmission distance can be further extended. Next, the 156.25-MHz monocycle pulses are experimentally transmitted over an 8.5-km SMF with a total dispersion of ~144 ps/nm. The waveform and the spectrum after the transmission are shown in Fig. 6.10 (b, c). Considering the 1.7-dB propagation loss in the SMF and the additional coupling loss in fiber connectors, the measured optical power of –7.0 dBm after transmission is within expectation. The shape of the monocycle pulses is well maintained, with a 10-dB fractional bandwidth of ~ 181% (10-dB bandwidth of 9.04 GHz at a central frequency of 5 GHz).

For the data modulation, we can work with either bi-phase modulation or pulse-position modulation. The bi-phase modulation can be implemented by modulating the phase shift in the DI between $\pi/2$ and - $\pi/2$ to change the pulse polarity. However, for high-speed modulation like 2.5 Gbit/s, thermal means of switching cannot meet the speed requirement. Instead, one can use a DI with a lithium niobate (LN) phase modulator in one arm to provide rapid phase change in

response to the high-speed electrical driving signal. This approach is practical for integrating the whole system onto a monolithic LN chip. A built-in delay should be provided between the two interfering arms. By adding an electrode to the LN phase modulator, the DI can thus perform high-speed bi-phase modulation. Alternatively, one can modify a PM based loop mirror [18] to a PM based DANLM to perform bi-phase modulation of UWB monocycle pulses generated at tunable fractional bandwidth through tunable delay between the interfering arms.

The pulse-position modulation is simple to implement by programming the pattern used to drive the PM. Here, we use "1000 0000" and "0010 0000" to represent bit 1 and bit 0, respectively. The encoding of a data sequence "11001110" at 2.5 Gbit/s is demonstrated in Fig. 6.11. The original UWB waveform before modulation is shown in Fig. 6.11 (a). All pulses are equally spaced in time. After data modulation, the UWB pulse train is depicted in Fig. 6.11 (b).

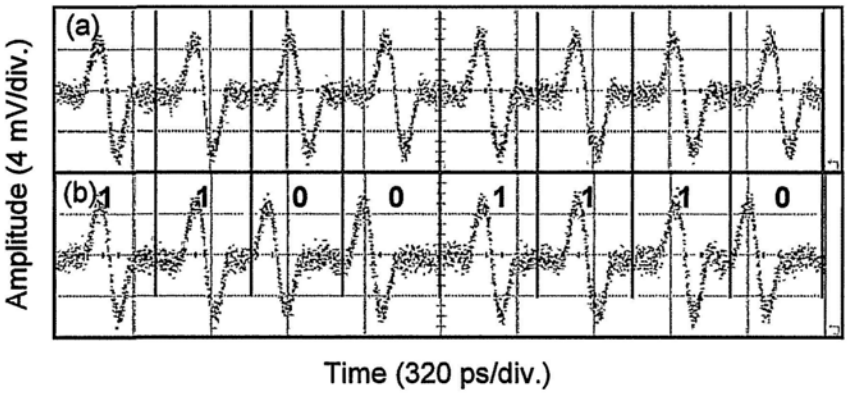

Fig. 6.11. (a) Original UWB pulse train before modulation. (b) UWB pulse train after pulse position modulation.

In conclusion, a UWB monocycle pulse generator is proposed and experimentally demonstrated. The generator utilizes delayed interference between the two arms of π/2-PSK signal in a fiber-based DI. With a proper delay, four different states of interference occur, resulting in the generation of a monocycle pulse. The pulse has a FWHM of 68 ps and a 10-dB fractional bandwidth of 168%. The proposed scheme is simple to implement, flexible to the operating wavelength, potentially integrable, and convenient for data modulation. The generated pulse is also tolerant to dispersion in the transmission fiber.

Reference

[1] J. Capmany and D. Novak, "Microwave photonics: combines two worlds," Nature Photon., vol. 1, pp. 319-330, 2007.

[2] Y. Liu, J. Yang, and J. P. Yao, "Continuous true-time-delay beamforming for phased array antenna using a tunable chirped fiber grating delay line," IEEE Photon. Technol. Lett., vol. 14, no. 8, pp. 1172–1174, Aug. 2002.

[3] F. Zeng and J. P. Yao, "All-optical bandpass microwave filter based on an electro-optic phase modulator," Optics Express, vol. 12, no. 16, pp. 3814–3819, Aug. 2004.

[4] G. C.Valley, "Photonic analog-to-digital converters," Opt. Express, vol. 15, no. 5, pp. 1955–1982, Mar. 2007.

[5] J. Yu, Z. Jia, L. Yi, Y. Su, G. Chang, and T.Wang, "Optical millimeterwave generation or up-conversion using external modulators," IEEE Photon. Tech. Lett., vol. 18, no. 1, pp. 265–267, Jan. 2006.

[6] M. H. Khan, H. Shen, Y. Xuan, L. Zhao, S. Xiao, D. E. Leaird, A. M. Weiner, and M. Qi, "Ultrabroad-bandwidth arbitrary radiofrequency waveform generation with a silicon photonic chip-based spectral shaper," Nature Photon., vol. 4, pp. 117-122, 2007.

[7] J. Yao, F. Zeng, and Q. Wang, "Photonic generation of ultrawideband signals," J. Lightwav. Technol., vol. 25, no. 11, pp. 3219-3235, Nov. 2007.

[8] U.S. Frequency Allocation Chart as of October 2003: http://www.ntia.doc.gov/osmhome/allochrt.pdf.

[9] M. Cotton, R. Achatz, J. Wepman, and P. Runkle, "Interference potential of ultrawideband signals part 2: measurement of gated-noise interference to C-band satellite digital television receivers," NTIA Report TR-05-429, Aug. 2005. http://www.its.bldrdoc.gov/pub/ntia-rpt/05-429/index.php

[10] Fed. Commun. Commission, Revision of Part 15 of the Commission's Rules Regarding Ultra-Wideband Transmission Systems, Apr. 2002. Tech. Rep., ET-Docket 98-153, FCC02-48.

[11] S. Pan and J. Yao, "UWB-over-fiber communications: modulation and transmission," J. Lightwave Technol., vol. 28, no. 16, pp. 2445-2455, Aug. 2010.

[12] J. Li, K. Xu, S. Fu, M. Tang, P. Shum, J. Wu, and J. Lin, "Photonic polarity-switchable ultra-wideband pulse generation using a tunable Sagnac interferometer comb filter," IEEE Photon. Technol. Lett., vol. 20, no. 15, pp. 1320-1322, Aug. 2008.

[13] F. Zeng, Q. Wang, and J. P. Yao, "All-optical UWB impulse generation based on cross phase modulation and frequency discrimination," Electron. Lett., vol. 43, no. 2, pp. 119–121, Jan. 2007.

[14] Q. Wang, F. Zeng, S. Blais, and J. Yao, "Optical ultrawideband monocycle pulse generation based on cross-gain modulation in a semiconductor optical amplifier," Opt. Lett., vol. 31, no. 21, pp. 3083–3085, Nov. 2006.

[15] J. Li, B. P.-P. Kuo, and K. K.-K. Wong, "Ultra-wideband pulse generation based on cross-gain modulation in fiber optical parametric amplifier," IEEE Photon. Technol. Lett., vol. 21, no. 4, pp. 212-214, Feb. 2009.

[16] H. Mu and J. Yao, "Polarity- and shape-switchable UWB pulse generation based on a photonic microwave delay-line filter with a negative tap coefficient," IEEE Photon. Technol. Lett., vol. 21, no. 17, pp. 1253-1255, Sep. 2009.

[17] M.-J. Zhang, T.-G. Liu, A.-B. Wang, J.-Y. Zheng, L.-N. Meng, Z.-X. Zhang, and Y.-C. Wang, "Photonic ultrawideband signal generator using an optically injected chaotic semiconductor laser," Opt. Lett., vol. 36, no. 6, pp. 1008-1010, Mar. 2011.

[18] M. P. Fok, K. L. Lee, and C. Shu, "Waveband-switchable SOA ring laser constructed with a phase modulator loop mirror filter," IEEE Photon. Technol. Lett., vol. 17, no. 7, pp. 1393-1395, Jul. 2005.

7 THESIS SUMMARY AND FUTURE WORK

This chapter summarizes the work presented in the previous chapters in section 7.1 and suggests some future work related to optical signal processing techniques of phase-modulated signals in section 7.2.

7.1 Summary

The thesis develops optical signal processing techniques for phase-modulated signals in fiber communication systems. In chapter 1, the functions provided by optical signal processing technology are classified. To support high-capacity communication networks, the current research emphasis is moving from amplitude-modulated signals to phase-modulated signals.

In chapter 2, 10-Gbit/s NRZ-OOK signal has been successfully converted to RZ-BPSK signal based on XPM together with pump-modulated FWM. Owing to the addition of the FWM stage, the degradation caused by SBS in the conversion is suppressed. In addition, the FWM stage provides a flexible wavelength conversion function. Specifically, it can convert the wavelength back to that of the original OOK signal to realize wavelength-preserved format conversion. The power gain of the generated RZ-BPSK signal is ~ 1.4 dB compared with the input NRZ-OOK signal. The heterogeneous multiplexing of a NRZ-OOK signal and a RZ-BPSK signal to produce a RZ-QPSK signal has also been investigated in this chapter.

In chapter 3, the polarization dependence of wavelength conversion techniques for phase-modulated signals is addressed. We take advantage of the birefringence in a 64-m highly nonlinear PCF to achieve polarization-insensitive FWM with a single pump. This technique eliminates the limitation on pump-to-pump wavelength detuning as required by dual-pump schemes for suppressing polarization dependence. Without the limitation, polarization-insensitive and wideband FWM are simultaneously achieved with dual pumps. The 3-dB down-conversion bandwidth is found to be 27 nm for 10-Gbit/s RZ-DPSK wavelength conversion. Based on the wide bandwidth, the technique is readily applied for polarization-insensitive wavelength multicasting. Using three pumps at unequally spaced wavelengths, a RZ-DPSK signal has been successfully multicasted to eight new wavelengths.

In chapter 4, the demodulation of phase-modulated signals at variable bit rates has been demonstrated. The function is achieved using delay interference with tunable optical delay introduced by wavelength conversion together with group velocity dispersion, either in a DANLM loop structure or a linear structure. We demonstrate a polarization-independent DANLM, consisting of 600-m SMF and 64-m PCF, using FWM with dual-orthogonal pumps and obtain demodulation results for RZ-DPSK signals at 10 and 12.5 Gbit/s. We also work on FWM with dual-parallel pumps to enhance the working bit-rate range of DANLM by increasing the delay to more than 300 ps. In addition to the loop structure, a linear structure with similar functionalties has been demonstrated, offering the potential for integration. We use a 41-m PCF and

a chirped FBG with a length of several centimeters to demodulate NRZ/RZ-DPSK signals at 5 and 10 Gbit/s.

In chapter 5, a clock recovery unit for NRZ-DPSK signal at variable bit rates is proposed and demonstrated. We first achieve a wideband clock recovery circuit for NRZ-DPSK signal through the preprocessing with a conventional fiber-based DI, followed by a loop mirror based on stimulated Brillouin scattering for bit-rate transparent clock extraction. The clock recovery unit covers a bit-rate range from 7.5 to 15 Gbit/s. Replacing the DI with a DANLM, an improved clock recovery circuit that operates at tunable bit rates over an extended range of 4 to 15 Gbit/s is achieved.

In chapter 6, the photonic generation of UWB signals has been demonstrated using delayed interference of a $\pi/2$-PSK signal. We generate polarity-switchable UWB monocycle pulsed with a fractional bandwidth of ~ 168%. Using pulse position modulation, the scheme can work at bit rates as high as 2.5 Gbit/s for wireless communication.

7.2 Future Work

To improve the performance of the investigated techniques described in the previous chapters, we list some suggestions for future work:

1. In chapter 3, we have demonstrated polarization-insensitive wavelength multicasting of DPSK signal. We have used unequally spaced pumps to eliminate crosstalk in the new copies of the signal. Owing to a large pump-probe detuning required by polarization dependence suppression, many wavelength channels are wasted in the ITU grid. To solve this problem, one may use a HNLF with sufficiently large birefringence to reduce the pump-probe detuning to the sub-nanometer level. At this level, the generated new copies can be matched to ITU grids of 0.8 or 1.6 nm, enhancing the bandwidth efficiency. The time jitter may increase due to the large birefringence but it can be compensated by a device providing a suitable differential group delay.
2. In chapter 4, bit-rate variable demodulation of phase-modulated signals has been achieved in a linear fiber structure. We use a 41-m nonlinear medium and a few-cm dispersive medium to demonstrate the function. Actually, the structure has the potential to be implemented on a single chip since both nonlinear and dispersive effects have been reported on silicon waveguides [1, 2].
3. In chapter 5, clock recovery for NRZ-DPSK signals has been demonstrated at variable bit rates. The demonstrated bit-rate range is ~ tens of Gbit/s. However, clock extraction based on SBS loop can work at 160 or even 320 Gbit/s. Such a high-speed clock recovery unit can be useful in modulation format conversion

from OTDM-ASK signal to OTDM-PSK signal [3].

4. In chapter 6, we have demonstrated photonic generation of UWB signals and data modulation in different formats. We also analyze the effects of dispersion on the transmission performance in an optical fiber. As a hybrid wireless and wireline communication system, the investigation on the transmission performance should ideally include the wireless part to complete the whole system using a pair of UWB antennae.

References

[1] N. Ophir, et al., "Continuous wavelength conversion of 40-Gbit/s data over 100 nm using dispersion-engineered silicon waveguide," IEEE Photon. Technol. Lett., vol. 23, no. 2, pp. 73-75, Jan. 2011.

[2] D. T. H. Tan, K. Ikeda, R. E. Saperstein, B. Slutsky, and Y. Fainman, "Chip-scale dispersion engineering using chirped vertical gratings," Opt. Lett. 33, 3013-3015 (2008).

[3] C. Schmidt-Langhorst, R. Ludwig, M. Galili, B. Huettl, F. Futami, S. Watanabe, C. Schubert, "160 Gbit/s all-optical OOK to DPSK in-line format conversion," in Proc. of ECOC 2006, Cannes, France, paper Th4.3.5.

APPENDICES

Appendix A. List of Publication

Journal papers:

[1] Y. Dai, J. Du, X. Fu, G. K. P. Lei, and C. Shu, "Ultrawideband monocycle pulse generation based on delayed interference of π/2 phase-shift keying signal," Opt. Lett., vol. 36, no. 14, pp. 2695-2697, Jul. 2011.

[2] Y. Dai and C. Shu, "Bit-rate variable DPSK demodulation based on cascaded four-wave mixing," Opt. Express, vol. 19, no. 5, pp. 2953-2959, Feb. 2011.

[3] Y. Dai and C. Shu, "Widely Tunable, Polarization-Insensitive Non-degenerate Four-Wave Mixing Wavelength Conversion for DPSK Signal," IEEE Photon. Technol. Lett., vol. 22, no. 15, pp. 1138-1140, Aug. 2010.

[4] G. K. P. Lei, Y. Dai, J. Du, and C. Shu, "Wavelength multicasting of DPSK signal with NRZ-to-RZ format conversion," Electron. Lett., vol. 47, no. 14, pp. 808-810, Jul. 2011.

[5] L. Wang, Y. Dai, G. K. P. Lei, J. Du, and C. Shu, "All-optical RZ-to-NRZ and NRZ-to-PRZ format conversions based on delay-asymmetric nonlinear loop mirror," IEEE Photon. Technol. Lett., vol. 23, no. 6, pp. 368-370, Mar. 2011.

[6] J. Du, Y. Dai, G. K. P. Lei, and C. Shu, "Reconfigurable all-optical two-channel demultiplexer based on modified dispersion asymmetric nonlinear optical loop mirror," Electron. Lett., vol. 46, no. 24, pp. 1613-1614, Nov. 2010.

[7] J. Du, Y. Dai, G. K. P. Lei, and C. Shu, "Reconfigurable two-channel demultiplexing using a single baseband control pulse train in a dispersion asymmetric NOLM," Opt. Express, vol. 18, no. 18, pp. 18691-18696, Aug. 2010.

[8] Y. Gao, Y. Dai, C. Shu, and S. He, "Wavelength interchange of phase-shift-keying signal," IEEE Photon. Technol. Lett., vol. 22, no. 11, pp. 838-840, Jun. 2010.

[9] J. Du, Y. Dai, G. K. P. Lei, W. Tong, and C. Shu, "Photonic crystal fiber based Mach-Zehnder interferometer for DPSK signal demodulation," Opt. Express, vol. 18, no. 8, pp. 7917-7922, Mar. 2010.

Conference paper:

[1] Y. Dai, J. Du, G. K. P. Lei, and C. Shu, "Wideband clock recovery for NRZ-DPSK signals," in Proc. of ACP 2010, paper FI 5.

[2] Y. Dai and C. Shu, "Tunable DPSK demodulation using variable optical delay in a straight-line interferometric structure," in Proc. of ECOC 2010, paper P1. 13.

[3] Y. Dai, G. K. P. Lei, J. Du, C. Shu, and M. P. Fok, "Bit-rate tunable clock recovery of NRZ-DPSK signal based on delay-asymmetric nonlinear loop mirror and stimulated Brillouin scattering loop," in Proc. of OFC 2010, paper OMT3.

[4] Y. Dai and C. Shu, "Polarization-insensitive wavelength multicasting of RZ-DPSK signal based on four-wave mixing in a photonic crystal fiber with residual birefringence," in Proc. of OFC 2010, paper OWP7.

[5] Y. Dai, C. Shu, and M. P. Fok, "Dual-pumped delay-asymmetric nonlinear loop mirror for DPSK demodulation at widely tunable bit rates," in Proc. of OECC 2009, paper FE6.

[6] Y. Dai and C. Shu, "Polarization-insensitive wideband wavelength conversion for DPSK signal by dual-pump four-wave mixing in a photonic crystal fiber," in Proc. of IEEE Photonics Society Summer Topicals 2009, paper MC2.3.

[7] Y. Dai, M. P. Fok, and C. Shu, "Polarization-insensitive delay-asymmetric nonlinear loop mirror for variable bit-rate DPSK demodulation," in Proc. of OFC 2009, paper OThM3.

[8] J. Du, Y. Dai, G. K. P. Lei, and C. Shu, "Reconfigurable all-optical two-channel demultiplexer based on modified dispersion asymmetric nonlinear optical loop mirror," in Proc. of ACP 2010, paper ThB 3.

[9] J. Du, Y. Dai, G. K. P. Lei, and C. Shu, "Dispersion asymmetric NOLM for reconfigurable all-optical two-channel demultiplexing using single baseband control pulse," in Proc. of ECOC 2010, paper P1. 15.

[10] J. Du, Y. Dai, G. K. P. Lei, H. Wei, and C. Shu, "RZ-to-NRZ and NRZ-to-PRZ format conversion using a photonic crystal fiber based Mach-Zehnder

Interferometer," in Proc. of OFC 2010, paper OMO4.

[11] J. Du, Y. Dai, G. K. P. Lei, W. Tong, and C. Shu, "Demodulation of DPSK signals using in-line Mach-Zehnder interferometer based on a Photonic crystal fiber," in Proc. of OECC 2009, paper FM6.

[12] C. Shu, Y. Dai, and M. P. Fok, "Optical signal processing with delay-asymmetric nonlinear loop mirror," in Proc. of ACP 2009, paper TuY2.

Appendix B. List of Figures

Fig. 2.1. Modulation formats in optical fiber communication systems. OOK: on-off keying; ODB: optical dual-binary; AMI: alternate mark inversion; 8QAM: 8 quadrature amplitude modulation; 16QAM: 16 quadrature amplitude modulation; BPSK: binary phase-shift keying; QPSK: quadrature phase-shift keying; 8PSK: 8 phase-shift keying; 16PSK: 16 phase-shift keying; PS-QPSK: polarization-switched QPSK; PolSK: polarization-shift keying.

Fig. 2.2. A data sequence "11010011000101" modulated in ODB and AMI formats.

Fig. 2.3. Constellation diagrams of 8QAM and 16QAM.

Fig. 2.4. Transmission systems using (a) DB/QPSK formats and (b) B/QPSK formats. DI: delay interferometer. d (n): the original data; D (n): transformed data with certain logic relation to the original data.

Fig. 2.5. Demodulation of binary PSK signal in a fiber-based DI. PS: phase shift.

Fig. 2.6. QPSK modulators: (a) parallel scheme; (b) serial scheme. MZM: Mach-Zehnder modulator; PM: phase modulator.

Fig. 2.7. Pump-modulated FWM to double the phase modulation depth.

Fig. 2.8. Experimental setup of NRZ-OOK to RZ-BPSK conversion using XPM plus FWM. TL: tunable laser; BPF: optical bandpass filter; PCF: photonic crystal fiber; DI: delay interferometer.

Fig. 2.9. Influence of SBS on OOK to BPSK conversion. (a, b) NRZ-OOK signal

with power under SBS threshold and the corresponding generated BPSK signal; (c, d) NRZ-OOK signal with power above SBS threshold and the corresponding generated BPSK signal.

Fig. 2.10. Optical spectra in the format conversion process when FWM between the XPM pump and XPM-probe varies. Inset: eye diagrams of NRZ-OOK signal when FWM is present and absent.

Fig. 2.11. Format conversion from NRZ-OOK to BPSK signal.

Fig. 2.12. Optical spectrum of pump-modulated FWM to convert π/2-BPSK to π-BPSK signal at the same wavelength of original OOK signal. CW-signal is set at 1563.7 nm.

Fig. 2.13. BER measurement of the generated BPSK signals. π-BPSK red: π-BPSK signal at the wavelength of 1553.9 nm; π-BPSK blue: π-BPSK signal at the wavelength of 1548.9 nm; π-BPSK original: π-BPSK signal at the wavelength of 1550.9 nm.

Fig. 2.14. Experimental setup to combine 10-Gbit/s RZ-BPSK and 10-Gbit/s NRZ-OOK to 10-Gbaud/s RZ-QPSK. TL: tunable laser; TDL: tunable optical delay line; BPF: bandpass filter.

Fig. 2.15. Conversion of 10-Gbit/s NRZ-OOK signal and 10-Gbit/s RZ-BPSK signal to 10-Gbaud/s RZ-QPSK signal. (b, c) demodulated RZ-BPSK signal and RZ-QPSK signal with phase shift in DI set at 0.

Fig. 2.16. Demodulated signals when the phase shift of DI is set to (a) π/4: constructive port of I channel; (b) 3π/4: destructive port of Q channel; (c)

5π/4: destructive of I channel; (d) 7π/4: constructive port of Q channel.

Fig. 2.17. Measurement of relative delay between the NRZ-OOK signal and RZ-BPSK signal.

Fig. 2.18. BER measurement of input NRZ-OOK signal, input RZ-BPSK signal, and generated RZ-QPSK signal.

Fig. 3.1. (a) Structure of OXC in a WDM system and (b) solution of wavelength blocking by wavelength conversion (Dash line: vacant channel; solid line: occupied channel). OXC: optical cross connect; WC: wavelength conversion.

Fig. 3.2. Partial degenerate and nondegenerate FWM.

Fig. 3.3. Polarization-insensitive FWM in conventional HNLF. PBS: polarization beam splitter.

Fig. 3.4. Polarization-insensitive degenerate FWM in birefringent HNLF.

Fig. 3.5. Polarization insensitive wavelength conversion of 10-Gbit/s RZ-ASK signal based on FWM with single pump in a birefringence PCF. (i, ii): polarization-fixed input; (iii, vi): polarization-scrambled input; (i, iii): polarization of pump aligned to principal axes; (ii, vi): polarization of pump aligned 45° offset to principal axes. PS: polarization scrambler; PC: polarization controller; PCF: photonic crystal fiber; BPF: bandpass filter.

Fig. 3.6. Polarization-insensitive nondegenerate FWM in birefringent fiber.

Fig. 3.7. Experimental setup to demonstrate polarization-insensitive, wideband wavelength conversion of RZ-DPSK signal based on FWM in

birefringent PCF. PC: polarization controller; PS: polarization scrambler; BPF: optical bandpass filter; DI: delay interferometer; PD: photodetector. BERT: bit error ratio tester; Inset: cross-section of the birefringent PCF [8].

Fig. 3.8. (a) Birefringent loop mirror using PCF and (b) measured transmission spectrum of the loop mirror.

Fig. 3.9. Polarization dependence of FWM in birefringent PCF on different signal-to-pump 1 wavelength detuning. RPD: residual polarization dependence; PPD: probe(signal)-to-pump1 detuning.

Fig. 3.10. FWM spectrum of polarization-insensitive RZ-DPSK wavelength conversion (pump2 is set at 1565.5 nm). The ASE peak is located at 1543 nm.

Fig. 3.11. Eye diagrams of the converted RZ-DPSK signals for polarization-fixed (left side) and polarization-scrambled (right side) input signals when pump 2 is set to different wavelengths: (a) 1565 nm; (b) 1555 nm; (c) 1545 nm; (d) 1540 nm; (e) 1540+10 nm. For (e), the wavelengths of both pump 1 and input signal are also increased by 10 nm.

Fig. 3.12. Measured wavelength conversion efficiency for dual-pump (black dots) and single-pump (blue squares) FWM. Only the down-conversion part is shown for dual-pump FWM.

Fig. 3.13. BER measurement at different polarization states of the input signal and wavelengths of pump 2.

Fig. 3.14. Wavelength multicasting of DPSK signal with equally-spaced pumps. C1-5: five copies generated in wavelength multicasting.

Fig. 3.15. Wavelength multicasting of DPSK signal with unequally-spaced pumps. C1-9: nine copies generated in wavelength multicasting; C0: vacant channels; Cp: idlers from FWM between pumps.

Fig. 3.16. Wavelength multicasting of DPSK signal with four unequally-spaced pumps. C1-9: nine copies generated in wavelength multicasting; C10-13: four additional copies generated owing to pump4; C0: vacant channels; Cp: idlers from FWM between pumps.

Fig. 3.17. Experimental setup of polarization-insensitive wavelength multicasting of DPSK signal using FWM in birefringent PCF.

Fig. 3.18. FWM spectra for RZ-DPSK wavelength multicasting; (a) pump-pump beatings without input signal; (b) wavelength multicasting with input signal (the input signal and the multicast channels are marked and are shown in red).

Fig. 3.19. Eye diagrams of the demodulated 10-Gbit/s RZ-DPSK multicast channels (in each pair, left: fixed polarization state of the input signal, right: time-varying polarization state of the input signal).

Fig. 3.20. BER measurements of the nine multicast channels (Inset: BER measurements of C3 at different polarization states of the input signal).

Fig. 4.1. Demodulation of DPSK using delay interferometer.

Fig. 4.2. (Color online) Tunable optical delay based on wavelength conversion plus

GVD.

Fig. 4.3. Structure of delay-asymmetric nonlinear loop mirror. SMF: single mode fiber; PCF: photonic crystal fiber; BPF: bandpass filter.

Fig. 4.4. Experimental setup of polarization-insensitive DANLM. PS: polarization scrambler; PBS: polarization beam splitter; SMF: single mode fiber; PCF: photonic crystal fiber; BPF: bandpass filter.

Fig. 4.5. Optical spectrum of polarization-insensitive FWM with dual-orthogonal pumps. P1: pump1; P2: pump2; C1, C2: converted wavelength from degenerate FWM between signal-P1 and signal-P2.

Fig. 4.6. Eye diagrams of demodulated 10-Gbit/s RZ-DPSK signal using (a, c): polarization-sensitive DANLM; (b, d): polarization-insensitive DANLM.

Fig. 4.7. Eye diagrams of demodulated 12.5-Gbit/s RZ-DPSK signal using (a, c): polarization-sensitive DANLM; (b, d): polarization-insensitive DANLM.

Fig. 4.8. BER measurement of the 10-Gbit/s DPSK signal demodulated by polarization-insensitive DANLM.

Fig. 4.9. (a) FWM with signal pump and (b) bandwidth-enhanced FWM with dual-parallel pump.

Fig. 4.10. Experimental setup of the dual-parallel pumped DANLM. P1: pump1; P2: pump2; SMF: single mode fiber; PCF: photonic crystal fiber; BPF: optical bandpass filter.

Fig. 4.11. Spectrum of FWM with dual-parallel pumps to produce 333-ps optical delay.

Fig. 4.12. Eye diagrams of demodulated 10-Gbit/s (a) and 3-Gbit/s (b) DPSK signals.

Fig. 4.13. BER measurements of DPSK demodulation with the conventional DI and the DANLM.

Fig. 4.14. Principle of DPSK demodulation based on cascaded FWM. S: signal; P: pump; I: idler.

Fig. 4.15. Setup of the bit-rate variable demodulator. TL: tunable laser; PM: phase modulator; MZM: Mach-Zehnder modulator; EDFA: erbium-doped fiber amplifier; PC: polarization controller; BPF: optical bandpass filter; PCF: photonic crystal fiber; CFBG: chirped fiber Bragg grating; BER: bit error ratio. Demodulator is shown in the dot-line rectangle area.

Fig. 4.16. Eye diagrams and optical spectra of the idlers centered at 1555 nm. (a) after the first FWM, (b) behind the chirped FBG, (c) after the second FWM with 0-phase shift, and (d) after the second FWM with π-phase shift. The measurement positions correspond to points A, B, and C in Fig. 4.15. Inset: incomplete depletion of idler 1.

Fig. 4.17. FWM spectra in the demodulation of (a) 10-Gbit/s and (b) 5-Gbit/s DPSK signals

Fig. 4.18. Demodulated NRZ-DPSK signals. Bit-rate variable demodulator: (a) 10-Gbit/s DB, (b) 10-Gbit/s AMI, (c) 5-Gbit/s DB, (d) 5-Gbit/s AMI; Standard DI: (e) 10-Gbit/s DB, (f) 10-Gbit/s AMI; and (g) BER measurement of the demodulated signals.

Fig. 4.19. Demodulated RZ-DPSK signals. Bit-rate variable demodulator: (a) 10-Gbit/s DB, (b) 10-Gbit/s AMI, (c) 5-Gbit/s DB, (d) 5-Gbit/s AMI; Standard DI: (e) 10-Gbit/s DB, (f) 10-Gbit/s AMI; and (g) BER measurement of the demodulated signals.

Fig. 5.1. SBS loop for clock recovery; (a) SBS loop; (b) working principle of clock recovery. ISO: optical isolator; DSF: dispersion shifted fiber; MZM: Mach-Zehnder modulator; PC: polarization controller. The probe is generated from the carrier-suppressed modulation of original signal. Dash line: spectrum before modulation; solid line: spectrum after modulation.

Fig. 5.2. RZ format generation using a DI. AMI: alternate mark inversion.

Fig. 5.3. Signal evolution in the wideband clock recovery circuit. DI: delay interferometer; NPR: nonlinear polarization rotation; SBS: stimulated Brillouin scattering.

Fig. 5.4. Experimental setup of wideband clock recovery circuit. ASE: amplified spontaneous emission; BPF: bandpass filter; VOA: variable optical attenuator; TL: tunable laser; PM: phase modulator; DI: delay interferometer; HNLF: highly nonlinear fiber; PBS: polarization beam splitter; ISO: optical isolator; DSF: dispersion shifted fiber; MZM: Mach-Zehnder modulator; SOA: semiconductor optical amplifier.

Fig. 5.5. Optical spectrum and waveform evolution in clock recovery of 10-Gbit/s NRZ-DPSK.

Fig. 5.6. RF spectrum (a) and SSB phase noise (b) of the recovered 10-GHz clock.

SSB: single sideband.

Fig. 5.7. (a) Input RZ-AMI signals after DI and (b) recovered clocks of NRZ-DPSK signals after SOA with bit-rate varying from 7.5 to 15 Gbit/s.

Fig. 5.8. RMS Time jitters of RZ-AMI signals and recovered clocks at different bit rates.

Fig. 5.9. Time jitter of recovered clock of 10-Gbit/s NRZ-DPSK signal at different input OSNR.

Fig. 5.10. RF spectra of (a) input NRZ-DPSK signal and (b)-(d) output RZ-AMI signals at different duty cycles.

Fig. 5.11. Experimental setup of the bit-rate tunable CR circuit for NRZ-DPSK signal. TL: tunable laser; PM: phase modulator; SMF: single mode fiber; PCF: photonic crystal fiber; BPF: bandpass filter; HNLF: highly nonlinear fiber; PBS: polarization beam splitter; ISO: isolator; DSF: dispersion shifted fiber; MZM: Mach-Zehnder modulator; SOA: semiconductor optical amplifier; VOA: variable optical attenuator; DI: delay interferometer.

Fig. 5.12. Optical spectrum and waveform evolution in the clock recovery of 10-Gbit/s NRZ-DPSK.

Fig. 5.13. Recovered clocks of NRZ-DPSK signals with bit-rates varying from 4 to 15 Gbit/s.

Fig. 5.14. (a) RF spectrum and (b) SSB phase noise of the recovered 10-GHz clock; (c) Time jitters of the recovered clocks and intensity ratios of clock tones

to information-bearing components at different bit rates.

Fig. 6.1. Microwave signal processing using microwave photonic technology.

Fig. 6.2. Band of UWB technology regulated by FCC.

Fig. 6.3. UWB impulse with spectrum precisely compliant with FCC definition.

Fig. 6.4. Three kinds of UWB signal waveforms.

Fig. 6.5. (color online) UWB generation based on phase-modulation to intensity-modulation conversion.

Fig. 6.6. UWB generation based on photonic microwave delay-line filter.

Fig. 6.7. Principle of UWB monocycle pulse generation based on delayed interference of $\pi/2$ PSK signal.

Fig. 6.8. Experimental setup. TL: tunable laser; PM: phase modulator; PD: photodetector; SMF: single mode fiber. Inset shows the input electrical waveform.

Fig. 6.9. (a) - (c) Generated UWB monocycle waveforms and (d) - (f) corresponding RF spectra. f: repetition rate; $\Delta\varphi$: phase shift between two arms in the DI.

Fig. 6.10. (Color online) (a) Simulated monocycle waveforms after transmission in a SMF of different lengths. (b) measured waveform and (c) measured RF spectrum after transmission in an 8.5-km SMF.

Fig. 6.11. (a) Original UWB pulse train before modulation. (b) UWB pulse train after pulse position modulation.

Appendix C. Abbreviations

AMI	alternate mark inversion
ASE	amplified spontaneous emission
ASK	amplitude shift keying
BER	bit error ratio
BPSK	binary phase-shift keying
CD	chromatic dispersion
DANLM	delay-asymmetric nonlinear loop mirror
DFG	different-frequency generation
DI	delay interferometer
DPSK	differential phase-shift keying
DQPSK	differential quadrature phase shift keying
DSF	dispersion-shifted fiber
EDFA	erbium-doped fiber amplifier
ER	extinction ratio
FBG	fiber Bragg grating
FCC	Federal Communications Commission
FWHM	full width at half maximum
FWM	four-wave mixing
GVD	group velocity dispersion
HNLF	highly nonlinear fiber
ITU	International Telecommunication Unit
MZM	Mach-Zehnder modulator
NPR	nonlinear polarization rotation
NRZ	nonreturn-to-zero
ODB	optical dual-binary
OOK	on-off keying
OPA	optical parametric amplifier
OSNR	optical signal-to-noise ratio

OTDM	optical time division multiplexing
OXC	optical cross connect
PBS	polarization beam splitter
PCF	photonic crystal fiber
PM	phase modulator
PMD	polarization mode dispersion
PolSK	polarization-shift keying
PPD	probe-to-pump detuning
PRBS	pseudo-random bit sequence
PSK	phase-shift keying
PS-QPSK	polarization-switched quadrature phase-shift keying
QAM	quadrature amplitude modulation
QPSK	quadrature phase-shift keying
RPD	residual polarization dependence
RZ	return-to-zero
SBS	stimulated Brillouin scattering
SFG	sum-frequency generation
SOA	semiconductor optical amplifier
SPM	self-phase modulation
SSB	single sideband
UWB	ultra-wideband
VOA	variable optical attenuator
WDM	wavelength division multiplexing
XGM	cross-gain modulation
XPM	cross-phase modulation